Non-adiabatic capillary tubes in high efficiency household refrigerator: an experimental study

PhD Thesis

Laetitia Bardoulet

Supervisors

Dr. D. José Miguel Corberán Salvador

Dr. D. Santiago Martínez Ballester

October 2018

To Quentin.

Acknowledgements

I finally have the pleasure and honour to thank the people who accompanied me during what was the longest race of my life. A PhD thesis is not only a technical challenge, it is also a personal challenge where you learn, through various questioning, how to be an investigator. I definitely would not have crossed the finish line without all the people mentioned here.

First, I would like to thank Prof. José Miguel Corberán Salvador who opened the doors of his institute (Instituto de Ingeniería Energética) to me and provided me with the opportunity to lead this PhD thesis. I express my deep gratitude to him for having trust in me, for always being present and supportive when my work was at a dead-end, for being very patient and always available when I needed him, despite his full agenda. *Muchas gracias José Miguel, por todo lo que he aprendido con usted.*

Thank you to Dr. Santiago Martinez Ballester, without whom this thesis would not exist, for sharing with me part of his vast knowledge of refrigeration, for continuing to supervise me despite his new job, and for his precious advice and support. *Gracias por tu apoyo Santi.*

Thank you to the Universidad Politécnica de Valencia and Generalitat valenciana for awarding me a grant.

Thank you to Prof. Alberto Coronas Salcedo (Universidad Rovira i Virgili, Tarragona), Prof. Ramón Cabello Lopez (Universidad Jaume I, Castellón), and Prof. Jose Fernandez Seara (Universidad de Vigo) for their useful comments and collaboration in the revision of this thesis.

Thank you to Prof. José Gonzálvez Maciá for trusting me and giving me the opportunity to participate in a research project in collaboration with the firm where I now have a position. *Gracias Pepe.*

Thank you to Estefanía for being the best office roommate ever, her friendship and daily support. *Gracias por haber estado siempre.*

Thank you to the inseparable Alex and Rafa for all the “valencianas” and coffee enjoyed in the always open “tears office” and their support in this adventure. To Alex, for his technical advice and help in the lab and Rafa for teaching me the most important informatics class lesson: in case of a problem, restart the computer. *Gracias chicos por vuestro apoyo.*

Thank you to Dr. Jorge Paya Herrero for all I have learnt during our work collaboration, advice for this thesis, support and friendship.

Thank you to all my other friends in the IIE: Alex, Antonio, Alberto and Javi for their help in the lab. Also, thank you to Fran, Emilio L., Emilio N., Carla, Maria, Joan, Paloma, Daniela, Fernando, Toni, Abdel, Luis, Barbara, and José Maria.

Thank you to my new friends in Pamplona, Alberto for his friendship and support and my great roommates José Luis and Juan Carlos.

Thank you to my new colleagues at B.S.H. for their support and especially to Sandra for our wonderful running trips.

Thank you to all my friends in France, Jeff for his precious support and advice during these years, Fouge for always trusting in and supporting me, Kevin and Rémy for their much-welcomed visits during the past three years, and Camille, Estelle, Gally, Flo, Greg, Guigui, Nono, Clément, Juju, Antonin, Julie, Elise, Marion, Lucie, and Thomas.

Thank you to Marvin for bearing with my doubts, sharing my joys and my pains, being supportive and always present for me. *Gracias Caramelito.*

And, thank you to my family, my sisters Coco and Mayou, Imed, my nephews Anissa and Sami and my parents for always having trusted in me more than I did myself, supporting me in all the choices I have made in life, and being such a united Family. *Merci à vous d´être toujours là.*

Abstract

Capillary tube with liquid-to-suction heat exchanger (CT-LSHX) is a component widely used in household refrigerators. Recent works have indicated that even when measuring subcooled conditions at the condenser outlet, the actual capillary tube inlet is two phase-flow.

The aim of this PhD thesis is to examine the actual conditions at the capillary tube inlet of a household refrigerator by using an innovative test bench.

Transparent tubes were set up at the condenser outlet and capillary tube inlet. The experimental visualisation campaign reveals that the capillary tube inlet was two-phase flow despite the measurement of a certain subcooling, regardless of the filter position (horizontal or vertical), flow direction (upward or downward) and refrigerant charge. This study also demonstrates that the filter was not acting as an accumulator since the liquid level of the capillary always followed the capillary tube entrance, regardless of the capillary tube length inside the filter. Two hypotheses were then posed to explain the phenomenon: a non-equilibrium condition of the refrigerant and/or an unbalanced matching between compressor and capillary tube, that is, the system would be equipped with a capillary tube with a notably large expansion capacity compared to the needs of the compressor.

The original refrigerant-to-air condenser was replaced by a refrigerant-to-water condenser to assess, from the heat balance at the water condenser, the refrigerant conditions at the condenser outlet and therefore, at the capillary tube inlet. Measurements indicate a non-equilibrium two-phase flow composed of subcooled vapour and liquid at the capillary tube inlet. To verify if the presence of two-phase flow was due to unbalanced matching between the capillary tube and compressor, the test bench design was modified by using a smaller capillary tube diameter and increasing compressor speed. Fully liquid conditions at the capillary tube inlet were reached with this new configuration.

A performance analysis comparison between a capillary tube inlet composed of vapour and liquid and a capillary tube inlet composed of only liquid was also performed. Results reveal that COP were higher in cases of fully liquid conditions at the capillary tube inlet.

Resumen

El tubo capilar con intercambio de calor líquido-succión (CT-LSHX) es un componente ampliamente utilizado en refrigeradores domésticos. Trabajos recientes han indicado que la entrada del tubo capilar era bifásica, aunque condiciones subenfriadas estaban medidas a la salida del condensador.

El objetivo de esta tesis doctoral es examinar las condiciones reales a la entrada del tubo capilar de un refrigerador doméstico mediante el uso de un banco de pruebas innovador. Se instalaron tubos transparentes a la salida del condensador y a la entrada del tubo capilar con el fin de visualizar el flujo.

La campaña de visualización experimental revela que el flujo a la entrada del tubo capilar era bifásico a pesar de la medición de un cierto subenfriamiento, independientemente de la posición del filtro instalado a la entrada del capilar (horizontal o vertical), la dirección del flujo (hacia arriba o hacia abajo) y la carga de refrigerante. Este estudio demuestra también que el filtro no estaba actuando como un acumulador ya que el nivel de líquido del capilar siempre siguió la entrada del tubo capilar, independientemente de la longitud del tubo capilar dentro del filtro. Se plantearon dos hipótesis para explicar el fenómeno: una condición de no equilibrio del refrigerante y/o un desequilibrio entre el caudal másico del compresor y del capilar, es decir, el sistema estaría equipado con un capilar no bastante restrictivo en comparación con las necesidades del compresor.

El condensador original refrigerante-aire fue reemplazado por un condensador refrigerante-agua para evaluar, a partir del balance de calor en el condensador de agua, las condiciones del refrigerante a la salida del condensador y, por lo tanto, a la entrada del tubo capilar. Las mediciones indican un flujo bifásico no equilibrado compuesto de vapor y líquido subenfriados a la entrada del tubo capilar. Para verificar si la presencia de flujo bifásico se debía a un desequilibrio entre el caudal másico del compresor y del capilar, el diseño del banco de prueba se modificó utilizando un diámetro de tubo capilar más pequeño y aumentando la velocidad del compresor. Con esta nueva configuración, se alcanzó a llenar de líquido el filtro y, por lo tanto, tener condiciones exclusivamente líquidas a la entrada del tubo capilar.

Se realizó una comparación de prestaciones entre un flujo bifásico y un flujo únicamente líquido a la entrada del capilar. Los resultados revelan que el COP fue mayor cuando la entrada del capilar era sólo líquida.

Resum

El tub capil·lar amb intercanvi de calor líquid-succió (CT-LSHX) és un component àmpliament utilitzat en refrigeradors domèstics. Treballs recents han indicat que l'entrada del tub capil·lar era bifàsica, encara que condicions sub-refredades estaven mesurades a l'eixida del condensador.

L'objectiu d'aquesta tesi doctoral és examinar les condicions reals a l'entrada del tub capil·lar d'un refrigerador domèstic mitjançant l'ús d'un banc de proves innovador. Es van instal·lar tubs transparents a l'eixida del condensador i a l'entrada del tub capil·lar amb la finalitat de visualitzar el flux.

La campanya de visualització experimental revela que el flux a l'entrada del tub capil·lar era bifàsic malgrat el mesurament d'un cert sub-refredament, independentment de la posició del filtre instal·lat a l'entrada del capil·lar (horitzontal o vertical), la direcció del flux (cap amunt o cap avall) i la càrrega de refrigerant. Aquest estudi demostra també que el filtre no estava actuant com un acumulador ja que el nivell de líquid del capil·lar sempre va seguir l'entrada del tub capil·lar, independentment de la longitud del tub capil·lar dins del filtre. Es van plantejar dues hipòtesis per a explicar el fenomen: una condició de no equilibri del refrigerant i/o un desequilibri entre el cabal màssic del compressor i del capil·lar, és a dir, el sistema estaria equipat amb un capil·lar no bastant restrictiu en comparació amb les necessitats del compressor.

El condensador original refrigerant-aire va ser reemplaçat per un condensador refrigerant-aigua per a avaluar, a partir del balanç de calor en el condensador d'aigua, les condicions del refrigerant a l'eixida del condensador i, per tant, a l'entrada del tub capil·lar. Els mesuraments indiquen un flux bifàsic no equilibrat compost de vapor i líquid sub-refredats a l'entrada del tub capil·lar. Per a verificar si la presència de flux bifàsic es devia a un desequilibri entre el cabal màssic del compressor i del capil·lar, el disseny del banc de prova es va modificar utilitzant un diàmetre de tub capil·lar més xicotet i augmentant la velocitat del compressor. Amb aquesta nova configuració, es va aconseguir omplir de líquid el filtre i, per tant, tindre condicions exclusivament líquides a l'entrada del tub capil·lar.

Es va realitzar una comparació de prestacions entre un flux bifàsic i un flux únicament líquid a l'entrada del capil·lar. Els resultats revelen que el COP va ser major quan l'entrada del capil·lar era només líquida.

Content

Acknowledgements v

Abstract vii

Resumen.. ix

Resum... xi

List of figures.. xvii

List of tables xxi

Nomenclature xxv

1. **Introduction.. 1**

1.1 Motivations 1

1.2 Working principles of a household refrigerator 3

1.2.1 Refrigerant loop 3

1.2.2 Air loop 4

1.3 CT-LSHX in household refrigerator system 8

1.3.1 Definition 8

1.3.2 Types of CT-LSHX 10

1.3.3 Refrigerant flow through the capillary tube 10

1.3.4 Parameters influencing the mass flow rate..................................... 12

1.3.5 Problems and consequences of using CT-LSHX 24

1.3.6 Recondensation and reverse heat transfer 24

1.3.7 Flow hysteresis 27

1.3.8 Noise 28

1.4 The importance of subcooled conditions 29

1.5 What are the actual conditions at the capillary tube inlet?......................... 30

1.6 Objectives and structure of the work 32

2. **Visualisation of the refrigerant flow at the capillary tube inlet of a household refrigerator 33**

2.1 Objectives 33

2.2 Experimental set up 33

2.2.1 Original apparatus 33

2.2.2 Modifications of the original apparatus 38

2.3 Experimental Campaign 47

2.3.1 Overall procedure 47

2.3.2 Refrigerant charge procedure 48

2.3.3 Find the optimal charge of refrigerant 48

2.3.4 Results and discussion 51

2.4 Conclusions 59

3. **Experimental assessment of vapour quality at the condenser outlet of a household refrigeration system 61**

3.1 Objective 61

3.2 Experimental set up 62

3.2.1 General overview of the tests bench 62

3.2.2 Instrumentation 63

3.3 Experimental campaigns 74

3.3.1 Procedure 74

3.3.2 PID set point 75

3.3.3 Reference conditions with air condenser 76

3.3.4 Tests repeatibility 79

3.3.5 Reproduction of optimal charge air condenser test without heater in the FZ 85

3.3.6 Reproduce test conditions with refrigerant-to-water HX 86
3.4 Analysis of the results and discussion 87
3.4.1 Visualisations.. 87
3.4.2 Determination of capillary tube inlet conditions............................ 88
3.4.3 Possible explanation of vapour at the capillary tube inlet.............. 95
3.5 Conclusions 96

4. **How to get full liquid conditions at the capillary tube inlet? 99**
4.1 Objectives 99
4.2 Modification of the test bench 99
4.2.1 Temperature regulation... 101
4.2.2 Temperature at the filter inlet 102
4.3 Experimental campaign 105
4.3.1 Tests conditions 105
4.3.2 Flow visualisation varying compressor speed.............................. 106
4.3.3 Results and discussion 109
4.4 Conclusions 120

5. **Performance comparison between liquid and vapour conditions at the capillary tube inlet 123**
5.1 Objectives 123
5.2 Experimental campaign 123
5.2.1 Procedure 123
5.2.2 Determination of optimal charges with 0.55 and 0.6 mm capillary tubes 124
5.3 Conclusions 129

6. **Conclusions and future works 131**

6.1 Conclusions 131
6.1.1 On the actual conditions at the capillary tube inlet 131
6.1.2 On the design improvement to ensure liquid conditions at the capillary tube inlet 132
6.2 Future works 133

References 135
Publications 139

List of figures

Figure 1: Refrigerant loop of a household refrigerator 4
Figure 2: Household refrigerator.. 5
Figure 3: Fan in the FZ cabinet 6
Figure 4: Damper between FF and FZ cabinets 6
Figure 5: Compressor and damper status vs temperatures evolution inside FF and FZ 6
Figure 6: Air distribution in FF and FZ cabinets... 7
Figure 7: NTC location inside FF and FZ cabinets 8
Figure 8: Set up of adiabatic (A) vs. non-adiabatic (B) capillary tube [20] 9
Figure 9: Flow pattern of non-adiabatic vs diabatic capillary tube [21] 9
Figure 10: Schematic of the capillary tube-suction line heat exchanger: (a) concentric, (b) lateral [21] 10
Figure 11: Evolution of refrigerant temperature along the capillary tube, adapted from [13]... 11
Figure 12: Refrigerant flow through capillary tube, adapted from [13] 12
Figure 13: Pressure-enthalpy diagram of recondensation phenomenon in CT-LSHX 25
Figure 14: Example of recondensation phenomenon [33] 25
Figure 15: Example of reverse heat transfer [18].. 26
Figure 16 : Pressure-enthalpy diagram of reverse heat transfer phenomenon in CT-LSHX 26
Figure 17: Hysteresis effect of mass flow rate versus subcooling [13].................... 27
Figure 18: Hysteresis effect of COP [13]... 27
Figure 19: Acceleration profile of the refrigerant flow [12] 28
Figure 20: Acceleration profile with additional heat exchanger at the condenser outlet [12]... 29

Figure 21: Effectiveness for different operating conditions with respect to subcooling [13] 30

Figure 22: Set up of the three capillary tubes around the suction line 42

Figure 23: Visualisation test bench 42

Figure 24: Refrigerant temperature and pressure measurements location 43

Figure 25: Outlet condenser temperature measurement 45

Figure 26: Air FF and FZ temperatures measurement locatio 45

Figure 27: Climatic chamber 47

Figure 28: Identification of time parameters for the calculation of the compressor energy consumption during a typical refrigeration dynamic cycle 50

Figure 29: Average compressor power through the refrigerant charge study 51

Figure 30: Temperatures along the condenser for optimal refrigerant charge (62.5 g) 52

Figure 31: Temperatures along the condenser for 73 g refrigerant charge 53

Figure 32: Evolution of subcooling through the refrigerant charge study 53

Figure 33: Refrigerant flow at the condenser outlet 54

Figure 34: Refrigerant flow in a condenser bend 55

Figure 35: Capillary tube inlet for tests 1, 2 and 3 58

Figure 36: Capillary tube inlet for tests 4, 5 and 6 58

Figure 37: Capillary tube inlet for tests 7, 8 and 9 58

Figure 38: Diagram of the tests bench 62

Figure 39 : Labview platform interface 74

Figure 40: Temperatures PID determination 76

Figure 41: Cooling capacity, COP and compressor power for different refrigerant charges 78

Figure 42: Subcooling for different refrigerant charges 79

Figure 43: Temperature along condenser for different charges tested 82

Figure 44: Gas chromatograph experimental set up 83

Figure 45: Two-phase flow capillary tube inlet 87

Figure 46: Visualisation of the condenser outlet with a)m_w=0.447 kg.min^{-1} b) m_w=0.190 kg.min^{-1} c) m_w =0.066 kg.min^{-1} 88

Figure 47: Water and condensing capacities varying water mass flow rate 89

Figure 48: Condensation pressure vs. water mass flow rate 90

Figure 49: Refrigerant mass flow rate vs. water mass flow rate 90

Figure 50: Subcooling evaluated from the pressure and temperature measurements and the assumption of thermodynamic equilibrium, and subcooling evaluated from the inlet refrigerant conditions and the heat measured on the water side. 91

Figure 51: Comparison between condenser outlet temperature and capillary tube inlet temperature 92

Figure 52: Approximate diagram for R600a/oil 94

Figure 53: Enthalpies evaluated from the pressure and temperature measurements and the assumption of thermodynamic equilibrium, and enthalpy evaluated from the inlet refrigerant conditions and the heat measured on the water side compared with data obtained by Lee et al. [16] 94

Figure 54: Refrigerant mass flow rates matching 96

Figure 55 : Test bench 100

Figure 56: Air evaporator inlet thermocouple location 101

Figure 57: Heat exchange inside refrigerant circuit 103

Figure 58: Set up of the anti-radiation shield around the RTD 104

Figure 59: Observed refrigerant liquid level for the different tests 106

Figure 60: Different liquid levels at the capillary tube inlet 107

Figure 61: Liquid level evolution at the capillary tube inlet for tests 2 and 6 108

Figure 62: Condenser outlet for different compressor speeds a) 1800 rpm b) 2500 rpm and c) 3500 rpm 108

Figure 63: Subcooling evaluated from the pressure and temperature measurements and the assumption of thermodynamic equilibrium (SC_pT), and subcooling evaluated from the inlet refrigerant conditions and the heat measured on the water side (SC_HX) 109

Figure 64: Refrigerant mass flow rate through tests campaign 110

Figure 65: Controlled parameters through tests campaign 111

Figure 66: Compressor power and resistance power through tests campaign 111

Figure 67: Hysteresis in the capillary tube mass flow rate [26] 112

Figure 68: Mass flow rate variation vs. SC_PT measured subcooling for different compressor speeds.. 113

Figure 69: Change in refrigerant mass flow rate from 1800 rpm to 2500 rpm 114

Figure 70: Evolution of cooling capacity, resistance power and compressor power across the tests.. 117

Figure 71: Re-evaluation of cooling capacity of the tests of test campaign 4.1 119

Figure 72: COP and liquid level inside filter for different refrigerant charges for the two tested capillary tubes, of 0.55 mm and 0.6 mm diameter respectively............ 126

Figure 73: Compressor power for different refrigerant charges for the two tested capillary tubes, of 0.55 mm and 0.6 mm diameter respectively 127

Figure 74: Refrigerant cooling capacity for different refrigerant charges for the two tested capillary tubes, of 0.55 mm and 0.6 mm diameter respectively.................. 127

Figure 75: Resistance power of 0.55 mm diameter and 0.6 mm diameter capillary tubes for different refrigerant charges 128

Figure 76: COP using air cooling capacity of 0.55 mm diameter and 0.6 mm diameter capillary tubes for different refrigerant charges 128

List of tables

Table 1: Review of CT-LSHX increase diameter effect on refrigerant mass flow rate 14

Table 2: Review of CT-LSHX total length increase effect on refrigerant mass flow rate 15

Table 3: Review of CT-LSHX heat exchange length increase effect on refrigerant mass flow rate 15

Table 4: Review of CT-LSHX inlet length increase effect on refrigerant mass flow rate 17

Table 5: Review of CT-LSHX suction diameter increase effect on refrigerant mass flow rate 18

Table 6: Review of CT-LSHX pressure inlet increase effect on refrigerant mass flow rate 19

Table 7: Review of CT-LSHX inlet subcooling increase effect on refrigerant mass flow rate 20

Table 8: Review of CT-LSHX evaporator superheat increase effect on refrigerant mass flow rate 21

Table 9: Review of CT-LSHX suction inlet pressure increase effect on refrigerant mass flow rate 22

Table 10: General description of the original apparatus 33

Table 11: Compressor data 34

Table 12: Condenser data 35

Table 13: Capillary tube and filter data 36

Table 14: Evaporator data 37

Table 15: Condenser modification 39

Table 16: Filter modification 40

Table 17: Capillary tube modification 41

Table 18: Evaporation and condensation pressures 43

Table 19: Refrigerant circuit temperatures 44

Table 20: Inside air FF+FZ temperatures 46

Table 21: Datalogger specifications 46

Table 22: Wattmeter specifications 46

Table 23: Test conditions for experimental campaign 2.1 49

Table 24: Tests matrix of experimental campaign 2.2 56

Table 25: Test input for experimental campaign 2.2 57

Table 26: Refrigerant mass flow meter 65

Table 27: Refrigerant-to-water condenser 66

Table 28: Condenser outlet 67

Table 29: Temperature measurement of the capillary tube inlet 68

Table 30: Water pump specifications 69

Table 31: Water temperatures 70

Table 32: Water mass flow meter 71

Table 33: Water-to-air heat exchanger 72

Table 34: Wattmeter specifications 73

Table 35: Temperature control 73

Table 36: PID temperature 76

Table 37: Test conditions for experimental campaign 3.1 77

Table 38: Test condition for experimental campaign 3.2 80

Table 39: Tests repetition 80

Table 40 : Gas chromatography of refrigerant sample 84

Table 41: Effect of nitrogen and oxygen on condensation temperature 84

Table 42: Test conditions for experimental campaign 3.3 85

Table 43: Optimal air condenser conditions 86

Table 44: Test conditions of experimental campaign 3.4 86

Table 45: Estimation of the radiation effect on the measurement of the vapor temperature at the capillary tube inlet 104

Table 46: Test conditions for experimental campaign 4.1 105

Table 47: Test conditions for experimental campaign 4.2 115

Table 48: Comparison of test with (test 1) and without (test 2) metastable length in capillary tube 116

Table 49: Cooling capacity calculated on the refrigerant side vs cooling capacity calculated on the air side 119

Table 50: Tests conditions of experimental campaign 5.1 124

Nomenclature

A	Surface, [m^2]
COP	Coefficient of Performance, [-]
c_p	Specific heat capacity, [kJ.kg^{-1}.K^{-1}]
G	Mass velocity [kg.m^{-2}.s^{-1}]
h	Specific enthalpy, [kJ.kg^{-1}]
L	Length, [m]
$\dot{m}$	Mass flow rate, [kg.s^{-1}]
P	Pressure, [bar]
$\dot{Q}$	Rate of heat transfer, [W]
R	Heater power, [W]
SC	Subcooling, [K]
SH	Superheat, [K]
T	Temperature, [ºC]
U	Global heat transfer coefficient [W.K^{-1}.m^{-2}]
$\dot{W}$	Rate of work, power [W]

Greek symbols

α	Air flow ratio, [-]
ε	Surface emissivity, [-]
τ	Time ratio, [-]
σ	Stefan-Boltzmann constant, (W. m^{-2} .K^{-4})

Subscripts

ave	Average
cap	Capillary tube
cond	Condenser
comp	Compressor
cool	Cooling
damp	Damper
dis	Discharge
evap	Evaporator
int	Interior
p	Pressure [bar]
in	Inlet

out	Outlet
ref	Refrigerant
suct	Suction
w	Water

Acronyms and abbreviations

CT	Capillary tube
COP	Coefficient of performance
FF	Fresh food compartment
FZ	Freezer compartment
HX	Heat exchanger
LSHX	Liquid-to-suction heat exchanger

Chapter 1

Introduction

1.1 Motivations

Innovations in household refrigeration are interesting from both the consumers and manufacturers points of view. Increases in energy prices provide an incentive for customers to buy low-consumption appliances, especially refrigerator and freezers since both represent the largest unit of energy consumption [1]. Private households are responsible for more than 25% of energy consumption in the EU, including 15% represented by refrigerators and freezers [1], [2]. The global market for energy efficient appliances is expected to represent 1030€ billion in 2020 [1]. Hence, it is a highly profitable challenge for manufacturers to investigate how to reduce consumers energy bills.

There are various ways to reduce energy consumption, for example:

- Improving insulation and, more generally, reducing heat gain [3]. The use of vacuum insulation panels in household refrigerators considerably reduces heat transfer. Indeed, they have a thermal resistance of approximately a factor of 10 higher than that of equally thick conventional polystyrene boards [4].
- Sizing and optimising the refrigerant circuit elements, such as the compressor [5], condenser [6], [7], evaporator and expansion device [5], [8]–[11].

In a household refrigerator, a capillary tube with liquid-to-suction heat exchanger (CT-LSHX) is the most widespread expansion device. Despite the simplicity of such a dispositive, CT-LSHX introduces complex phenomena due to simultaneous two-phase flow expansion and heat transfer.

Some of the negative consequences of these phenomena are noise [12], which is becoming an important quality issue, flow hysteresis, flow oscillations and reduction of CT-LSHX effectiveness [13], which affects global efficiency.

Studies investigating how to solve this noise problem report that it disappears when there is sufficient subcooling at the capillary tube inlet [12]. Another important consequence of the liquid absence at the condenser outlet is loss of global efficiency due to the reduction of cooling capacity given the same compression work.

Boend and Melo [14] developed a correlation to predict the mass flow rate through the capillary tube, and obtained a good prediction of the mass flow rate, except for the tests with subcooling of less than 5 K. By visualisation of the capillary tube inlet, the authors concluded that even with a certain subcooling, the inlet was a two-phase flow. As a possible explanation, they pointed out that, at the capillary inlet, there is a non-equilibrium mixture of subcooled liquid and saturated vapour, instead of a purely liquid phase.

Inan et al. [15] identified, by X-ray equipment, fully liquid conditions at the capillary tube inlet. The value for the subcooling was of 5 K when quasi-steady conditions were reached. Thus, concerning the inlet conditions at the capillary tube, observations by Inan et al. [15] differ from those by Boeng and Melo [14], possibly from running the system with different refrigerant mass flow rates due to using different refrigerants.

Lee et al. [16] visualised a two-phase refrigerant flow at the inlet of the capillary tube of a commercial refrigeration system working with R600a, and concluded that the refrigerant was in a non-equilibrium state where both subcooled liquid and subcooled vapour coexist at the capillary tube inlet.

Ko and Jeong [17] complemented this previous work by studying the effect of a non-equilibrium subcooled two-phase flow on the performance of a vapour compression refrigeration system. These authors claimed that the COP may be overestimated by 19.4% if the thermodynamic properties table is used for a refrigerant non-equilibrium state.

The subcooled conditions at the capillary tube inlet, estimated from measuring the temperature on the wall surface, are always reported in the literature. However, the cited problems of noise and conclusions of others works [14], [16], [17] point out that these conditions may not be real, which, if true, would mean that there is a room for efficiency improvement and, more generally, energy consumption.

Different reasons may offer explanation, namely: non-equilibrium between subcooled phase and saturated vapour at the capillary inlet [14], non-equilibrium between subcooled liquid and subcooled vapour [16], [17] and/or insufficient compressor capacity compared with the expansion device capacity of the capillary tube used, which would mean a capillary tube too large for that compressor.

For these reasons, an experimental work is needed to deepen the actual inlet capillary tube conditions of a household refrigerator.

1.2 Working principles of a household refrigerator

The purpose of this section is to give some keys about the overall working of a domestic refrigerator. A more detailed description of each component will be provided in the next chapter.

1.2.1 Refrigerant loop

Figure 1 presents a basic diagram of the refrigerant loop components in a household refrigerator. The working is based on a vapour compression cycle.

The refrigerant, in a saturated vapour state, enters the compressor. The vapour is then compressed, which increases both its pressure and temperature. The refrigerant releases ambient heat through the condenser and moves to the frame heater, where it follows the door frame to avoid condensation on the door seal.

After passing through the filter dryer, the refrigerant enters the capillary tube in a subcooled liquid state.

The expansion occurs due to the CT-LSHX; pressure and temperature are reduced to finally enter the evaporator where the warm air of the cabinet is circulated with a fan. This warm air evaporates the liquid refrigerant, which leaves the evaporator in a saturated vapour state and returns to the compressor to commence another compression cycle.

There are many refrigerator architectures that differ in their number of different temperature compartments. There are also some varying configurations for evaporator choice, but no frost and normal are typical selections. No frost units are usually equipped with a fin a tube heat exchanger, while the normal unites usually use a roll-bond or tube-on-sheet heat exchanger.

The thesis focuses on no-frost refrigerators with two separated cabinets for fresh and frozen food, since these are most commonly used in Spain.

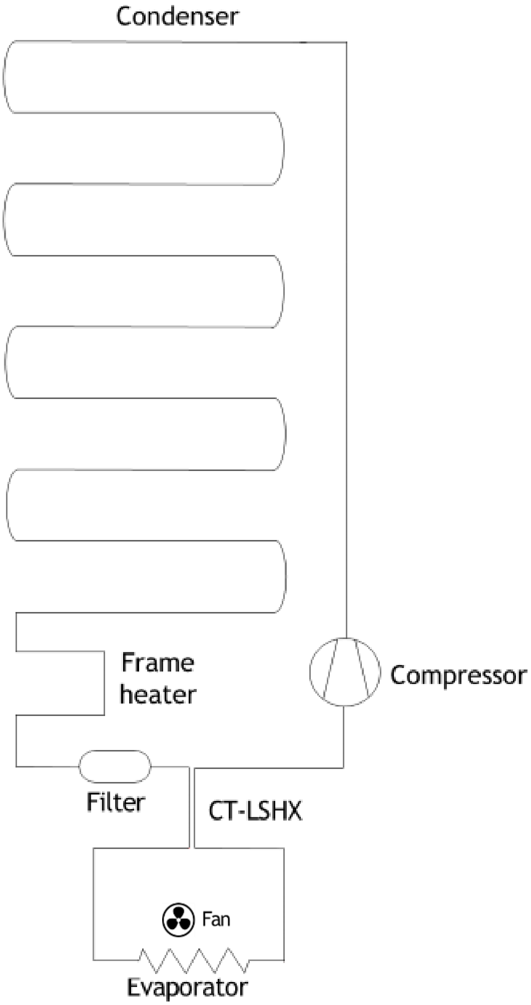
Condenser
Frame heater
Compressor
Filter
CT-LSHX
Fan
Evaporator

Figure 1: Refrigerant loop of a household refrigerator

1.2.2 Air loop

This refrigerator is composed of fresh food (FF) and freezer (FZ) compartments, as illustrated in Figure 2.

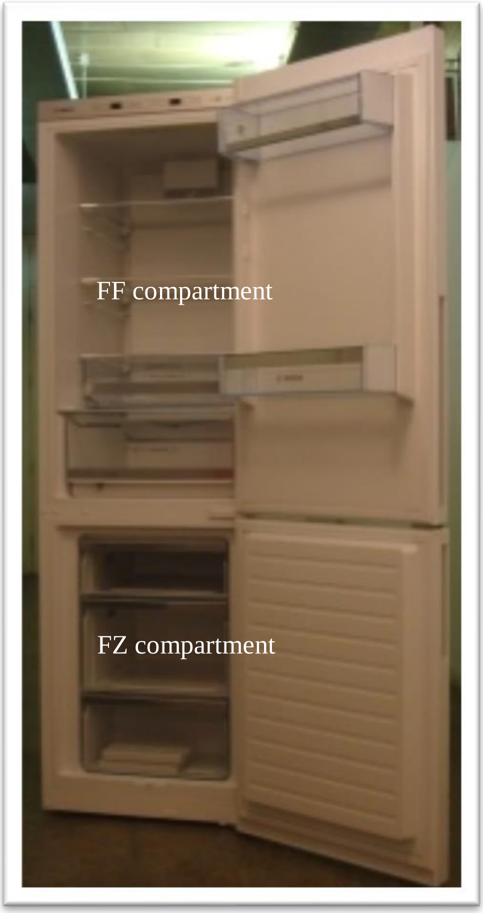

Figure 2: Household refrigerator

The evaporator is in the FZ and a fan (Figure 3) located close to the evaporator, supplies fresh air to both compartments, alternating between two modes. Namely, FZ mode (only the freezer is supplied with fresh air) and FF+FZ mode (fresh food and freezer cabinets are both supplied with fresh air). A trapdoor, named damper (Figure 4) is located between both cabinets, which allows alternating FZ and FF+FZ modes, according to the FF temperature. Figure 5 represents a complete compressor cycle. At T1, the compressor starts, the damper opens and fan operates. This is the FF+FZ mode, where air from the evaporator is supplied to both the fresh food cabinet and freezer cabinet as depicted in Figure 6.

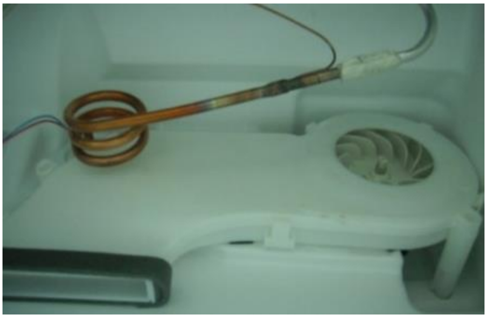

Figure 3: Fan in the FZ cabinet

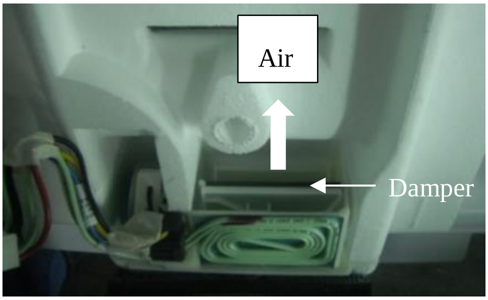

Figure 4: Damper between FF and FZ cabinets

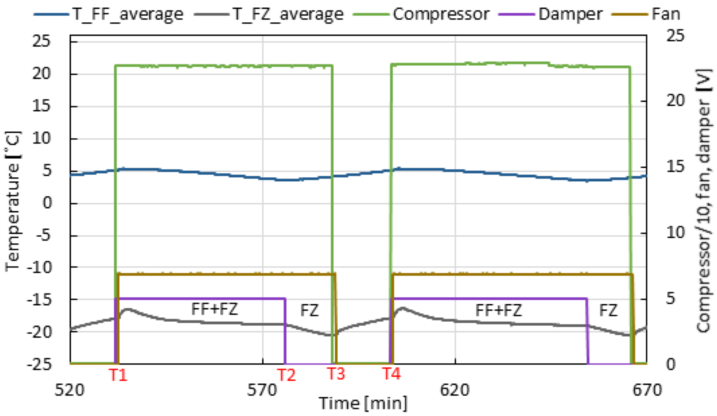

Figure 5: Compressor and damper status vs temperatures evolution inside FF and FZ

At T2, the damper closes. Here, the air temperature inside the fresh food cabinet reaches a lower temperature value within a control range (in this case, the temperature set point is -18 ºC for the FZ and 4 ºC for the FF, where both temperatures correspond to the average temperature of each compartment).

The refrigerator then switches to FZ mode, where air from the evaporator is only supplied to the freezer. At T3, once the freezer also achieves the lower temperature value within the control range, the compressor switches off, the damper closes and the fan no longer operate until the temperature of either the FF or FZ reaches the largest limit in the set range (T4).

Measurement of the temperature inside the cabinets was carried out with NTC (location depicted in Figure 7).

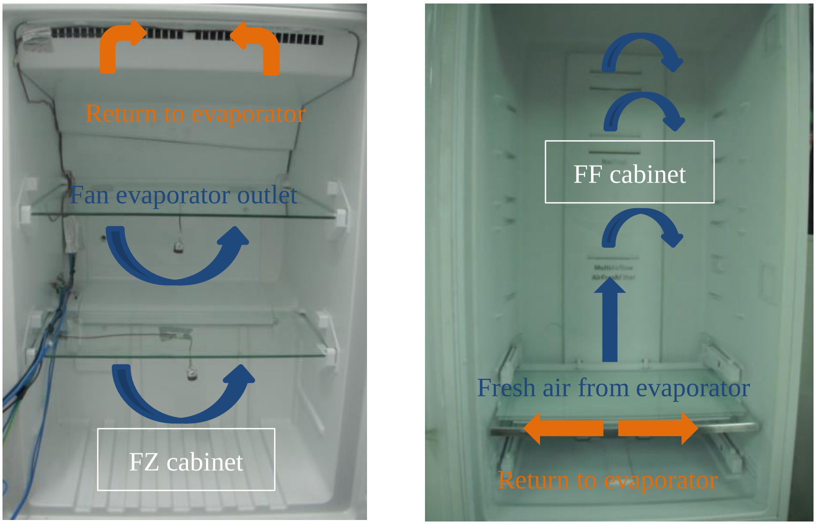
Return to evaporator
Fan evaporator outlet
FZ cabinet
FF cabinet
Fresh air from evaporator
Return to evaporator

Figure 6: Air distribution in FF and FZ cabinets

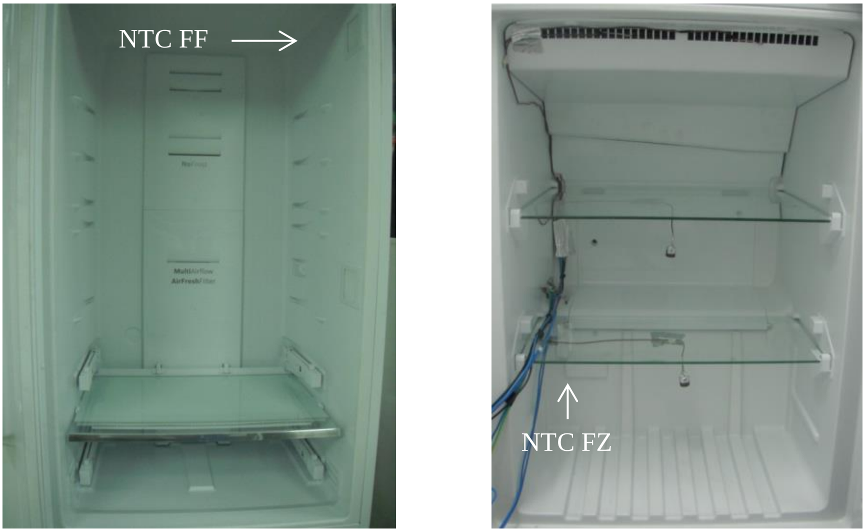

Figure 7: NTC location inside FF and FZ cabinets

1.3 CT-LSHX in household refrigerator system

1.3.1 Definition

A capillary tube is a copper tube with a small diameter, and which is used as an expansion device. Generally, the tube has an inner diameter ranging from 0.5 mm to 2 mm and a length between 1 m to 6 m [18].

The capillary tube can be non-adiabatic or adiabatic (Figure 8). Unlike the adiabatic capillary tube (configuration (A) in Figure 8), the non-adiabatic capillary tube is placed in thermal contact with the compressor suction line (configuration (B) in Figure 8). In the latter case, the term is capillary tube with liquid-to-suction line heat exchanger (CT-LSHX), and it prevents suction line sweating, increases refrigerating capacity and efficiency and reduces the risk of liquid slugs in the compressor. Another advantage is that pressure equalises through the system during the off cycle and reduces the starting torque required by the compressor motor [19]. Some inconveniences include the incapacity to control the superheat and the limited range of use. Figure 9 compares the flow patterns described by adiabatic and non-adiabatic flows of the refrigerant R134a in the same capillary tube. The adiabatic flow follows a path close to an isenthalpic line, whereas the non-adiabatic flow is projected toward the line of saturated liquid, increasing the amount of liquid in the two-phase mixture and decreasing the vapour quality at the evaporator inlet [21].

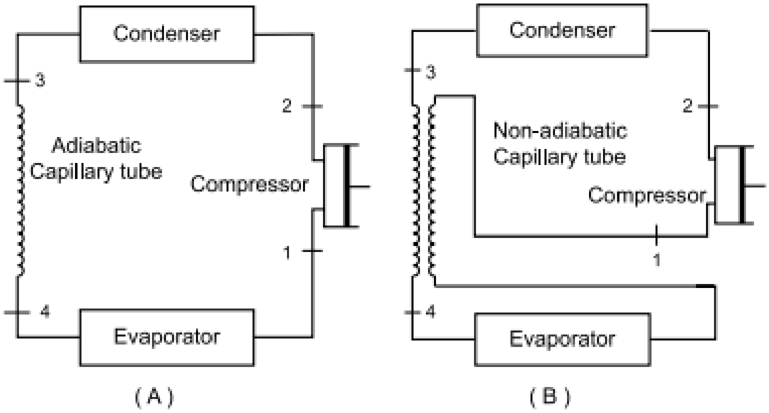
Condenser
3
2
Adiabatic
Capillary tube
Compressor
1
4
Evaporator
(A)
Condenser
3
2
Non-adiabatic
Capillary tube
Compressor
1
4
Evaporator
(B)

Figure 8: Set up of adiabatic (A) vs. non-adiabatic (B) capillary tube [20]

Due to its simplicity and low cost, CT-LSHX is widely adopted in household refrigerators. A such, this thesis focuses on explaining this type of capillary tube.

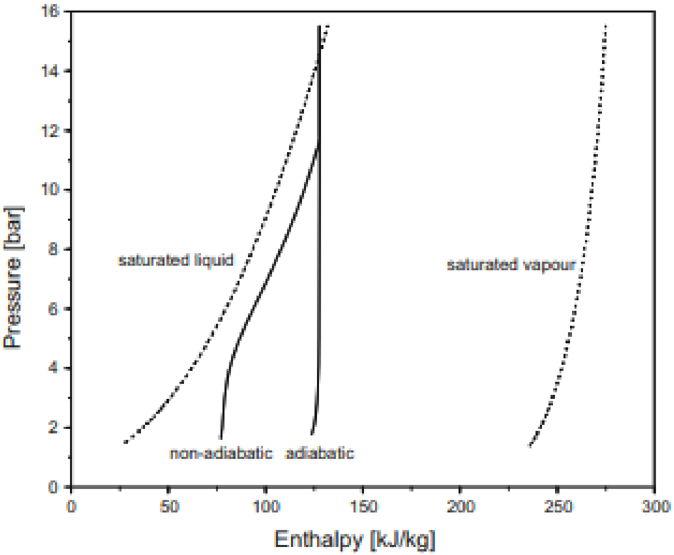

Figure 9: Flow pattern of non-adiabatic vs diabatic capillary tube [21]

1.3.2 Types of CT-LSHX

CT-LSHX can be placed in contact with the suction line in two main ways: concentric and lateral [18], [21], [22].

The capillary tube passes through the suction line for the concentric configuration, whereas in the lateral configuration (Figure 10) it is welded to the suction line. Therefore, it is important to highlight three length parameters that influence the refrigerant mass flow rate and, more generally, refrigerator efficiency:

- total length (L_{cap}) of the capillary tube
- inlet length (L_{in}) corresponding to the adiabatic capillary tube length from the outlet of the condenser
- heat exchange length (L_{HX}), where the suction line and capillary tube are in thermal contact

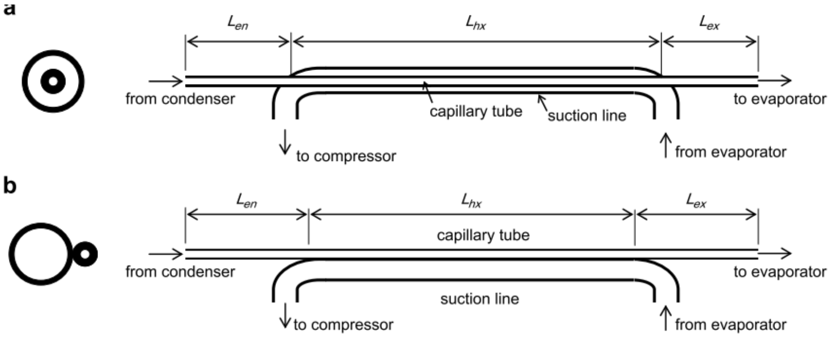
a
L_{en}
L_{hx}
L_{ex}
from condenser
to evaporator
capillary tube
suction line
to compressor
from evaporator
b
L_{en}
L_{hx}
L_{ex}
capillary tube
from condenser
to evaporator
suction line
to compressor
from evaporator

Figure 10: Schematic of the capillary tube-suction line heat exchanger: (a) concentric, (b) lateral [21]

1.3.3 Refrigerant flow through the capillary tube

Before describing how capillary tube parameters influence system performance, it is important to understand the evolution of the refrigerant condition inside the capillary tube.

Figure 11 presents the temperature profile along the capillary tube.

Normally, the refrigerant enters the adiabatic region of the capillary tube as subcooled liquid and initially experiences a linear pressure drop due to friction as refrigerant temperature remains constant [23]. Once the non-adiabatic heat exchange region is reached, the refrigerant temperature decreases due to the heat transfer to the suction line side. At a point, pressure drops below the saturation pressure, flashing occurs and vaporisation begins.

Then, the pressure drop decreases rapidly due to two-phase friction and vapour acceleration. The continued pressure drop results in a decreasing saturation temperature. As the flashing keeps on going, the quality of the refrigerant increases until the capillary tube outlet is reached, where a choked condition typically occurs [23].

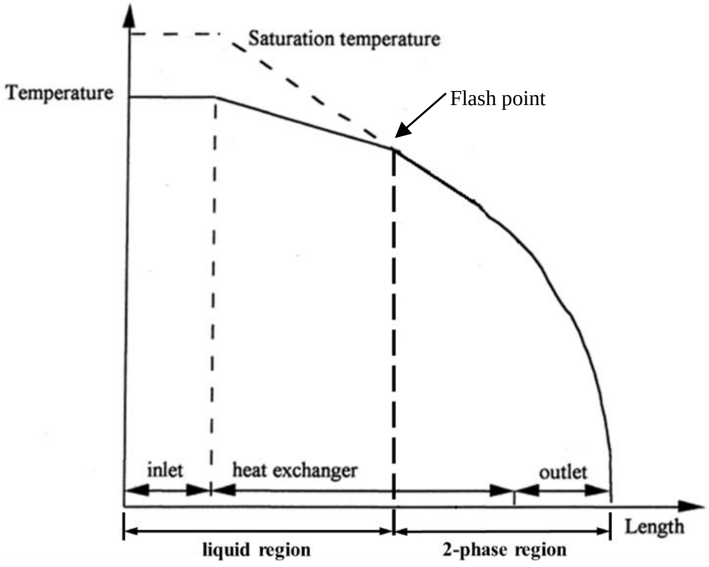

Figure 11: Evolution of refrigerant temperature along the capillary tube, adapted from [13]

Nevertheless, the creation of a metastable length is possible [13], [24]–[26]. Figure 12 illustrates the refrigerant temperature profile along the capillary tube in this case. As explained, when refrigerant temperature crosses the saturation temperature line, flashing flow may occur. However, vaporisation can be delayed, an under pressure of vaporisation is produced, and the liquid becomes superheated. Here, a liquid region exists at pressures below the saturation pressure and refrigerant is in a metastable state because a finite amount of superheat is required for the formation of the first vapour bubble [27].

When this superheated liquid disappears, an equilibrium two-phase region appears and the vaporisation process starts; the first vapour bubble is formed at the flash point and the pressure gradient increases due to both friction and vapour acceleration.

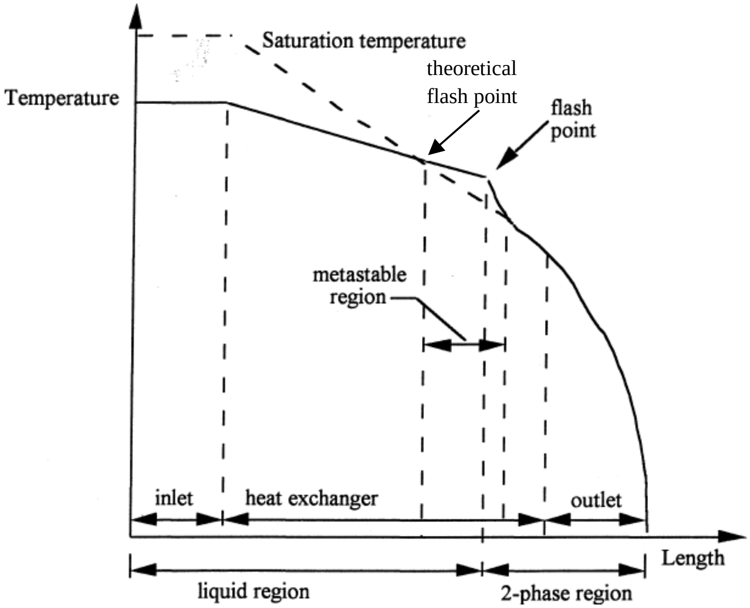
Saturation temperature
theoretical flash point
Temperature
flash point
metastable region
inlet
heat exchanger
outlet
Length
liquid region
2-phase region

Figure 12: Refrigerant flow through capillary tube, adapted from [13]

The existence of a metastable region results in a higher mass flow rate than would otherwise exist under equilibrium conditions [13], [24], [26], [27], because total liquid length increases and reduces two phase length. The overall flow resistance is reduced, thereby, mass flow rate is higher. Li et al. [28] showed that metastable behavior increases for longer capillary tube or lower capillary tube diameter.

1.3.4 Parameters influencing the mass flow rate

1.3.4.1 Geometric variables and operating conditions

Table 1 to Table 5 present a literature review of the different geometric parameters that influence the refrigerant mass flow rate. Each table provides a list of works including a summary, the refrigerant used, type of the study and tests conditions for each work.

The most influencing parameter is the capillary tube inlet diameter (Table 1). The larger the capillary tube diameter the higher the mass flow rate due to smaller frictional effects.

The mass flow rate decreases when the capillary tube total length (Table 2) increases from the increase of frictional resistance.

With an increase in the heat exchange length (Table 3), the refrigerant mass flow rate rises due to the increased heat transfer between the capillary tube and suction line. Indeed, the higher the heat transfer, the larger the volume of capillary tube occupied by subcooled liquid, and the higher the mass flow rate.

An increase in the capillary tube inlet length (Table 4) tends to diminish the refrigerant mass flow rate, but in an insignificant proportion. The same scenario occurs with the suction line inlet diameter (Table 5), which does not significantly influence flow rate.

Table 6 to Table 9 present a literature review of the different operating conditions that influence the refrigerant mass flow rate.

The mass flow rate significantly increases with the augmentation of the capillary tube inlet pressure (Table 6).

An increase in the inlet subcooling (Table 7) results in an increase in the length of the subcooled liquid region and a delay in the flashing point. As a result, overall flow resistance is reduced and mass flow rate increases.

Conversely, an increase in the evaporator superheat (Table 8) leads to a decline in mass flow rate because of the increase in suction line temperature and thus, a decrease in heat transfer.

Suction inlet pressure (Table 9) has a minor impact on the mass flow rate when choked flow conditions are present at the capillary tube outlet, which is typically the case.

Table 1: Review of CT-LSHX increase diameter effect on refrigerant mass flow rate

Authors	Refrigerant	Study type	Tests conditions	Comments
Liu and Bullard [13]	R134a	Experimental/ Numerical	Ø$_{cap}$= {0.0291 in; 0.032 in;0.0362 in;0.039}	The larger the Øcap the higher the mass flow rate, the lower the underpressure of vaporisation, and the shorter the length of the metastable flow in the single-phase liquid
Bittle [25]	R134a R152a R12	Experimental	Ø$_{cap}$ = {0.026 in;0.031in}	Empirical correlation in which the Øcap increase is the not the most influencing parameter, calculated effect of Øcap increase : +5.06 lbm/hr
Mendonca et al. [29]	R134a	Experimental	Ø$_{cap}$= {0.61 mm;0.83 mm}	Increase of refrigerant mass flow rate from 1.94kg/h to 5.44 kg/h when Øcap is larger. Flash point location not affected
Wolf and Pate [23]	R134a, R22 R410a, R600a R152a	Experimental	Ø$_{cap}$= {0.026 in; 0.031 in;0.034 in;0.039 in;0.042 in}	Empirical correlation to predict the mass flow rate which increase of around 50% from the lower to the larger Øcap tested
Melo [30]	R600a	Experimental	Ø$_{cap}$= {0.553 mm;0.776 mm}	Empirical correlation to predict the mass flow rate which increases dramatically with Øcap
Dirik [31]	R134a	Experimental	Ø$_{cap}$ = {0.66 mm;0.8mm}	Increase in mass flow rate for more than 50%

Table 2: Review of CT-LSHX total length increase effect on refrigerant mass flow rate

Authors	Refrigerant	Study type	Tests conditions	Comments
Bittle [25]	R134a R152a R12	Experimental	L_{cap}= {96 in;130 in}	Calculated effect of L_{HX} increase: -1.8 lbm/hr
Wolf and Pate [23]	R134a R22 R410a R600a R152a	Experimental	L_{cap}= {80 in;105 in;130 in;155 in; 180 in}	Empirical correlation to predict the mass flow rate which decreases of 25% from the minimum to the maximum L_{cap} due to additional frictional resistance
Melo [30]	R600a	Experimental	L_{cap}= {3 m;4 m}	Empirical correlation to predict the mass flow rate which decreases with the increase of L_{cap}, third most influencing parameters on mass flow rate after inlet pressure and $Ø_{cap}$

Table 3: Review of CT-LSHX heat exchange length increase effect on refrigerant mass flow rate

Authors	Refrigerant	Study type	Tests conditions	Comments
Bittle [25]	R152a	Experimental	L_{HX}= {40 in;70 in}	Calculated effect of L_{HX} increase : +0.20 Ibm/hr. The increase in heat exchange length is directly related to an increase in heat transfer area, and thus, heat transfer rate
Wolf and Pate [23]	R134a R22 R410a R600a R152a	Experimental	L_{HX}= {20 in;40 in;60 in;80 in; 100 in}	Higher mass flow rate (+14%) due to the increased liquid length created by the increased contact of both the capillary tube and the suction line
Melo [30]	R600a	Experimental	L_{HX} = {1 m;2.2 m}	Empirical correlation to predict the mass flow rate which increases with the increase of L_{HX}

Table 4: Review of CT-LSHX inlet length increase effect on refrigerant mass flow rate

Authors	Refrigerant	Study type	Tests conditions	Comments
Bittle [25]	R134a R152a R12	Experimental	L_{in}= {6 in;20 in}	Calculated effect of L_{in} increase: -0.14 Ibm/hr
Mendonca et al. [29]	R134a	Experimental	L_{in}= {1.1 m;2.3 m}	Refrigerant mass flow few affected (1.94 kg/h to 1.77 kg/h) but capillary tube flow pattern very affected: flashing point moves downward when L_{in} increases
Wolf and Pate [23]	R134a R22 R410a R600a R152a	Experimental	L_{in}= {6 in; 15 in;24 in}	Not significant parameter in the empirical correlation
Melo [30]	R600a	Experimental	L_{in}= {0.6 m;0.2 m}	Few significant parameter in the empirical correlation

Table 5: Review of CT-LSHX suction diameter increase effect on refrigerant mass flow rate

Authors	Refrigerant	Study type	Tests conditions	Comments
Bittle [25]	R134a R152a R12	Experimental	Ø$_{suct}$= {0.201 in;0.319 in}	Calculated effect of Ø$_{suct}$ increase: +0.08 Ibm/hr
Wolf and Pate [23]	R134a R22 R410a R600a R152a	Experimental	Ø$_{suct}$ = {0.194 in; 0.2565 in;24 in}	Not significant parameter in the empirical correlation
Melo [30]	R600a	Experimental	Ø$_{suct}$= {0.201 in;0.319 in}	Not significant parameter in the empirical correlation

Table 6: Review of CT-LSHX pressure inlet increase effect on refrigerant mass flow rate

Authors	Refrigerant	Study type	Tests conditions	Comments
Bittle [25]	R134a R152a R12	Experimental	T_{cond} = {85 ºF; 132 ºF}	Most influencing parameter on mass flow rate that increases of +6.48 lbm/hr
Mendonca et al. [29]	R134a	Experimental	p_{in} = {9 bar;14 bar}	Mass flow rate increase from 1.93 kg/h to 2.58 kg/h Flash point location not affected
Wolf and Pate [23]	R134a R22 R410a R600a R152a	Experimental	p_{in} = {60 to 100 psia} (for R600a)	Empirical correlation to predict the mass flow rate which significantly increases with the increase of p_{in}
Melo [30]	R600a	Experimental	p_{in} = {5 bar to 6.53 bar}	Empirical correlation to predict the mass flow rate which significantly increases with the increase of p_{in}

Table 7: Review of CT-LSHX inlet subcooling increase effect on refrigerant mass flow rate

Authors	Refrigerant	Study type	Tests conditions	Comments
Wolf and pate [23]	R134a R22 R410a R600a R152a	Experimental	SC= {5 ºF to 35 ºF} (for R600a)	Empirical correlation to predict the mass flow rate which increases when SC increases because of the longer liquid length in the capillary tube
Melo [30]	R600a	Experimental	SC= {5 K to 10 K}	Empirical correlation to predict the mass flow-rate which increases when SC increases
Bittle [25]	R134a R152a R12	Experimental	SC = {5 ºF to 10 ºF}	Calculated effect of SC increase: +0.24 Ibm/hr

Table 8: Review of CT-LSHX evaporator superheat increase effect on refrigerant mass flow rate

Authors	Refrigerant	Study type	Tests conditions	Comments
Bittle [25]	R134a R152a R12	Experimental	SH = {5 ºF to 10 ºF} (for R134a)	Calculated effect of SH increase: -0.56 Ibm/hr
Wolf and pate [23]	R134a R22 R410a R600a R152a	Experimental	SH= {5 ºF to 45 ºF} (for R600a)	Empirical correlation to predict the mass flow rate which decreases when SH increases because of the reduction of the heat exchange effect

Table 9: Review of CT-LSHX suction inlet pressure increase effect on refrigerant mass flow rate

Authors	Refrigerant	Study type	Tests conditions	Comments
Wolf and Pate [23]	R134a R22 R410a R600a R152a	Experimental	p_{suct} = {10 to 21 psia} (for R600a)	Critical flow at the exit of the capillary tube so p_{suct} did not affect the mass flow rate
Bittle [25]	R134a R152a R12	Experimental	p_{suct} = {19 psia; 24 psia}	Calculated effect of p_{suct} increase: -0.4 Ibm/hr

1.3.4.2 Lubricant oil

To the authors knowledge, there is no work related to the effect of oil in the refrigerant circuit of a household refrigerator.

That said, using a test bench filled with R134a, Bittle [25] studied the effect of 3% oil concentration (by mass) and calculated that the mass flow rate would rise by 0.12 lbm/hr, a level he judged as not significant for his empirical equation prediction of mass flow rate.

Wolf and Pate [23] performed tests with R134a mixing with different esther oil concentrations. For a 1.5% oil concentration (by mass), the authors observed a decline in the refrigerant mass flow rate by around 8.5% and 10% for 4.7% oil concentration, a level they considered statistically significant.

1.3.4.3 Refrigerant charge

The higher the refrigerant charge, the higher the mass flow rate [5], [9], [10]. Capillary tube selection is a fair trade between refrigerant charge and capillary tube geometric parameters to minimise energy consumption of the refrigerator.

Boeng and Melo [9] conducted an experimental study to identify the optimal combination of refrigerant charge and a capillary tube in a refrigerator-freezer equipped with R600a. To vary the expansion device capacity (capillary length + capillary diameter), the authors used a metering valve in series with a capillary tube with a larger internal diameter than the original one. A maximum COP can be found for a given valve opening degree when varying the refrigerant charge. The higher the valve opening degree (and thus, the higher the capillary tube diameter), the lower the refrigerant charge required to reach the system maximum COP.

Björk and Palm [10] used a single door and compartment refrigerator filled with R600a and varied the expansion device capacity of a capillary tube with a needle valve set up at the inlet of a capillary tube. The authors found that the energy consumption had a minimum for certain combinations of expansion device capacity and refrigerant charge.

Hermès et al. [32] used a dynamic model to assess the influence of capillary tube parameters and refrigerant charge. These authors found a deviation of ±10% in the experimental data, according to the model. The findings demonstrate that the energy consumption of a frost-free refrigerator working with R134a can be reduced by 8% by changing the original capillary tube inner diameter, heat exchange capillary tube length and refrigerant charge.

1.3.5 Problems and consequences of using CT-LSHX

Due to simultaneous two-phase flow expansion and heat transfer, CT-LSHX introduces complex phenomena such as reverse heat transfer and recondensation [18]. Some of the negative consequences of these phenomena are noise [12], which is becoming an important quality issue; flow hysteresis and flow oscillations and reduction of the CT-LSHX effectiveness [13].

1.3.6 Recondensation and reverse heat transfer

In the heat exchange region, when the heat transferred to the suction line is sufficient, two-phase refrigerant in the capillary tube can lead to recondensation of the refrigerant vapour [18], as illustrated in Figure 13.

When the refrigerant flows into the capillary tube-suction line heat exchange region, it loses heat to the suction line side, as described section 1.3.3. The quality decreases and, sometimes, the refrigerant can be in a complete condensation state. As a result, refrigerant quality may reduce to zero and the recondensation phenomenon occurs, as illustrated in Figure 14.

If the heat exchanger region lengthens, the heat transfer increases [18]. For this reason, the temperature of the suction line may be higher than that of the capillary tube at the end of the heat exchanger region (Figure 15). As a result, the heat begins to transfer from the suction line to the capillary tube via a process known as a reverse heat transfer, as illustrated in Figure 16.

Bansal and Yang [18] concluded that a longer heat exchanger length, approximately 60% of total length, is responsible for the reserve heat transfer.

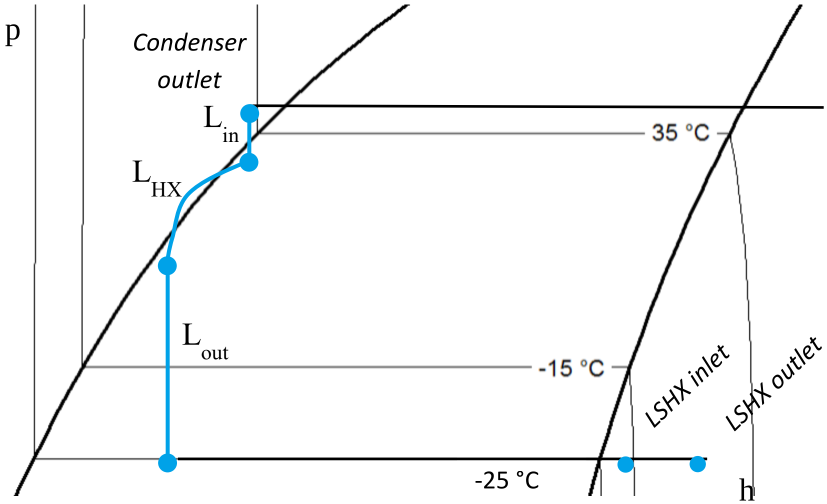
p
Condenser outlet
L_{in}
L_{HX}
L_{out}
35 °C
-15 °C
-25 °C
LSHX inlet
LSHX outlet
h

Figure 13: Pressure-enthalpy diagram of recondensation phenomenon in CT-LSHX

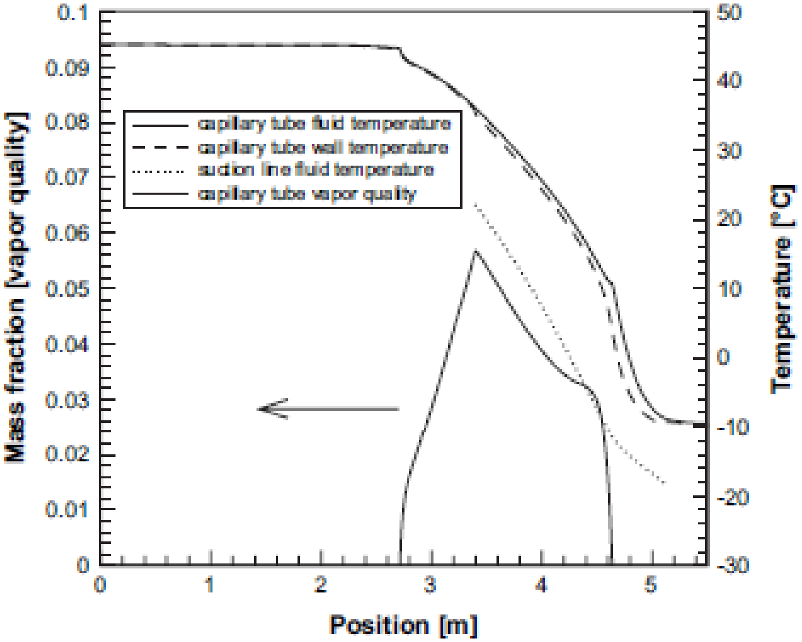

Figure 14: Example of recondensation phenomenon [33]

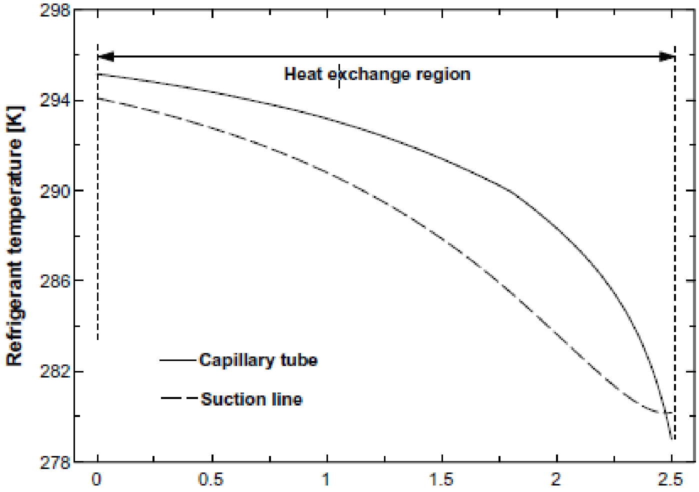

Figure 15: Example of reverse heat transfer [18]

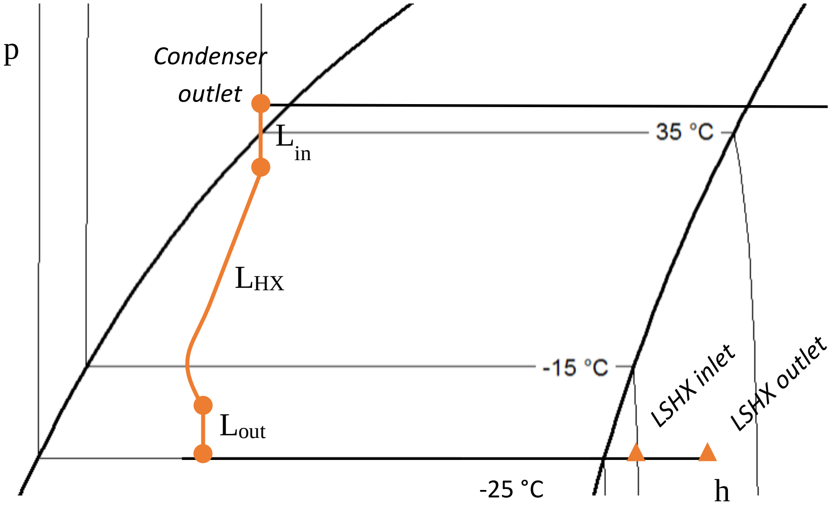
p
Condenser outlet
L_{in}
35 °C
L_{HX}
-15 °C
LSHX inlet
LSHX outlet
L_{out}
-25 °C
h

Figure 16 : Pressure-enthalpy diagram of reverse heat transfer phenomenon in CT-LSHX

1.3.7 Flow hysteresis

Flow hysteresis is a consequence of reverse heat transfer and recondensation. Meyer and Dunn [26] have demonstrated a hysteresis effect of mass flow rate when it is plotted as subcooling increasing and decreasing. For the same level of subcooling, a variation of almost 10% in the mass flow rate measurement is observable.

Liu and Bullard [13] repeated these experiments with CT-LSHX and observed similar hysteresis (Figure 17) and highlighted the non-repeatability of this hysteresis effect, noting that such hysteresis could introduce control instabilities in refrigerators equipped with variable speed compressors. The authors emphasise that the effect on COP could be as large as 6% (Figure 18).

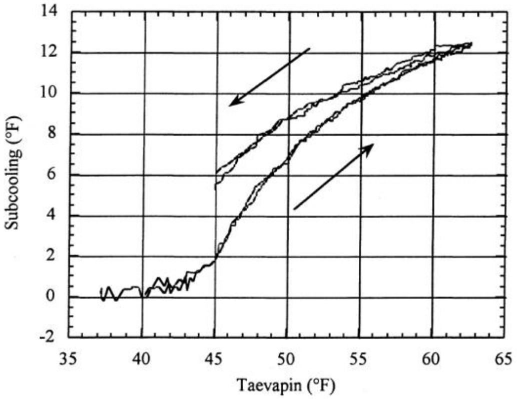

Figure 17: Hysteresis effect of mass flow rate versus subcooling [13]

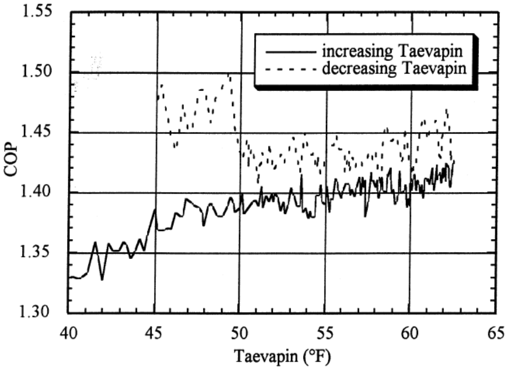

Figure 18: Hysteresis effect of COP [13]

1.3.8 Noise

Another possible consequence of recondensation is noise. It occurs when a refrigerant vapour bubble in the capillary tube is surrounded by subcooled liquid and kept colder than the vapour. This temperature difference allows the vapour to reject heat to the liquid and condense. As the vapour condenses, the bubble volume decreases and, if this volume reduction is sufficiently high, the bubble implodes and shockwaves are created [12].

Hartmann and Melo [12] explains that after compressor start-up, there is a substantial amount of liquid refrigerant in the evaporator. An important amount of cold liquid through the suction line is moved due to the pressure drop induced by the compressor start up. The vapour bubbles inside the capillary tube quickly lose heat producing even the recondensation phenomenon (See section 1.3.6). When recondensation takes place, the bubbles in the capillary tube collapse and generate shockwaves.

According to Hartmann and Melo [12], the shockwaves that move to the condenser encounter other pockets of vapour and are dissipated; however, those that proceed to the evaporator encounter no restrictions, excite it and generate noise. The authors used an accelerometer to measure vibration induced by the refrigerant flow in the heat exchanger region (Figure 19), where the peaks indicate when the noise is produced.

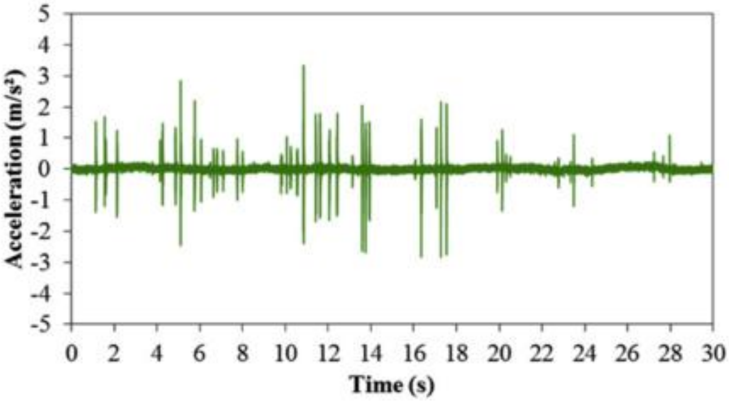

Figure 19: Acceleration profile of the refrigerant flow [12]

1.4 The importance of subcooled conditions

A consequence of an absence of liquid at the condenser outlet is a loss of global efficiency due to the reduction of cooling capacity given the same compression work.

Another benefit of getting subcooling in systems with CT-LSHX is avoiding the noise issue previously reported (section 1.3.8). Hartmann and Melo [12] solved the noise problem by adding an internal heat exchanger at the condenser outlet, ensuring a certain level of subcooling at the capillary tube inlet and avoiding the entrance of vapour (Figure 20). This subcooling helps to avoid recondensation because the liquid is further from the saturation line during the heat exchange region, and therefore prevents from noise.

An alternative and quite simple solution is to place the heat exchange length of the capillary tube inmmediatly after the filter, reducing therefore the inlet adiabatic length as much as possible. Liu and Bullard [13] observed flow oscillations in experimental data only for subcooling inferior to 5 K, and demonstrated that the hysteresis effect was higher for lower subcooling. Furthermore, these authors found that the CT-LSHX effectiveness decreased with a subcooling decrease (Figure 21). Surprisingly, however, by developing a model based on experimental data, the CT-LSHX effectiveness was almost not affected by an increase in vapour quality from 2% to 10% at the capillary tube inlet. Liu and Bullard [13] proposed that the two-phase frictional pressure drop determines the temperature difference for the heat exchanger. Higher inlet quality produces a greater temperature drop, and therefore, a greater temperature difference near the suction line inlet. As a result, the suction line outlet temperature is higher due to the increased heat transfer.

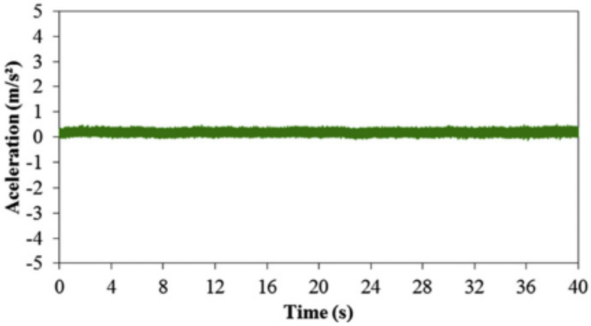

Figure 20: Acceleration profile with additional heat exchanger at the condenser outlet [12]

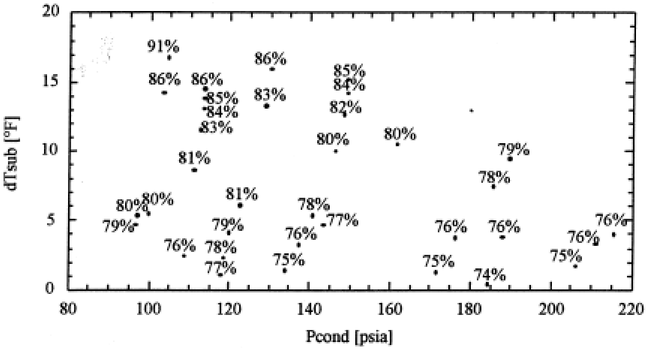

Figure 21: Effectiveness for different operating conditions with respect to subcooling [13]

Wolf and Pate [23] tested different quality levels for refrigerants R600a, R22, R134a and R410a in a wide range of operating conditions. For R600a, the mass flow rate dropped of 55% between two operating points of 5.9% and 12.5% quality, respectively.

Bittle [25] measured a decrease of about 13% in mass flow rate when the quality inlet conditions increased from 0% to 5% for R134a.

1.5 What are the actual conditions at the capillary tube inlet?

Some works conclude that the subcooled conditions at the capillary tube inlet may not be real, which, if true, would mean that there is a room for efficiency improvement and, more generally, energy consumption.

As mentioned, Boeng and Melo [9] performed an experimental study to identify the optimal combination of refrigerant charge and capillary tube by varying the expansion device capacity. These researchers then complemented this work by applying a model [21] to examine correlations between degree of valve opening and the equivalent capillary diameter. This study revealed a good prediction of the mass flow rate, except for tests with fully open valves or subcooling of less than 5 K. By visualisation of the capillary tube inlet, the authors concluded that even with a subcooling of 5 K, two-phase flow was present at the inlet. As a possible explanation, Boeng and Melo highlight that at the capillary inlet, there was a non-equilibrium mixture of subcooled liquid and saturated vapour instead of a purely liquid phase. Findings also revealed that the vapour quality at the capillary tube inlet ranged from 2% to 12%, depending on the refrigerant charge.

Lee et al. [16] visualised a two-phase refrigerant flow at the inlet of the capillary tube of a commercial refrigeration system working with isobutane. These researchers set up a transparent tube at the condenser outlet and an oil separator at the compressor discharge, and measured both the vapour and liquid temperatures, as the condensation pressure. This study revealed that the refrigerant was in a non-equilibrium state where both subcooled liquid and subcooled vapour coexisted at the capillary tube inlet. The authors subsequently proposed a method to calculate the enthalpy for non-equilibrium refrigerant conditions and could estimate the vapour quality for different condensing pressures ranging from 2.44% to 4.29% at the condenser outlet.

Ko and Jeong [17] complemented previous work by studying the effect of a non-equilibrium subcooled two-phase flow on the performance of a vapour compression refrigeration system. The authors estimated that the COP may be overestimated by 19.4% if the thermodynamic properties table is used, which implicitily assumes equilibrium, for a refrigerant non-equilibrium state.

Using X-ray equipment, Inan et al. [15] visualised the filter, accumulator at the evaporator outlet, and section at the evaporator inlet in a refrigerator-freezer equipped with R134a. This study clearly identified fully liquid conditions at the capillary tube inlet and, within a few minutes after compressor start-up, the filter was completely full of liquid. The value of subcooling was 5 K when quasi-steady conditions were reached.

A reason for this difference observed by Inan et al. [15] and other authors [9], [16] could be due to running the system with different refrigerant mass flow rates and using different refrigerants.

Various explanations are thus provided to explain the presence of two-phase flow at the capillary tube inlet. As stated by Lee et al. [16], an explanation of the presence of vapour, although a certain subcooling is measured, is the non-equilibrium state of the refrigerant composed of subcooled liquid and subcooled vapour. Whereas Boend and Melo propose non-equilibrium between saturated vapour and subcooled liquid.

1.6 Objectives and structure of the work

The main objectives of this thesis are first, to determine a fundamental explanation of actual conditions at the capillary tube inlet of a household refrigerator system and second, improve apparatus design to ensure required subcooling and continuously provide liquid at the capillary tube inlet. To achieve these goals, this work has been structured as follows:

First, a review of the literature in CT-LSHX was carried out, which reveals that subcooled conditions at the capillary tube inlet may not be real, and thus, there is a possibility to improve energy consumption of household refrigerators.

Chapter 2 focuses on visualisations of the condenser outlet and capillary tube inlet to examine the actual conditions of the refrigerant at the capillary tube inlet by designing an innovative test bench based on a household refrigerator.

To determine conditions at the capillary tube inlet, chapter 3 provides an assessment of refrigerant conditions at the condenser outlet, and therefore, at the capillary tube inlet, by modifying the previous test bench.

Chapter 4 describes the design improvement implemented to obtain fully liquid conditions at the capillary tube inlet.

Finally, chapter 5 presents a performance comparison between both the original and improved design.

Chapter 2

Visualisation of the refrigerant flow at the capillary tube inlet of a household refrigerator

2.1 Objectives

This chapter focuses on visualisations of the condenser outlet and capillary tube inlet of a household refrigerator to examine actual conditions of the refrigerant at the capillary tube inlet. Several filter positions were tested, as well as different lengths of the capillary tube within the filter to investigate the effect of orientation on the flow pattern at the condenser outlet and capillary tube inlet.

2.2 Experimental set up

2.2.1 Original apparatus

The original apparatus was a Siemens high-efficiency refrigerator-freezer. A general description of the original apparatus is presented in Table 10.

Table 10: General description of the original apparatus

Refrigerator type	High efficiency 2 doors no frost refrigerator–freezer
Energy consumption	0.48 kWh day^{-1}
Energy class	A+++
Refrigerator cabinet volume	211 l
Freezer cabinet volume	86 l
Refrigerant	R600a
Refrigerant original charge	50 g

The following tables describe the different component of the refrigerator following the refrigerant flow. For each component, the red element on the schema indicates the described item.

Table 11 presents the hermetic reciprocating compressor used in the appliance.

Table 12 presents the original tubes and wire condenser data.

After passing through the frame heater, the refrigerant enters the drier filter and capillary tube (Table 13).

Then the refrigerant enters the evaporator (Table 14).

Table 11: Compressor data

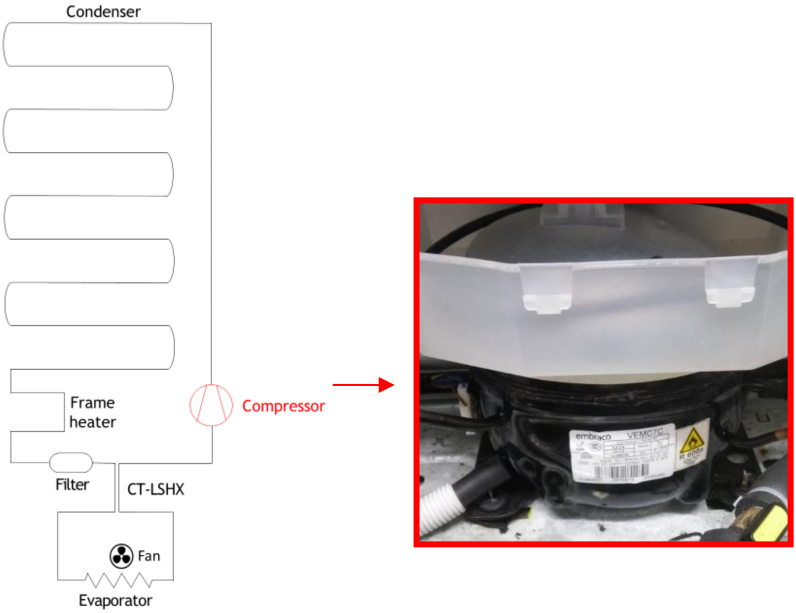
Condenser
Frame heater
Compressor
Filter
CT-LSHX
Fan
Evaporator
embraco
VEMC7C
R 600a

Type	Hermetic reciprocating
Brand/Model	Embraco VEMC7C
Displacement	7 cm^3
Range of speed	1400 rpm to 4500 rpm

Table 12: Condenser data

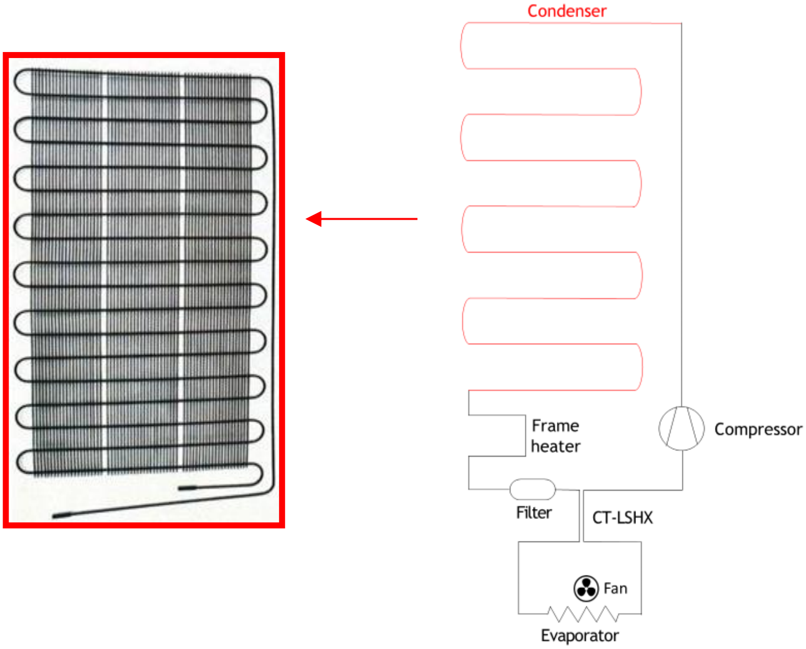
Condenser
Frame
heater
Compressor
Filter
CT-LSHX
Fan
Evaporator

Type	Tube and wires
Tube and wire material	Steel
Exterior tube diameter/thickness	4.75 mm/0.7 mm
Width	444.5 mm
Total tube length	13.3 m
Transversal spacing	50 mm
Wire diameter	1.3 mm
Wire pitch	6.75 mm
Convection	Free

Table 13: Capillary tube and filter data

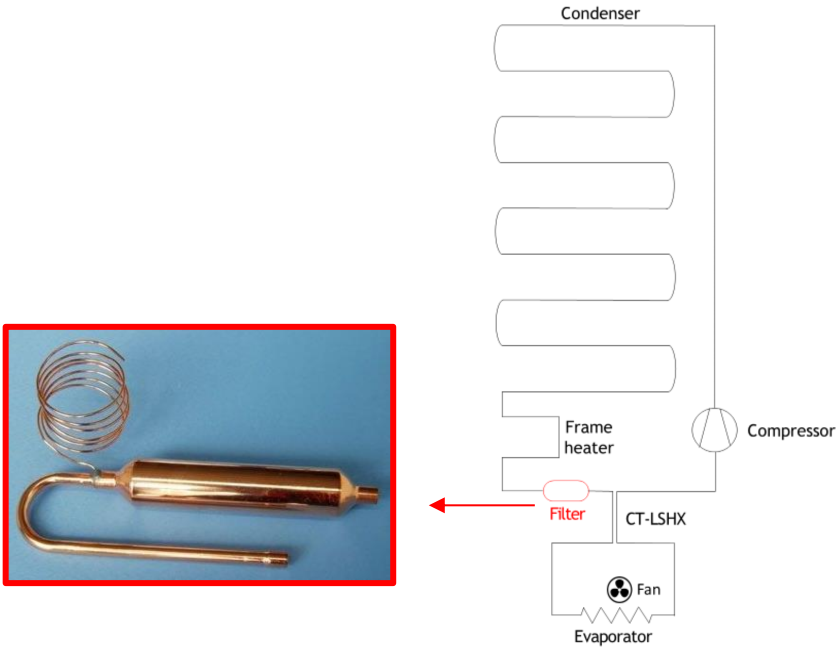
Condenser
Frame heater
Compressor
Filter
CT-LSHX
Fan
Evaporator

Filter	
Body material	Copper
Desiccant material	Zeolite balls
Capillary tube	
Type	LSHX
Material	Copper
Diameter	0.6 mm
Total length	2.44 m
Heat exchange length	1.3 m

Table 14: Evaporator data

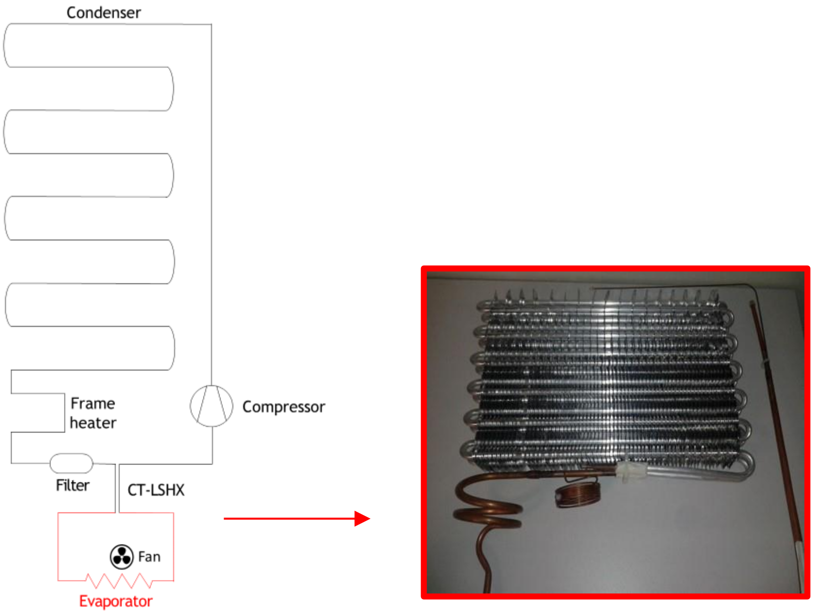
Condenser
Frame heater
Compressor
Filter
CT-LSHX
Fan
Evaporator

Type	Fin and tube
Tube and fin material	Aluminium
Exterior tube diameter/thickness	8 mm / 0.7 mm
Width	330 mm
Longitudinal spacing	19 mm
Transversal spacing	22 mm
Fin thickness	0.17 mm
Fin pitch	8.75 mm
Convection	Forced convection with a fan supplied with continuous voltage of 7V or 9V
No frost	Yes, resistance of 200 W

2.2.2 Modifications of the original apparatus

2.2.2.1 Refrigerant circuit

The refrigerant circuit was carefully modified so as to not add unnecessary extra length nor alter the original working of the apparatus. The frame heater was moved from the condenser outlet to the compressor outlet to visualise the condenser outlet.

The original condenser was modified by removing 1.5 m from the original length, which was replaced by a transparent tube to visualise the refrigerant flow (Table 15).

The original capillary tube was replaced by an experimental facility, comprised of three identical capillary tubes, to test different filter drier positions. The filter drier was modified to a transparent tube of PFA filled with zeolite balls (Table 16).

Each capillary tube was connected to a different transparent filter placed at the capillary tube inlet, as per the original configuration. Two filters were in vertical positions, but with opposite flow directions, while the third was horizontally oriented, to investigate the effect of orientation on the flow patterns at the condenser outlet and capillary tube inlet. A valve at the inlet of each filter made it possible to select the capillary tube and filter to be tested.

Each capillary tube was wrapped around the suction line, as depicted in Figure 22. Both the original length and diameters of the three capillary tubes were maintained. However, the length of the capillary tube within the filter could be varied (see Table 17).

This set of capillary tubes, filters, and valves was installed in the capillary test section (Figure 23), which was insulated accordingly.

Table 15: Condenser modification

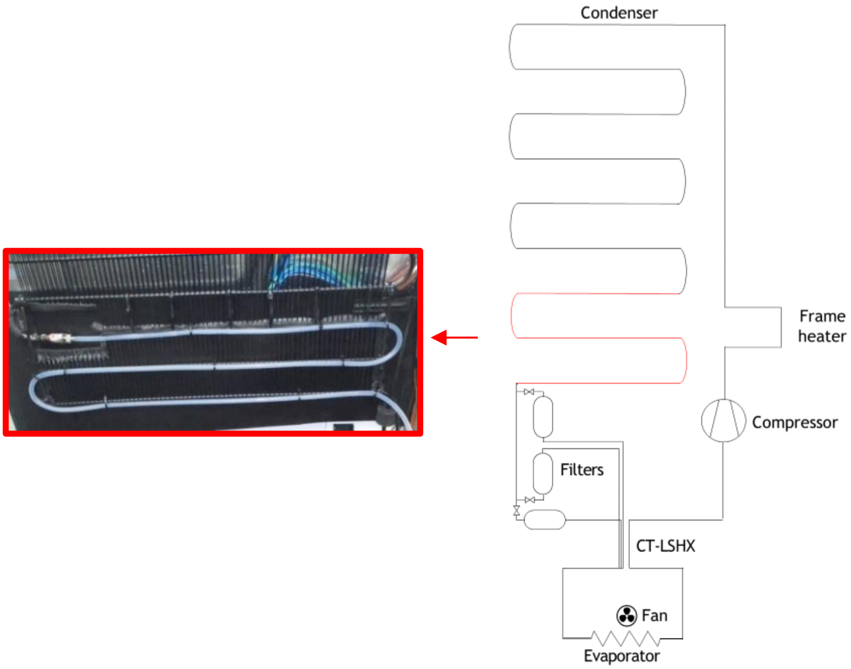
Condenser
Frame heater
Compressor
Filters
CT-LSHX
Fan
Evaporator

Material	PFA
Tube and wire material	steel
Exterior/interior tube diameter	6 mm/4 mm
Transparent tube length	1.5 m

Table 16: Filter modification

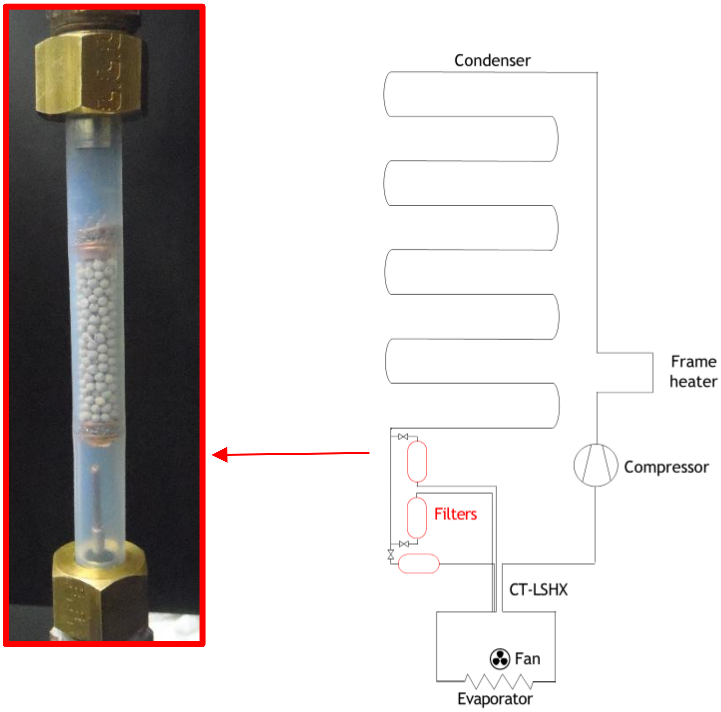
Condenser
Frame heater
Compressor
Filters
CT-LSHX
Fan
Evaporator

Material	PFA
Internal/external diameter	9/12 mm
Total transparent length	130 mm
Zeolite balls length	75 mm

Table 17: Capillary tube modification

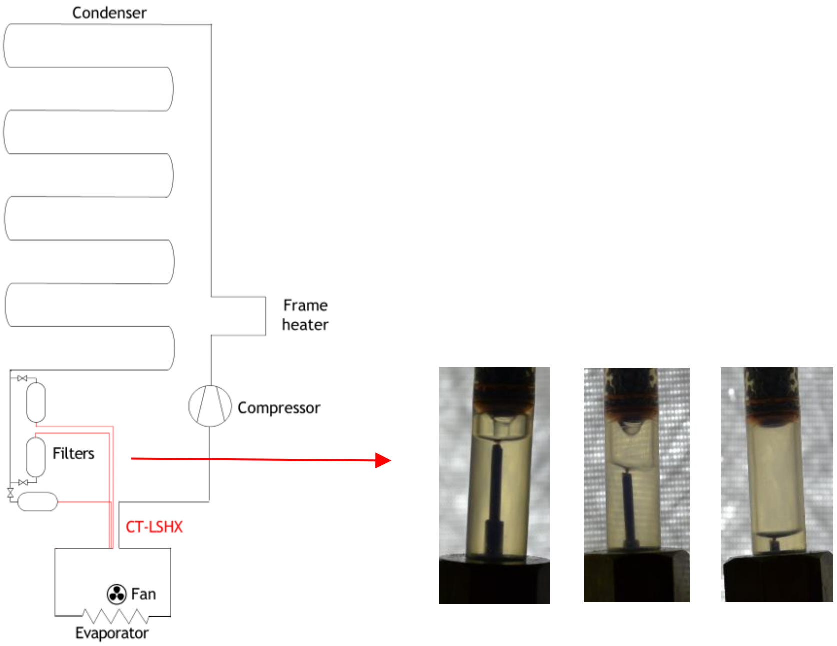
Condenser
Frame heater
Compressor
Filters
CT-LSHX
Fan
Evaporator

Type	LSHX
Diameter	0.6 mm
Total length	2.44 m
Length of capillary tubes within the filter	variable
Heat exchange length	1.3 m

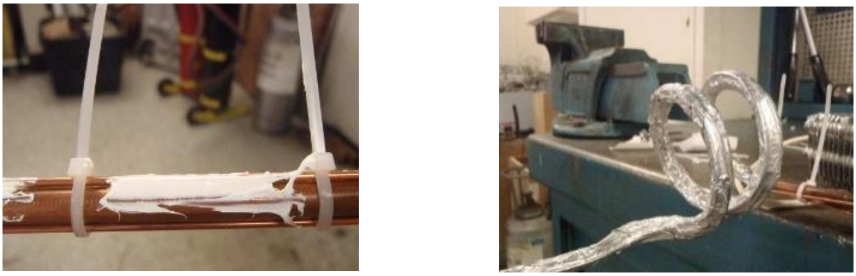

Figure 22: Set up of the three capillary tubes around the suction line

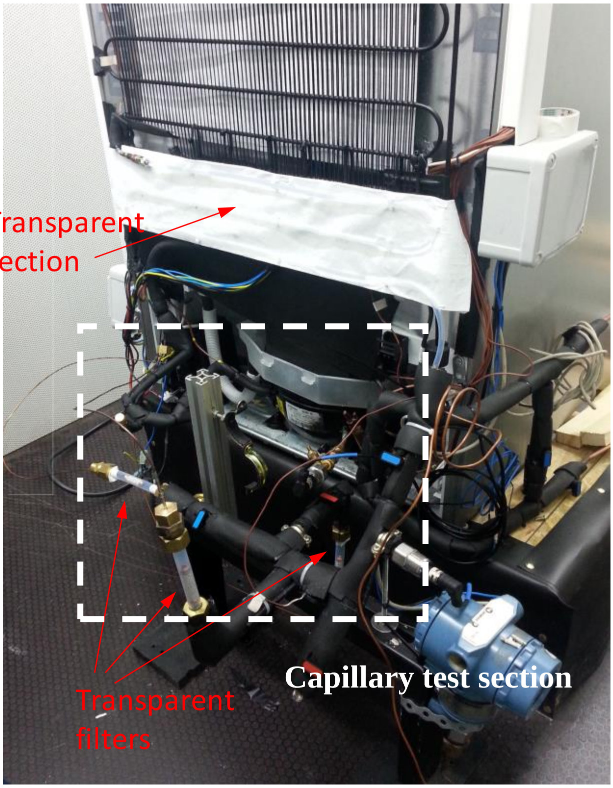
Transparent section
Capillary test section
Transparent filters

Figure 23: Visualisation test bench

2.2.2.2 Instrumentation

i. Pressure and temperature measurements

Figure 24 illustrates the location of the pressure and temperature instrumentations set up along the refrigerant circuit.

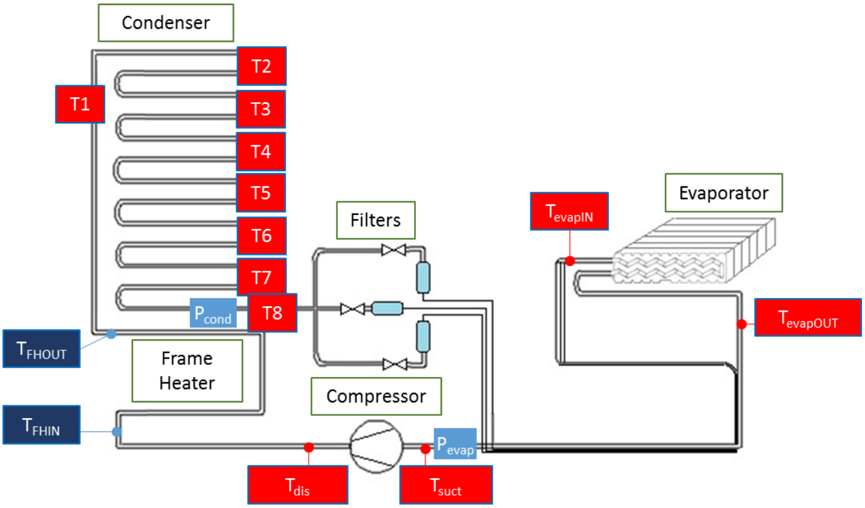
Condenser
T1
T2
T3
T4
T5
T6
T7
T8
P_{cond}
T_{FHOUT}
Frame Heater
T_{FHIN}
Filters
Compressor
T_{evapIN}
Evaporator
$T_{evapOUT}$
P_{evap}
T_{dis}
T_{suct}

Figure 24: Refrigerant temperature and pressure measurements location

Condensation and evaporation pressures were measured with two pressure transducers. The specifications are listed in Table 18. The condensation (respectively, evaporation) pressure transducer was located at the condenser outlet (respectively, evaporator).

Table 18: Evaporation and condensation pressures

Brand	Emerson
Model	PT5-07M
Span	-0.8 to 7 bars
Total accuracy*	± 1% FS (± 0.078 bar)

*includes non-linearity, hysteresis, repeatibility

Table 19 presents the refrigerant circuit temperatures specifications. The thermocouples from T1 to T8 had a lower uncertainty because temperature measurement was compensated for using the reference junction compensation method, which consisted of correcting the voltage signal measured at the desired point by voltage generated at a reference junction placed in an isotherm block where the temperature was measured with an accurate RTD.

Then, thermocouples were calibrated by comparing the temperatures measured with a temperature probe of uncertainty ± 0.2 K in a wide range (0 ºC to 60 ºC). The uncertainty for T1 to T7 presented in Table 19 correspond to the maximum uncertainty observed for this set of thermocouples. Since T8 was used to calculate SC, and more precision was needed, the actual value was given in this case.

Table 19: Refrigerant circuit temperatures

	Location	Thermocouples type	Accuracy
T1 to T7	Condenser	T-Type	±0.3 K
T8	Outlet condenser	Thermowell	±0.2 K
T_{evapIN}	Inlet evaporator	T-Type	±0.5 K
$T_{evapOUT}$	Outlet evaporator	T-Type	±0.5 K
T_{suct}	Inlet compressor	T-Type	±0.5 K
T_{dis}	Outlet compressor	T-Type	±0.5 K

The remaining thermocouples measurement was not compensated for by the voltage of the reference junction. Verification of the proper measurement was performed using the same calibration method described above. The uncertainty corresponds to the maximum temperature difference found between the set of thermocouples.

To confirm that the tests were performed within the same conditions, a set of thermocouples were set up inside the FF and FZ compartments, as depicted in Figure 26. Table 20 presents the thermocouples specifications.

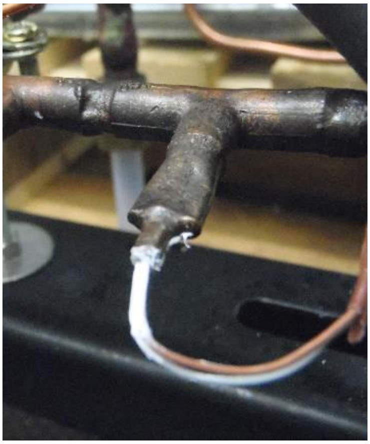

Figure 25: Outlet condenser temperature measurement

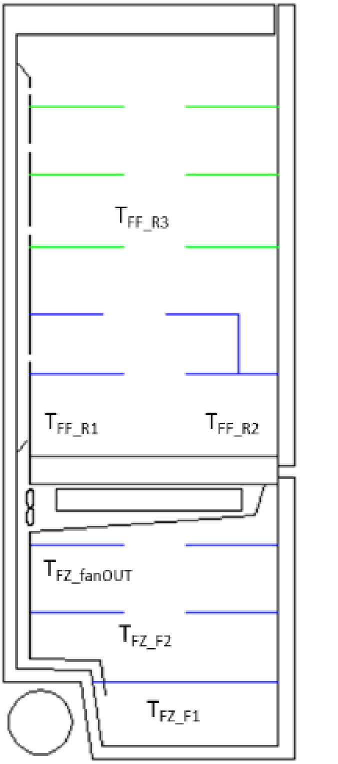
T_{FF_R3}
T_{FF_R1}
T_{FF_R2}
T_{FZ_fanOUT}
T_{FZ_F2}
T_{FZ_F1}

Figure 26: Air FF and FZ temperatures measurement locatio

Table 20: Inside air FF+FZ temperatures

	Location	Thermocouples type	Accuracy
T_{FF_R1} to T_{FF_R3}	FF compartment	T-Type	±0.5K
T_{FZ_F1} and T_{FZ_F2}	FZ compartment	T-Type	±0.5K
T_{FZ_fanOUT}	Fan outlet	T-Type	±0.5K

ii. Data acquisition

Specifications of the data logger used to register temperature, pressure and voltage data are listed in Table 21.

Table 21: Datalogger specifications

Brand	Agilent
Model	34970A
Error for current specifications*	± (0.05% reading + 0.02% of range)
Error for thermocouple type T	±1˚C

*Considers measurement error, switching error, transducer conversion error

iii. Power measurement

Table 22 presents the specifications of the wattmeter used for power measurements.

Table 22: Wattmeter specifications

Brand	Gossen Metrawatt
Model	Energy
Power accuracy	± (0.4% reading + 0.02)
Power accuracy for 30 W	± 0.14 W

iv. Climatic chamber

The experimental apparatus is placed in a climatic chamber (Figure 27) where temperature was regulated with PID.

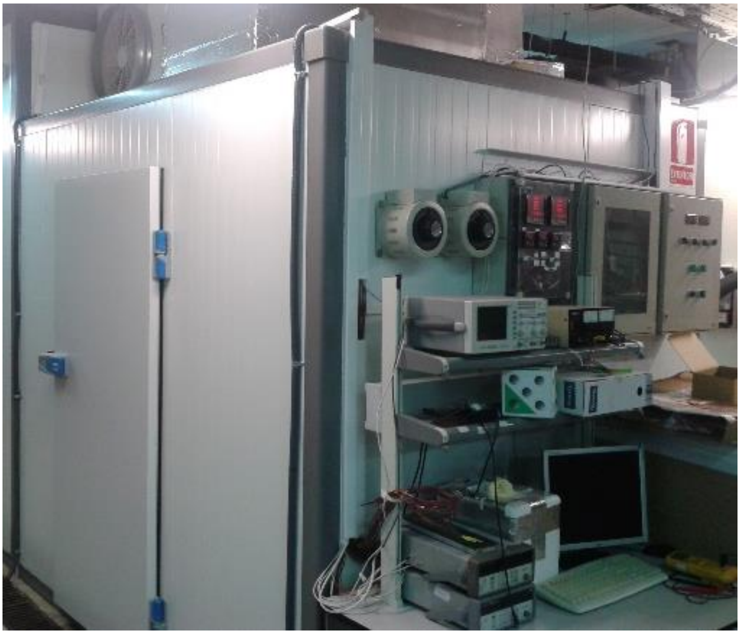

Figure 27: Climatic chamber

2.3 Experimental Campaign

2.3.1 Overall procedure

Due to the piping modification, it was necessary to determine the new optimal charge for the refrigerant. Then, nine different filter and capillary tube configurations were tested, involving three filter orientations, and for each filter, three positions of the capillary tube within the filter to investigate the effect of orientation on the flow pattern at the condenser outlet and capillary tube inlet.

The total capillary tube length was always kept constant.

2.3.2 Refrigerant charge procedure

A special charging setup was designed to charge refrigerant in the test bench so that it was always connected to the main test bench. A pipe connected the bottle of refrigerant to the suction of the compressor. Flow rate could be modified by a metering valve, to slowly and accurately charge the refrigerant circuit, which was incremented by a certain amount of refrigerant per tests. The bottle was placed on a scale of ±0.01 g accuracy during the entire experimental campaign.

2.3.3 Find the optimal charge of refrigerant

For overcharged conditions, refrigerant mass flow rate and pressure ratio increases and thus, the power consumption increases and the cooling capacity decreases. For undercharged conditions, refrigerating capacity is reduced and compressor reliability may be degraded due to high discharge temperatures. Therefore, it is essential to have the optimum amount of charge in the heat pump to ensure high performance operation and high system reliability [9], [10], [34].

The original system, charged with 50 g of R600a, was carefully modified to minimise extra volumes and other modifications that could affect the original performances.

The additional volume mainly came from the liquid side in the capillary tube and filter test section. A first estimation of the extra refrigerant charge required to fill this extra volume returned a result of 10.6 g. The additional volume on the vapour side was negligible since both refrigerant density and extra volume were notably low on this side.

To compensate for the additional volume introduced, a charge study was performed using the same method as household appliance manufacturers to accurately determine the new optimal charge. This parametric study tested different charges at increments of 5 g per test.

The global appliance energy consumption was also analysed for each test. An average of the consumption of five cycles was conducted. The optimal charge minimised energy consumption the most. Test conditions are listed in Table 23.

Table 23: Test conditions for experimental campaign 2.1

Parameter	Configuration
FF average temperature (°C)	4
FZ average temperature (°C)	-20
Climate chamber temperature (°C)	25
Temperature regulation	Electronics
Compressor speed (rpm)	1600
Test type	Dynamics
Capillary tube diameter (mm)	0.6
Filter position	Horizontal
Test aim	Charge study

For the explanation of the overall working of the refrigerator, reader is referred to chapter 1, section 1.2.

Eq. 2.1 presents the energy consumption calculation for one compressor cycle.

$$\dot{W}_{average\_Cycle} = \tau_{compON}(\tau_{dampOFF}\dot{W}_{FZ} + \tau_{dampON}\dot{W}_{FF+FZ}) \qquad 2.1$$

With,

$$\tau_{compON} = \frac{T_3 - T_1}{T_4 - T_1} \qquad 2.2$$

$$\tau_{dampON} = \frac{T_2 - T_1}{T_3 - T_1} \qquad 2.3$$

$$\tau_{dampOFF} = 1 - \tau_{dampON} \qquad 2.4$$

$\dot{W}_{FF+FZ}$ is the average power when the damper was opened.

$\dot{W}_{FZ}$ is the average power when the damper was closed.

Time parameters for Eq. 2.2 to Eq. 2.4 are identified in Figure 28.

τ_{compON} is the ratio of time the compressor was working over the total time cycle (Eq. 2.2).

τ_{dampON} is the ratio of time the damper was opened over the time the compressor was working (Eq. 2.3).

$\tau_{dampOFF}$ is the ratio of time the damper was closed when the compressor was working (Eq. 2.4).

Results are presented on Figure 29, and reveal that the optimal refrigerant charge was between 57.9 g and 67.8 g. Following the trend curve, it was decided the tests should run with 62.5g as the optimal refrigerant charge, even though the average power at this charge seemed higher, perhaps due to measurement uncertainty.

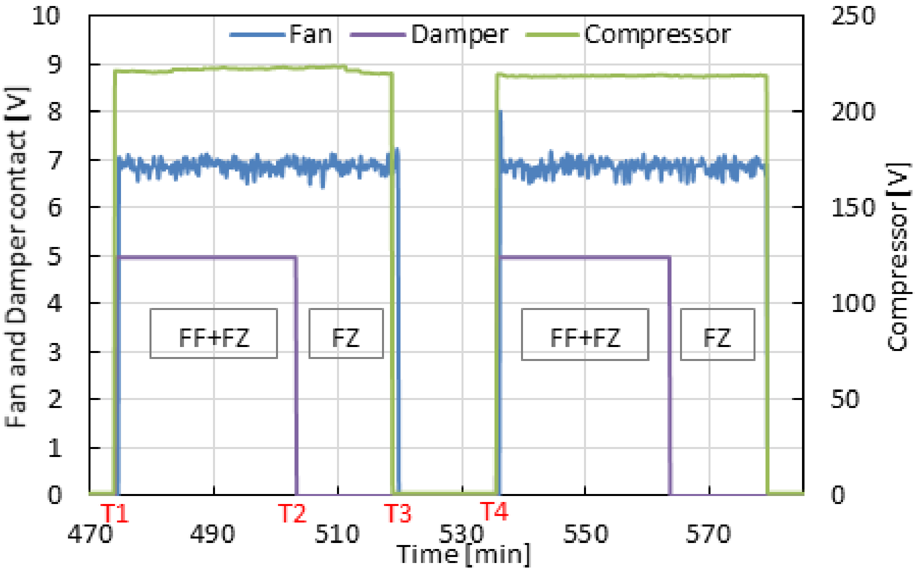

Figure 28: Identification of time parameters for the calculation of the compressor energy consumption during a typical refrigeration dynamic cycle

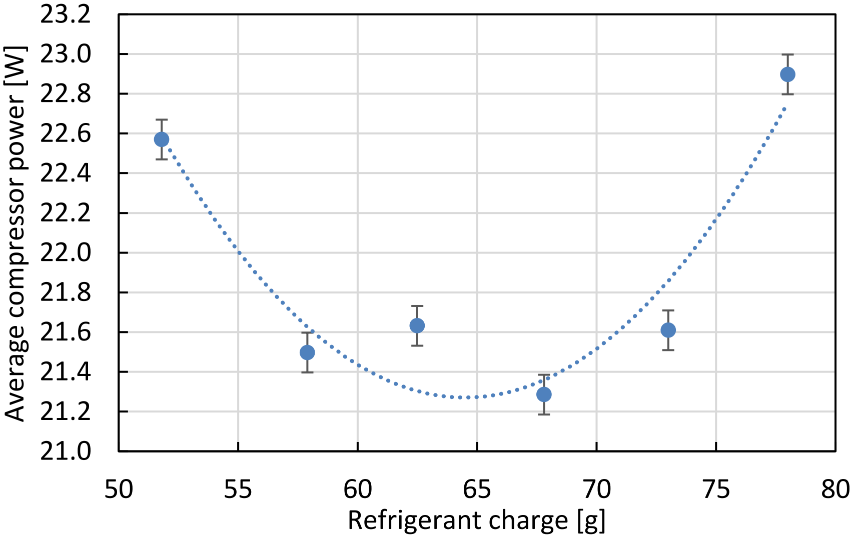

Figure 29: Average compressor power through the refrigerant charge study

2.3.4 Results and discussion

2.3.4.1 Temperature profiles

The condenser temperature profile for the optimal refrigerant charge is presented in Figure 30. Uncertainty of the condensation temperature is ±0.5 ºC. In both operating modes, the saturation temperature (obtained from the outlet condenser pressure) was always slightly higher than the temperature measured by the thermocouples on the wall, where condensation was expected to be present.

Although the thermocouple was highly insulated from the ambient surroundings, this difference could be explained by a certain longitudinal heat conduction and uncertainty of measurements. Figure 30 demonstrates that the temperature value barely changed from T1 to T5, which could be understood as the condenser area where the two-phase flow was present.

The temperature measured by thermocouples T6 to T8 decreased from the value at T5, which suggests that a certain subcooling was present. To study the effect of the refrigerant charge on the condenser temperature profile, a set of tests with different refrigerant charges was carried out. Figure 31 depicts the case with the largest refrigerant charge (73 g). In this case, the analysis of the condenser temperature profile indicated that subcooling began at temperature T4, earlier than in the optimal charge case.

The temperature difference between T5, T6, and T7 became more important until T8 was reached, where the temperature appeared to stop decreasing. This finding could be explained by the temperature almost reaching that of the climatic chamber and thus, no more heat could be exchanged. As expected, the temperature condensation and subcooling were higher than in the optimal charge case.

Figure 32 illustrates the subcooling evolution when the refrigerant charge increased. The reported subcooling was defined as the difference between the saturated temperature and the value of T8 at the last moment before the compressor shut down. The non-linear trend of subcooling could be explained by the uncertainty of the temperature measurements and/or the difficulty of testing at exactly the same operating conditions.

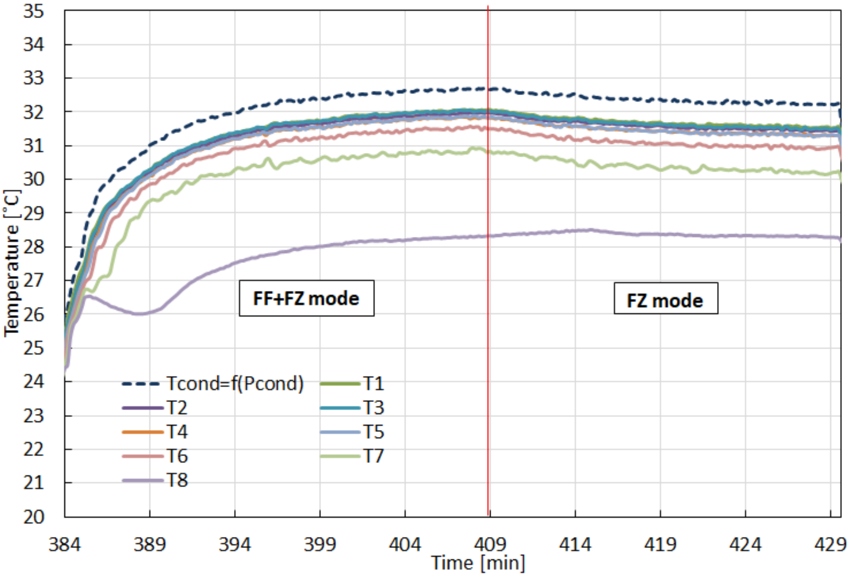

Figure 30: Temperatures along the condenser for optimal refrigerant charge (62.5 g)

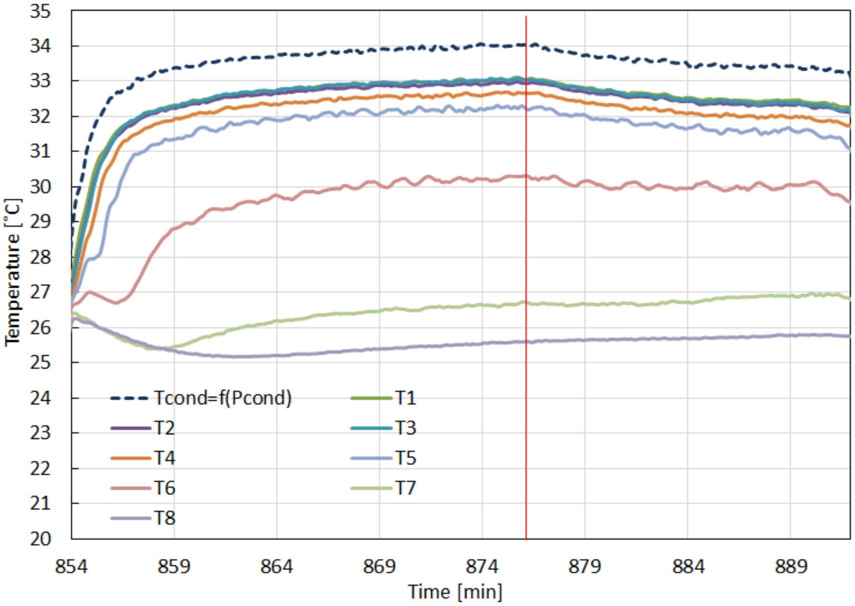

Figure 31: Temperatures along the condenser for 73 g refrigerant charge

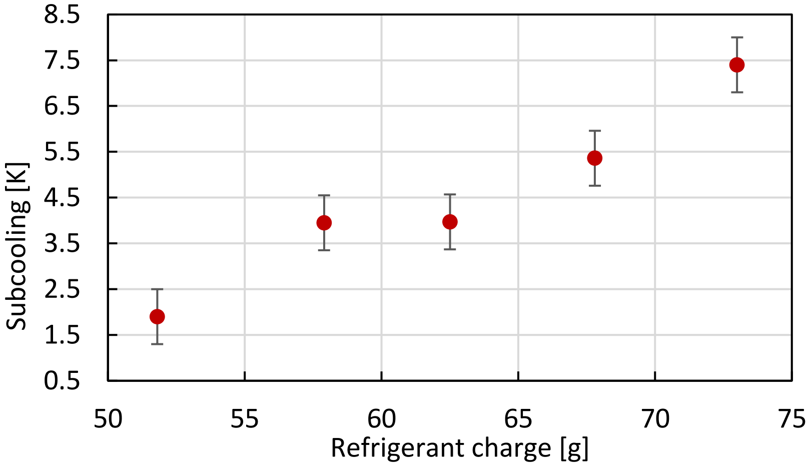

Figure 32: Evolution of subcooling through the refrigerant charge study

2.3.4.2 Visualisation of the flow pattern at the condenser outlet

Figure 33 and Figure 34 present images of the transparent section built in the tube-and-wire condenser when the refrigerator was running with the optimal refrigerant charge, which minimised energy consumption. The two figures reveal the presence of two-phase flow at the condenser outlet, evident by the presence of both liquid and vapour.

This visualisation did not reveal noticeable differences between the two operating refrigerator modes, FF+FZ and FZ. The images were taken when transient phenomena, due to the start-up of compressor, had finished and quasi-steady state conditions were established.

The situation analyzed corresponded to a very low mass velocity G of about 20 kg m^{-2} s^{-1} in FF+FZ. Under the test conditions, the flow pattern correlation of Thome et al. [35] predicted a stratified regime for all vapour qualities, especially at the outlet of the condenser.

From Figure 33 and Figure 34, this flow regime could also be characterized as a stratified regime, where the liquid filled the bottom of the tube while the vapour was present only in the upper part. An intermittent stratified wavy flow appeared when the liquid phase occupied the full cross-section in some sections due to some minor liquid waves.

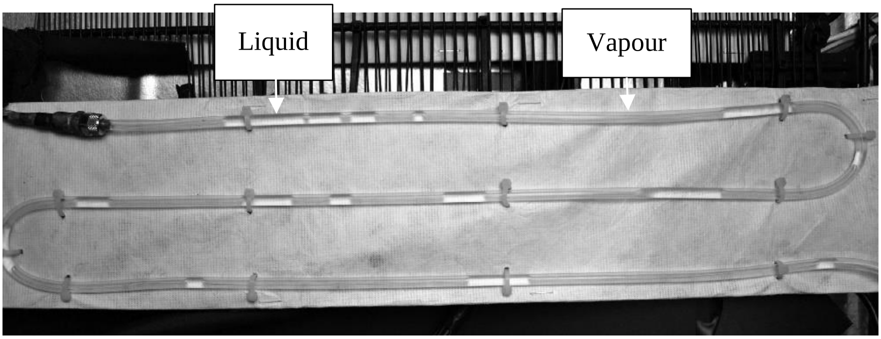

Figure 33: Refrigerant flow at the condenser outlet

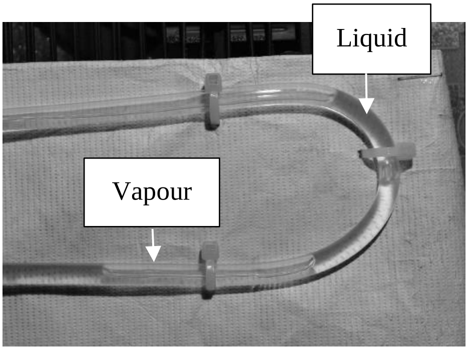

Figure 34: Refrigerant flow in a condenser bend

It was observed that the U-bends separate the two phases: the liquid was pushed by the gravity centrifugal forces towards the external part of the curve and, at the same time, the vapour occupied the internal part. At the outlet of these U-bends, the flow became more stratified, as shown in Figure 34.

Overall, elongated bubbles moved through the condenser until they reached the filter and the capillary tube inlet. The same flow pattern was observed for all the refrigerant charges tested, including one of the highest charges (73 g). It is expected that the void fraction had slightly changed. However, this type of measurement is beyond the scope of the present work, because the main objective here is to investigate whether two-phase flow was present at the condenser outlet and if it persisted even with a large increase in charge.

Contrary to the conclusions drawn from the temperature field analysis, with these visualisations, it can be concluded that there was no subcooled liquid. Boend and Melo [9] observed this situation at the capillary tube inlet and explained it as a non-equilibrium mixture of subcooled liquid and saturated vapour.

However, the transparent section was relatively long in this study, and could be considered adiabatic compared with a normal tube, and sufficient length enabled an equilibrium state or, at least, revealed some evolution towards equilibrium. That said, no evolution towards this end was observed. Further experimental studies are required to characterise the actual condenser outlet conditions.

To analyse whether these conclusions were affected by the refrigerant charge, the same visualisations were performed with a charge of 77 g, which is a relatively large charge for these systems because, at this charge, frost appears in the suction line. The visualisations of both tests were essentially the same.

2.3.4.3 Visualisation of the refrigerant flow at the capillary tube inlet

Figure 35, Figure 36 and Figure 37 depict the flow conditions at the capillary tube inlet for all the arrangements shown in Table 24 and according to the tests input presented in Table 25. Like the outlet condenser visualisation, the images did not show noticeable differences between the two operating modes, FF+FZ and FZ. Also, in this case the images were taken when the quasi-steady state conditions were established. Figure 35 reveals the different flow condition at the capillary tube inlet during tests 1 to 3 of Table 24, which were characterized by having the capillary tube inlet at the bottom of the filter and the refrigerant flowing downwards. The liquid filled the bottom of the filter until it reached the level defined by the capillary tube inlet section. The flow at this section was quite unstable, displaying fast and short oscillations (approximately 1 mm) due to the droplets falling from the filter. The flow condition mostly corresponded to the scenario depicted Figure 35, which illustrates that once the liquid reached the capillary tube inlet, a small vortex appeared. This phenomenon highlighted that the capillary tube draws in both liquid and vapour.

Table 24: Tests matrix of experimental campaign 2.2

Filter orientation	Flow direction	Capillary tube position inside the filter	Test n^{o}
Vertical	Downwards	Top	1
		Middle	2
		Low	3
Vertical	Upwards	Top	4
		Middle	5
		Low	6
Horizontal	Horizontal	Top	7
		Middle	8
		Low	9

To demonstrate that the filter was not working as a liquid accumulator, the position of the capillary within the filter was varied (Tests 2 and 3) with respect to Test 1. These figures demonstrate that the liquid level always followed the capillary tube inlet. Figure 35 shows that, regardless of its position, the capillary tube always drew in refrigerant with a certain amount of vapour. In fact, the filter always contained a constant amount of vapour and liquid that came from the filter walls and from the liquid droplets. This amount depended on the position of the capillary tube within the filter.

Figure 36 displays the corresponding tests for the filter mounted in the opposite direction; the refrigerant came from the bottom and flowed up until it reached the capillary tube inlet. Vapour bubbles flowing through the liquid and reaching the upper part of the filter can be observed in the pictures. Stronger oscillations than in the previous case were present at the interface, as evident by the abrupt interruption of bubbles, which flowed towards the capillary inlet. In this case, the interface was quite irregular, and the capillary tube drew in both liquid and vapour alternately. As in the previous case, the liquid level followed the displacement of the capillary tube inlet (Tests 5 and 6). Test 4 revealed a situation that may have been somewhat confusing if the capillary tube inlet was not visible since this situation would suggest that it was fully filled with liquid, however, this was not the case.

Table 25: Test conditions for experimental campaign 2.2

Parameter	Configuration
FF average temperature (°C)	4
FZ average temperature (°C)	-18
Climate chamber temperature (°C)	25
Temperature regulation	Electronics
Compressor speed (rpm)	1600
Refrigerant charge (g)	62.5
Test type	Dynamic
Condenser	Air
Capillary tube diameter (mm)	0.6
Filter position	According to Table 24
Test aim	Visualisation of condenser outlet and capillary tube inlet

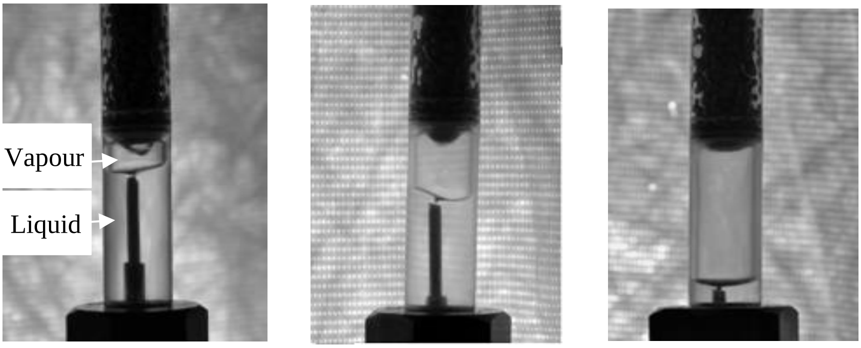

Test nº1 Test nº2 Test nº3

Figure 35: Capillary tube inlet for tests 1, 2 and 3

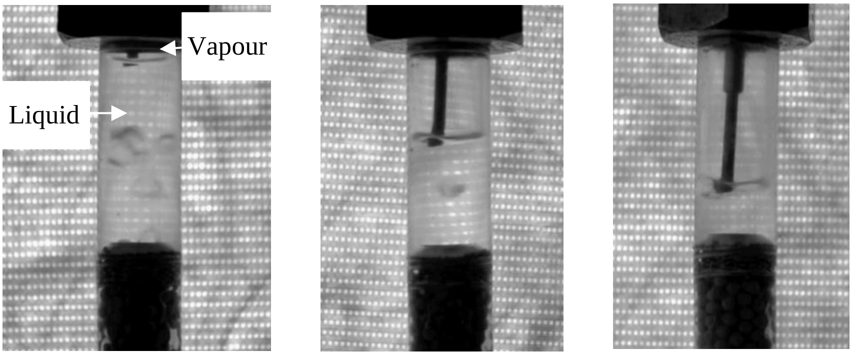

Test nº4 Test nº5 Test nº6

Figure 36: Capillary tube inlet for tests 4, 5 and 6

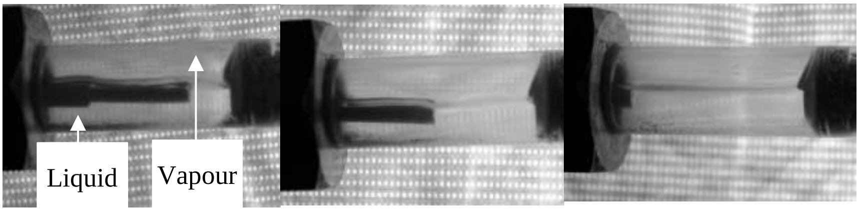

Test nº7 Test nº8 Test nº9

Figure 37: Capillary tube inlet for tests 7, 8 and 9

Figure 37 shows pictures of the horizontally oriented filter. In these operating conditions, only a tiny vortex appeared at the capillary tube inlet. No significant change was observed when the capillary tube inlet was moved along the filter. From here, the liquid–vapour interface could be considered practically motionless in all cases. This finding is critical because it suggests that the capillary tube inlet could be constantly drawing in a certain amount of vapour in steady conditions. This observation is somewhat unclear in Figure 35 and Figure 36 because gravity was affecting the vapour–liquid interface through the action of either bubbles or droplets.

Note that the measurements were performed once the system reached steady conditions, meaning that the compressor supplied the same mass flow rate as the capillary tube. This condition was achieved with the liquid–vapour interface depicted in Figure 35 to Figure 37. Therefore, if the conditions were the same, this interface will always be present at the inlet section of the capillary tube once steady conditions were reached. This explains why the interface always followed the capillary tube inlet regardless of its position within the filter.

The visualisation in Figure 35 to Figure 37 illustrates the presence of two-phase flow at the capillary tube inlet, confirming that the filter was not operating as a liquid receiver. Therefore, if thermodynamic equilibrium between the two phases is assumed, condensation in the condenser cannot be considered complete. The unbalanced matching between compressor and capillary tube could be an explanation for such observations; that is, the system would be equipped with a capillary tube with a larger expansion capacity compared with the needs of the compressor. This situation would cause the system to work at a less efficient operating point compared to a system working with effective subcooling.

The same tests were performed again with a large charge (for this kind of system) of 77 g. All tests revealed the same type of vapour–liquid interface at the capillary tube inlet. Therefore, the capillary tube still drew in a mixture of vapour and liquid, regardless of its orientation and position. The same conclusions from the tests with 62.5 g are applicable to these observations.

2.4 Conclusions

This experimental work aims to visualise the refrigerant flow at the condenser outlet and capillary tube inlet. To expand upon the studies examining the actual refrigerant conditions in the condenser outlet of these refrigeration systems, a novel experimental test bench was designed and mounted on a high efficiency household refrigerator. The main results are summarised as follows:

- The temperature profile analysis revealed the presence of subcooled liquid at the condenser outlet, which increased in value as the refrigerant charge increased.

- Visualisation of the condenser outlet revealed the presence of two-phase flow regardless the refrigerant charge. The dominant flow regime appeared to be stratified, while in some sectors, intermittent flow appeared.

- Regardless the orientation of the filter, capillary tube position inside and refrigerant charge, the capillary was always drawing in a mixture of liquid and vapour. In all tested filters, the liquid level followed the capillary entrance, demonstrating that the filter was not operating as a liquid receiver.

- The visualisations did not qualitatively change even with a charge increase of 15 g.

This visualisation work cannot alone demonstrate that the refrigerant was not fully condensate in the condenser, these findings clearly demonstrate that there are two phases. A non-equilibrium condition could explain this observation, and thus, the purpose of the next chapter is to determine the thermodynamic conditions at the capillary tube inlet by measuring the heat released during the condensation process. In the authors opinion, the compressor required a more restrictive capillary tube, which was tested and the results are presented in chapter 4.

Chapter 3

Experimental assessment of vapour quality at the condenser outlet of a household refrigeration system

3.1 Objective

An experimental visualisation campaign was detailed in the previous chapter, and results revealed that the capillary tube inlet was two-phase flow, regardless of filter position (horizontal or vertical), flow direction (upward or downward) and refrigerant charge.

Findings also demonstrated that the filter did not act as an accumulator since the liquid level of the capillary always followed the capillary tube entrance, regardless of the length of the capillary tube inside the filter. Various hypotheses can be posed to explain this phenomenon. For example, a non-equilibrium condition of the refrigerant or unbalanced matching between compressor and capillary tube; that is, the system would be equipped with a capillary tube with a very large expansion capacity compared with the needs of the compressor.

This chapter describes the test bench used where the original refrigerant-to-air condenser was replaced by a refrigerant-to-water condenser to enable, first, a larger variation of the condensation conditions, and second, assessment of the refrigerant conditions at the outlet of the condenser from the heat balance at the water condenser, and therefore, at the inlet of the capillary tube.

3.2 Experimental set up

3.2.1 General overview of the tests bench

With the aim of determining the actual vapour quality or degree of subcooling at the capillary tube inlet, a new test bench was designed. To accurately calculate the heat exchanged during the condensation process, the original condenser was replaced by a refrigerant-to-water heat exchanger, as depicted in Figure 38.

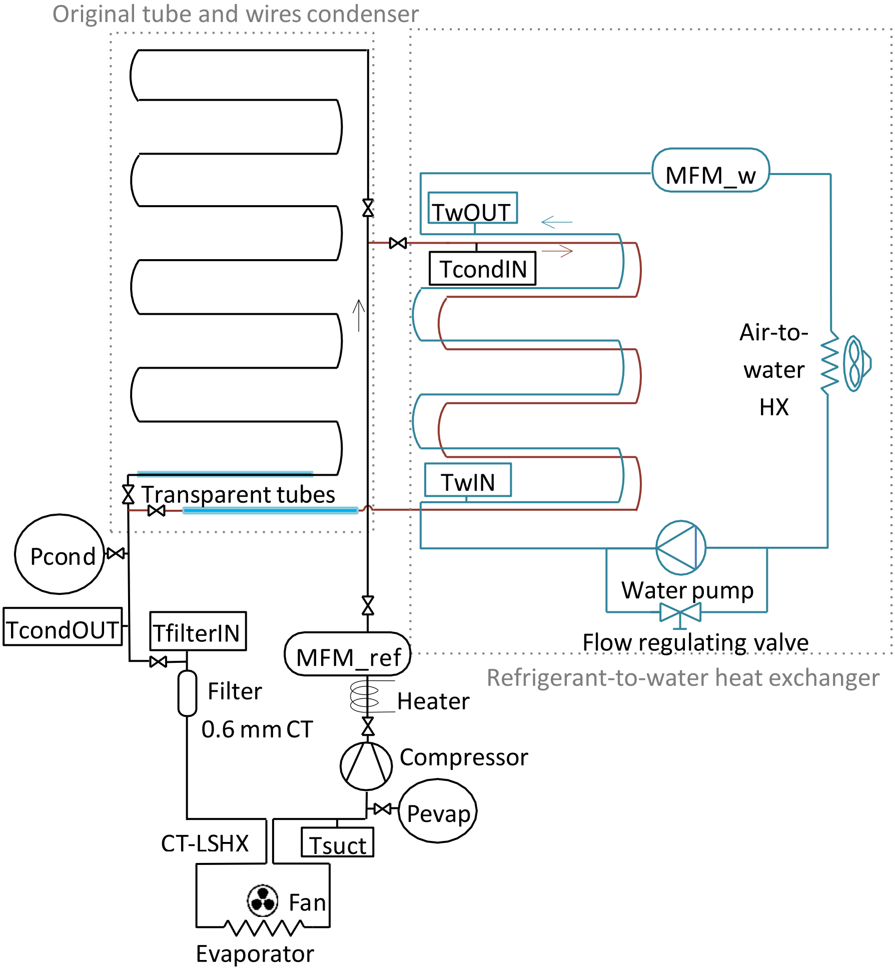
Original tube and wires condenser
MFM_w
TwOUT
TcondIN
Air-to-
water
HX
TwIN
Transparent tubes
Pcond
TcondOUT
TfilterIN
MFM_ref
Water pump
Flow regulating valve
Refrigerant-to-water heat exchanger
Filter
0.6 mm CT
Heater
Compressor
Pevap
CT-LSHX
Tsuct
Fan
Evaporator

Figure 38: Diagram of the tests bench

A system of valves enabled selection between the original condenser and refrigerant-to-water heat exchanger. Existing instrumentation, such as temperature and pressure measurements were improved and new instrumentation was added to allow estimation of enthalpy at the capillary tube inlet.

3.2.2 Instrumentation

Special attention was paid to the instrumentation selection to minimise measurement uncertainty about the determination of the enthalpy and vapour quality at the capillary tube inlet.

3.2.2.1 Refrigerant side

For the description of the refrigerator, evaporator and compressor, see chapter 2, section 2.2.1 and for the filter dryer, see section 2.2.2.1.

For this set of experiments, the filter dryer was in a vertical position. Due to the extra piping length added for the new refrigerant circuit, it was decided that the existing piping length should be reduced by removing the frame heater from the discharge line.

The following tables describe both refrigerant and water circuits items. The described item is highlighted in red in the schema. The sequence of descriptions corresponds to the flow (refrigerant or water) path.

All data presented in the following tables list the contribution of each individual measurement and were used to calculate the total uncertainty of the estimated parameters. In some cases, the datalogger measurement uncertainty was calculated but neglected because of its insignificant value with respect to the uncertainty of the considered equipment. For the technical description of the datalogger, see chapter 2, Table 21.

At the compressor discharge, the refrigerant mass flow rate was measured with a mass flow meter, as presented in Table 26. According to the mass flow meter provider advices, and since the condenser outlet appeared to be two-phase flow (chapter 1), it seemed the ideal location of the mass flow meter was at the compressor discharge, where only one-phase flow (vapour) was expected. Nevertheless, during installation start up, large oscillations were observed in the refrigerant mass flow rate measurement. Although the mass flow meter was set up close to the compressor discharge, it appeared that refrigerant started to condense before mass flow measurement, resulting in the observation of mass flow oscillations due to the presence of two-phase flow. To obtain only vapour at the mass flow meter inlet, a heater wire of a constant power of 10 W was set up and wrapped around the pipe at the inlet of the mass flow meter with the aim of heating the refrigerant and evaporating any possible liquid droplet.

Then, the refrigerant arrived at the refrigerant-to-water heat exchanger region where the condenser inlet temperature was measured (Table 26).

The refrigerant moved through the heat exchanger, carefully insulated from the surroundings. The heat exchanger was composed of two welded twin tubes, as depicted in Table 27.

A transparent tube set up at the outlet of the condenser enabled visible refrigerant flow. Condensation pressure was measured with a pressure transducer and the temperature at the condenser outlet was determined with a thermocouple placed inside a thermowell in contact with the refrigerant (Table 28).

Then, the refrigerant entered the capillary tube through the vertical filter. The filter configuration was slightly modified (the original configuration is explained in chapter 2, Table 16), namely, an RTD was added at the inlet of the filter, as depicted in Table 29. The aim was to measure the vapour temperature (TfilterIN), if present, at the capillary tube inlet and evaluate the difference with the liquid temperature.

Table 26: Refrigerant mass flow meter

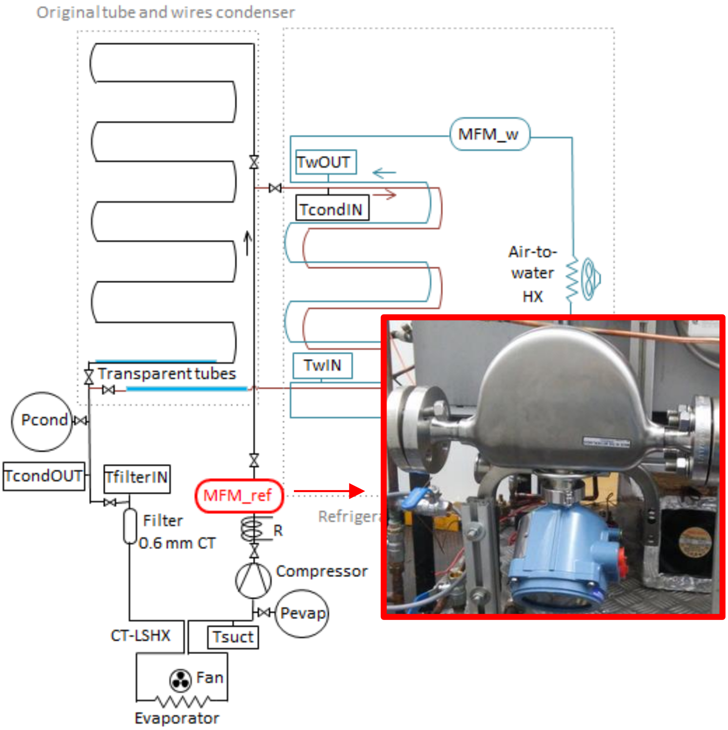
Original tube and wires condenser
MFM_w
TwOUT
TcondIN
Air-to-water HX
TwIN
Transparent tubes
Pcond
TcondOUT
TfilterIN
MFM_ref
Refriger
Filter
0.6 mm CT
R
Compressor
Pevap
CT-LSHX
Tsuct
Fan
Evaporator

Type	Coriolis
Brand	Micromotion
Model	CMFS010
Span	0 to 0.4167 g.s^{-1}
*Reference accuracy**	±0.25% of rate
Total accuracy (datalogger accuracy negligible)	±0.0005 g.s^{-1} for 0.2 g.s^{-1} flow rate

**includes linearity, repeteability, hysteresis*

Table 27: Refrigerant-to-water condenser

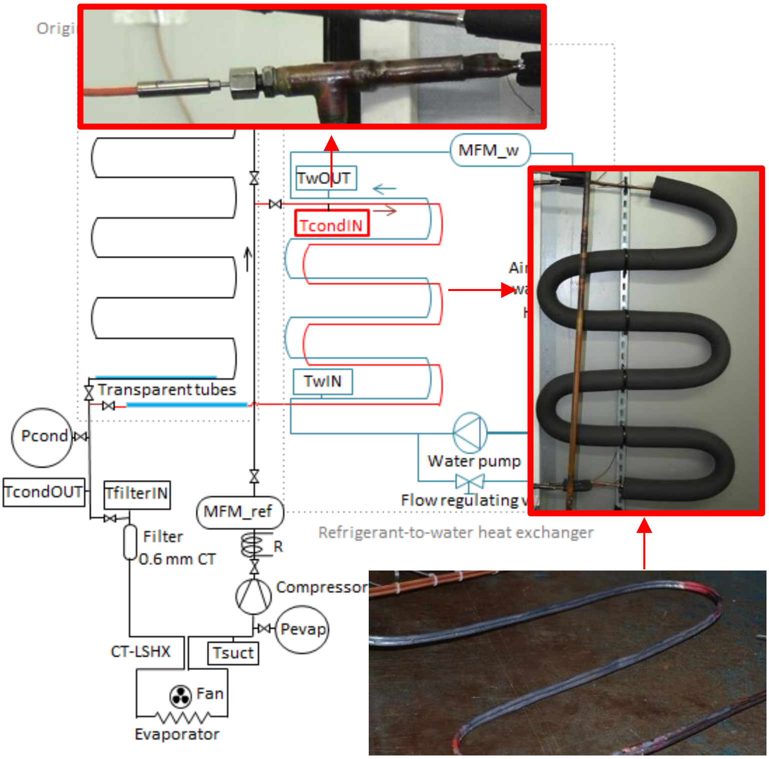
Origi
MFM_w
TwOUT
TcondIN
Ai
wa
Transparent tubes
TwIN
Pcond
Water pump
TcondOUT
TfilterIN
MFM_ref
Flow regulating v
Refrigerant-to-water heat exchanger
Filter
0.6 mm CT
R
Compressor
Pevap
CT-LSHX
Tsuct
Fan
Evaporator

TcondIN	
Type	RTD – Pt100
Class	1/10
Accuracy @ 40 ºC	±0.05 K
Total accuracy including data logger	±0.078 K

Refrigerant-to-water heat exchanger	
Type	Counter flow twin tubes
Exterior tube diameter/thickness	3.16 mm/0.8 mm
Width	50 mm
Total length	2460 mm
Tubes material	Copper

Table 28: Condenser outlet

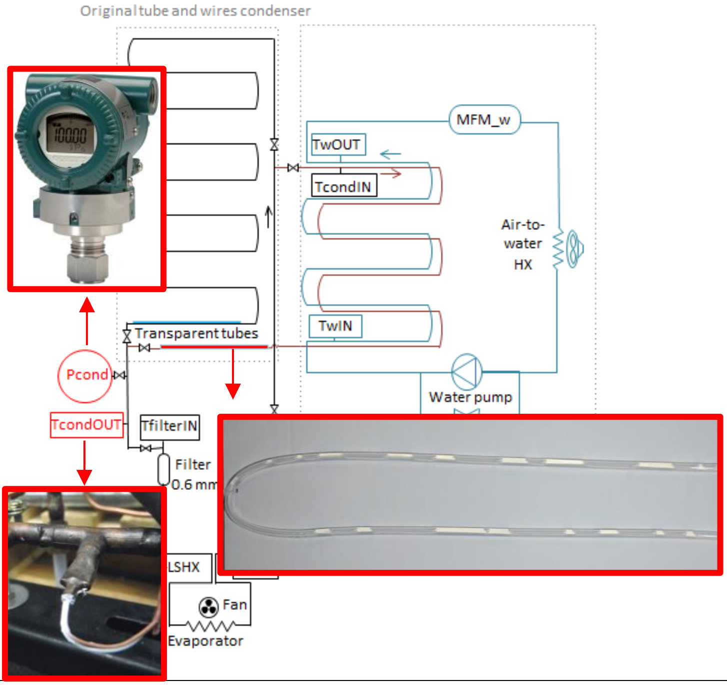
Original tube and wires condenser
MFM_w
TwOUT
TcondIN
Air-to-water HX
TwIN
Water pump
Transparent tubes
Pcond
TcondOUT
TfilterIN
Filter
0.6 mm
LSHX
Fan
Evaporator

Transparent tube	
Material	PFA
Internal diameter	4 mm
Length	1000 mm
Pcond	
Brand	Yokogawa
Model	EJA510E
Span	0 to 8 bars Abs
Upper Range limit (URL)	20 bars
Reference accuracy	±0.055% FS
Stability for 3 years	±0.2% URL
Total accuracy (datalogger negligible)	±0.04 bar
TcondOUT	
Type	T-type thermocouple
Accuracy	±0.2 K

Table 29: Temperature measurement of the capillary tube inlet

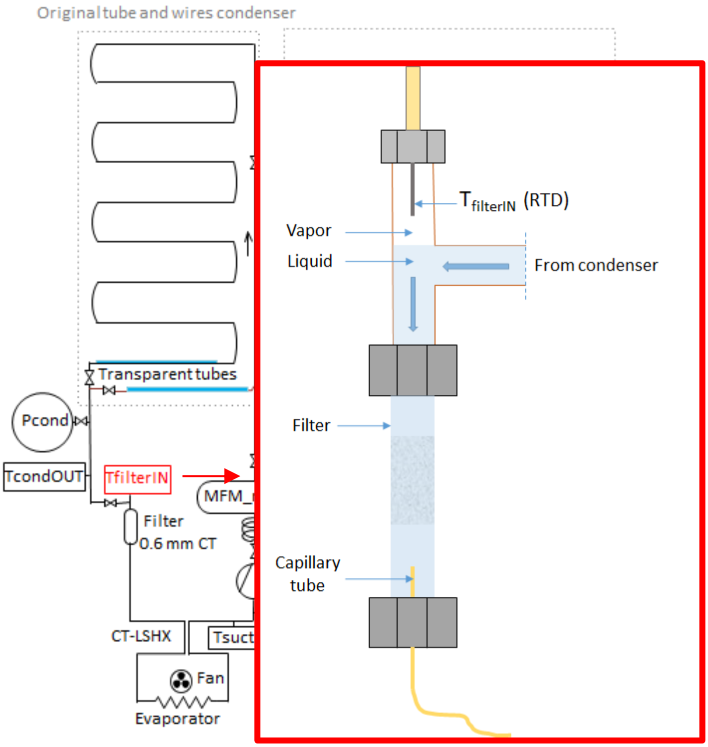
Original tube and wires condenser
Transparent tubes
Pcond
TcondOUT
TfilterIN
MFM_
Filter
0.6 mm CT
CT-LSHX
Tsuct
Fan
Evaporator
$T_{filterIN}$ (RTD)
Vapor
Liquid
From condenser
Filter
Capillary
tube

TfilterIN	
Type	RTD – Pt100
Class	1/10
Accuracy @ 20 ºC	±0.04 K
Total accuracy including data logger	±0.07 K

3.2.2.2 Water side

A closed circuit was built for the water side.

A pump powered the water loop (Table 30). The water mass flow rate was adjusted with a by-pass system.

The water inlet temperature and water outlet temperature were measured at both the inlet and outlet of the refrigerant-to-water condenser (Table 31). The water mass flow rate was measured at the heat exchanger outlet (Table 32).

A fan provided a constant airflow to a fin and tube heat exchanger to remove the heat from the water at the condenser outlet (Table 33) and achieve a constant water inlet temperature.

Table 30: Water pump specifications

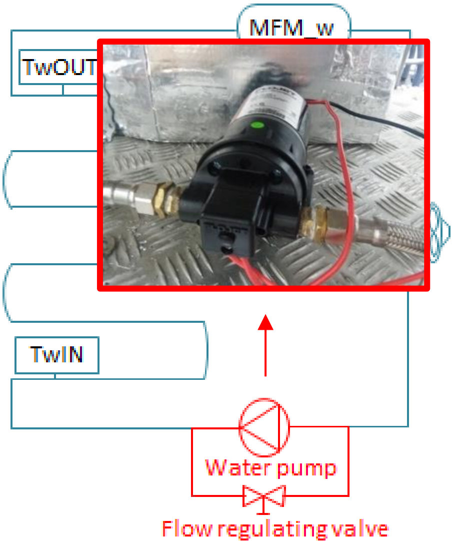

Brand/ model	Flojet/Duplex II
Type	Diaphragm pump
Max flow rate	8.1 l/min

Table 31: Water temperatures

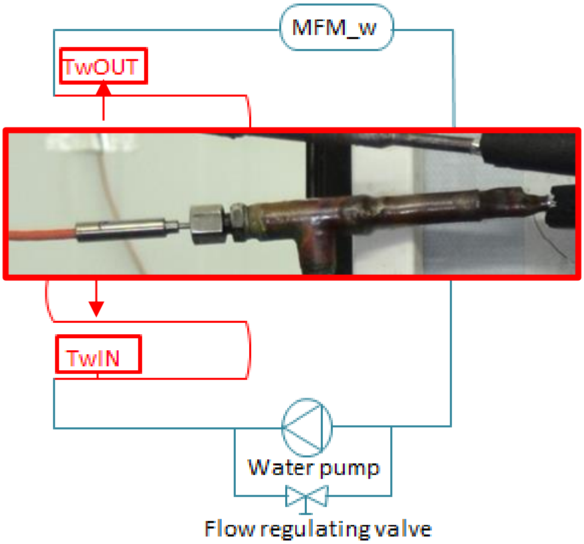
MFM_w
TwOUT
TwIN
Water pump
Flow regulating valve

Type	RTD – Pt100
Class	1/10
Accuracy @ 25 ºC	±0.042 K
Total accuracy including data logger	±0.07 K

Table 32: Water mass flow meter

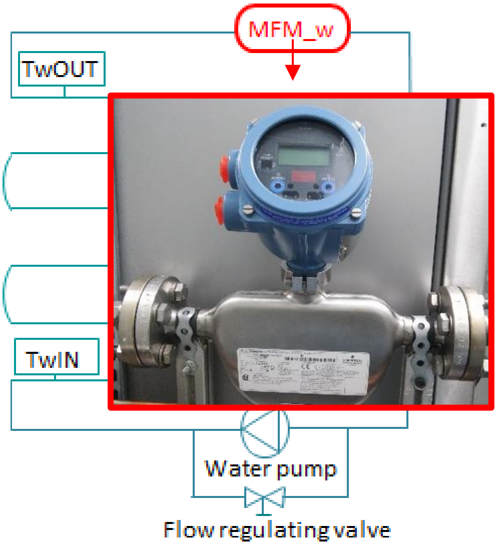
MFM_w
TwOUT
TwIN
Water pump
Flow regulating valve

Type	Coriolis
Brand	Micromotion
Model	CMFS015
Span	0 to 1 kg.min^{-1}
*Reference accuracy**	±0.1% of rate
Total accuracy (datalogger accuracy negligible)	±0.0003 kg.min^{-1} for 0.3 kg.min^{-1} flow rate

**includes repeatibility, linearity and hysteresis*

Table 33: Water-to-air heat exchanger

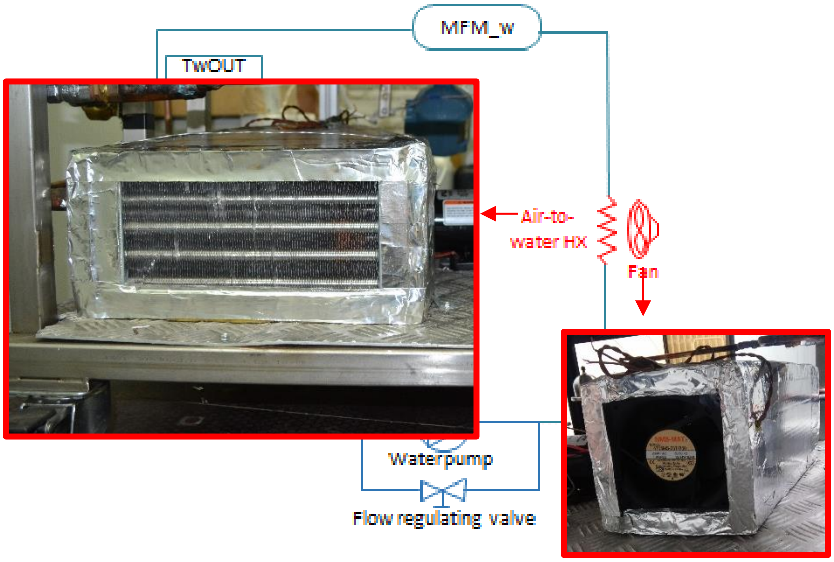
MFM_w
TwOUT
Air-to-water HX
Fan
Water pump
Flow regulating valve

Type	Fin and tubes
Exterior tube diameter/thickness	9.52/0.4 mm
Longitudinal spacing	22 mm
Transversal spacing	25.4 mm
Fin thickness	0.1 mm
Fin pitch	2.1 mm

The experimental apparatus was in a climatic chamber kept at 25°C and equipped with the same system for data acquisition described in chapter 2, section 2.2.

3.2.2.3 Power measurement

Technical data of the wattmeter are described Table 34.

Table 34: Wattmeter specifications

Brand	Camille Bauer
Model	Aplus
Power accuracy	± (0.16% reading + 0.04% range)
Power accuracy for 30 W	± 1.2 W

3.2.2.4 Control software

The system was controlled by a software using a labview platform to enable different temperature set points and modify the compressor displacement (Figure 39). The objective was to imitate the original control by having the possibility to modify parameters, such as compressor velocity and FF and FZ temperatures. The compressor velocity could be set from 1400 rpm to 4500 rpm. The temperature regulation was controlled using the information provided by a set of thermocouples (TFZ_control for the FZ and TFF_control for the FF), set close to the temperature measurement used by the refrigerator electronics (chapter 2, Figure 7). Descriptions of both thermocouples are presented in Table 35.

Table 35: Temperature control

	Location	Thermocouples type	Accuracy
TFF_control	Refrigerator inside air	T-Type	±0.5K
TFZ_control	Freezer inside air	T-Type	±0.5K

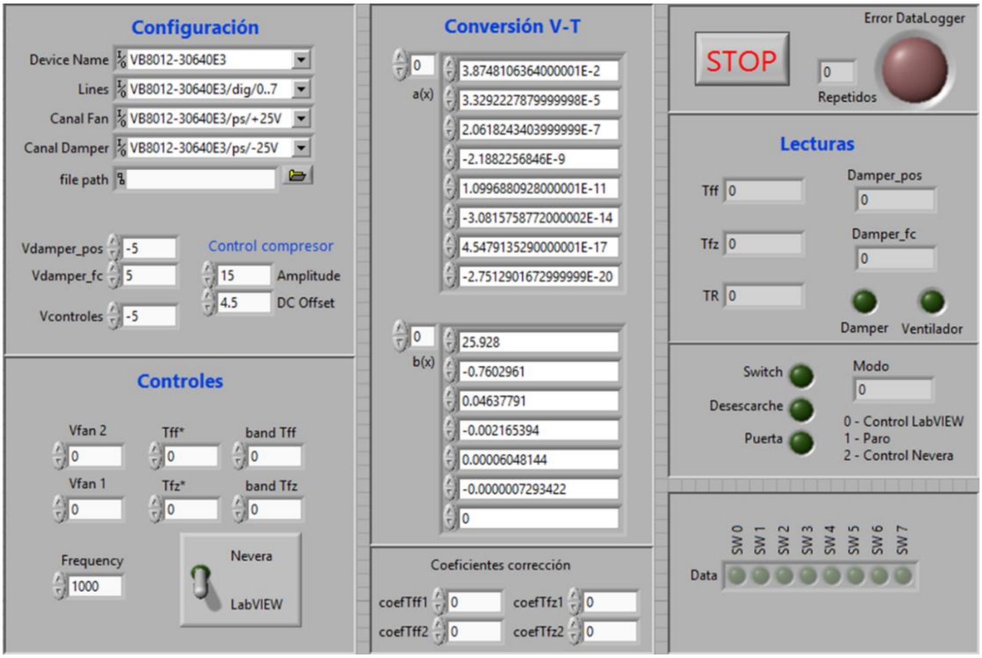
Configuración
Control compresor
Controles
Nevera
LabVIEW
Conversión V-T
Coeficientes corrección
STOP
Error DataLogger
Lecturas
Damper
Ventilador
Switch
Desescarche
Puerta
SW 0
SW 1
SW 2
SW 3
SW 4
SW 5
SW 6
SW 7
Data

Device Name VB8012-30640E3
Lines VB8012-30640E3/dig/0..7
Canal Fan VB8012-30640E3/ps/+25V
Canal Damper VB8012-30640E3/ps/-25V
file path

Vdamper_pos -5
Vdamper_fc 5
Vcontroles -5
15 Amplitude
4.5 DC Offset

Vfan 2 0
Tff* 0
band Tff 0
Vfan 1 0
Tfz* 0
band Tfz 0
Frequency 1000

a(x) 0
3.8748106364000001E-2
3.3292227879999998E-5
2.0618243403999999E-7
-2.1882256846E-9
1.0996880928000001E-11
-3.0815758772000002E-14
4.5479135290000001E-17
-2.7512901672999999E-20

b(x) 0
25.928
-0.7602961
0.04637791
-0.002165394
0.00006048144
-0.0000007293422
0

coefTff1 0
coefTfz1 0
coefTff2 0
coefTfz2 0

0 Repetidos

Tff 0
Tfz 0
TR 0
Damper_pos 0
Damper_fc 0

Modo 0
0 - Control LabVIEW
1 - Paro
2 - Control Nevera

Figure 39 : Labview platform interface

3.3 Experimental campaigns

3.3.1 Procedure

The following experimental campaigns were conducted to determine the conditions at the capillary tube inlet:

- Experimental campaign 3.1: determination of the optimal refrigerant charge with the original condenser and new piping system.
- Experimental campaign 3.3: with the optimal charge previously determined, a test was performed without the heater in the FZ compartment, but maintaining the original condenser, to reproduce easier, and with more accuracy (with the refrigerant-to-water HX), the operating conditions determined in experimental campaign 3.1.
- Experimental campaign 3.4: refrigerant-to-water HX was used to determine the capillary tube inlet conditions. The refrigerant charge was slowly increased until operating parameters were close to those determined in

experimental campaign 3.3. Then, a fine-tuning was performed, varying the water mass flow rate to match almost exactly the refrigerant conditions of the original unit.

Experimental campaign 3.2 included a study of repeatability through a test campaign.

3.3.2 PID set point

In chapter 2, dynamic tests were done. Steady tests were conducted in this experimental campaign because it is the best way to analyse and understand the refrigerant cycle. To reflect the behaviour of an actual household refrigerator as much as possible, temperatures inside the FF and FZ and compressor velocity were identical to the manufacturer settings, therefore, the performance and operation were analogous.

The temperature inside the FF and FZ were maintained constant by a PID regulating the maximum power of a 200 W heater inside each cabinet. The thermocouples T_{FF_PID} and T_{FZ_PID} connected to the PID inside the FF and FZ were located close to the original FF and FZ temperature measurements, respectively (chapter 2, Figure 7).

During normal operation, the compressor alternates switching on and off in such a way that the temperature cycles and is, on average, 4ºC and -18ºC, inside the FF and FZ, respectively. It would have been improper to put these temperatures as PID setting points because they represent the average temperature of all drawers of each cabinet and not at the sensor location.

To determine the PID temperature setting points (T_{FF_PID} and T_{FZ_PID}), a dynamic test was run with the apparatus original electronics. In this configuration, a temperature of T_{FF_PID} and $T_{FZ\_PID,}$ equal to 8ºC and -20 ºC, respectively was observed (Figure 40). The temperature difference with respect to the manufacturer set point can be explained by both the location of T_{FF_PID} and T_{FZ_PID} and the air distribution inside each cabinet.

Table 36 describes the thermocouples T_{FZ_PID} and T_{FF_PID}.

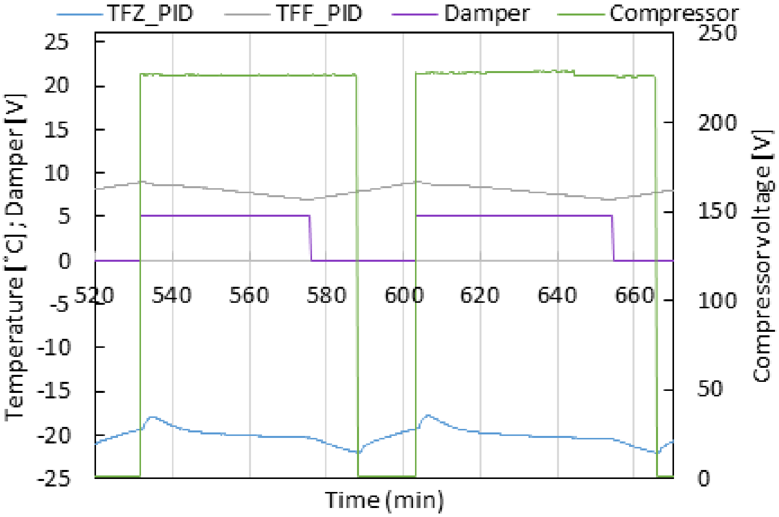

Figure 40: Temperatures PID determination

Table 36: PID temperature

	Location	Thermocouples type	Accuracy
T_{FF_PID}	Refrigerator inside air	T-Type	±0.5 K
T_{FZ_PID}	Freezer inside air	T-Type	±0.5 K

3.3.3 Reference conditions with air condenser

3.3.3.1 Optimal charge with air condenser

Table 37 lists the reference conditions for this set of tests. The aim was to determine the optimal refrigerant charge with the air condenser, considering the piping modifications. The refrigerator was kept in operation for 24 hours under steady state conditions for each charge of refrigerant tested. To analyse the data, an average of the last 30 minuts measured values were calculated when steady state conditions were reached. The different calculations were then determined with those average values.

Table 37: Test conditions for experimental campaign 3.1

Parameter	Configuration
T_{FF_PID} (°C)	8
T_{FZ_PID} (°C)	-20
Climate chamber temperature (°C)	25
Temperature regulation	PID+heater
Compressor speed (rpm)	1600
Control type	Labview
Test type	Steady
Condenser	Air
Capillary tube inner diameter (mm)	0.6
Filter position	Vertical
Test aim	Charge study

3.3.3.2 Results and discussion

The refrigerant charge was varied from 74.5 g to 90 g. Results with 90 g are not included in the data analysis because suction was frozen, and therefore, it was impossible to reach the required temperature inside the cabinets. The optimal charge is that which maximised the COP.

The cooling capacity, considering the presence of the CT-LSHX, was calculated as per Eq. 3.1.

$$\dot{Q}_{cool} = \dot{m}_{ref}(h_{suct} - h_{condOUT}) \tag{3.1}$$

The COP is calculated as presented in Eq. 3.2.

$$\text{COP} = \frac{\dot{Q}_{cool}}{\dot{W}_{comp}} \tag{3.2}$$

Figure 41 presents the cooling capacity calculated from the refrigerant side, measured compressor power and corresponding COP. The compressor power increased almost linearly with the refrigerant charge and in a proportion equal to 14% from the lowest to the highest refrigerant charge. The cooling capacity also increased when the charge increased, but reached a maximum around 82 g and then started to decrease. This saw the COP have first a moderate increase with refrigerant charge, a maximum around 80 g, and then a decrease with a significant negative slope. Similar results can be found in the literature [9], [34].

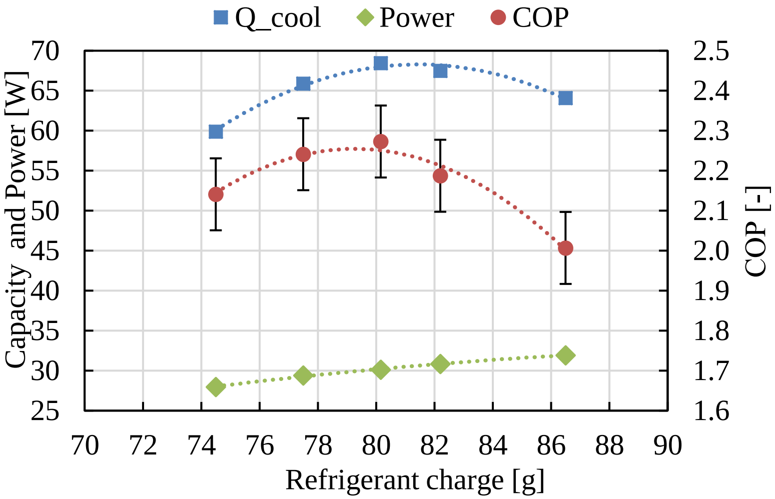

Figure 41: Cooling capacity, COP and compressor power for different refrigerant charges

Although the refrigerant charge was increased by almost 20 g, few variations were visible in the subcooling calculated with the condenser pressure outlet and temperature at the condenser outlet, namely SC_{pT}, which varied from 9.2 K for the lowest refrigerant charge to 10.1 K for the highest (Figure 42).

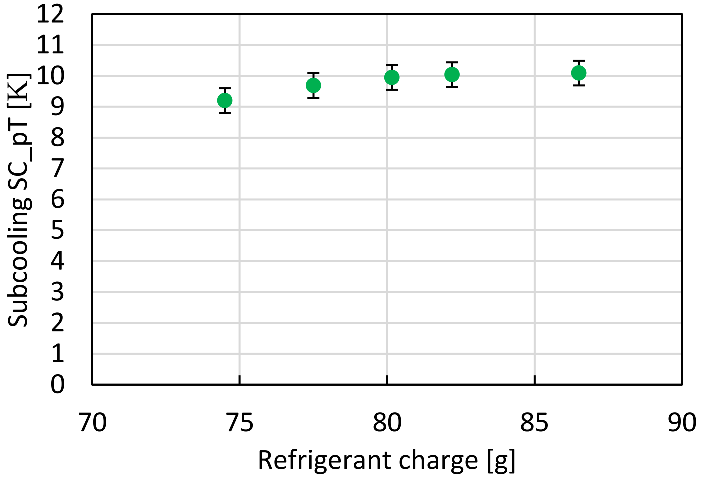

Figure 42: Subcooling for different refrigerant charges

Various repetitions of the same experimental campaign were conducted and variations observed in the subcooling measurement. Thus, it was decided that an experimental campaign to study the test repeatability should be conducted to explain possible deviations along the campaign.

3.3.4 Tests repeatibility

The heater was only operating in the FF compartment to determine if the system could reach the same temperature inside the FZ compartment between the different tests. Table 38 describes the tests condition for this experimental campaign.

Table 39 compares the test repetition results. Test 2 was repeated five days after test 1.

The COP decreased because of the cooling capacity decline due to a lower refrigerant mass flow rate during test 2. An increase in the subcooling of 1.7 K, due to a reduction of the outlet condenser temperature, was also observed.

Other works have demonstrated variation in subcoooling for same condition, reporting a certain hysteresis [13]. However, it is possible that the increase in subcooling and a decrease in refrigerator performance could indicate the presence of non-condensable in the refrigerant circuit. Therefore, the next work tested for the presence of air.

Table 38: Test conditions for experimental campaign 3.2

Parameter	Configuration
T_{FF_PID} (°C)	8
Climate chamber temperature (°C)	25
Temperature regulation	PID+heater in FF
Compressor speed (rpm)	1600
Refrigerant charge (g)	83.5
Condenser	Air
Control type	Labview
Test type	Steady
Capillary tube inner diameter (mm)	0.6
Filter position	Horizontal
Test aim	Repeatibility study

Table 39: Tests repetition

Parameter	Value for test 1	Value for test 2	Difference
SC_{pT} (K)	7.1	8.8	+1.7 K
P_{evap} (bar)	0.73	0.72	-1%
P_{cond} (bar)	4.83	4.90	1%
T_{suct} (°C)	1.6	1.6	0%
$T_{condOUT}$ (°C)	29.3	28.1	-4%
$\dot{m}_{ref}$ ($g.s^{-1}$)	0.260	0.252	-3%
Compressor power (W)	32.7	32.5	-1%
Cooling capacity (W)	75.9	74.3	-2%
COP (-)	2.32	2.28	-1.7%
T_{FZ} (°C)	-17.9	-18.2	º-2%

3.3.4.1 Study on the possible presence of air in the system

Many works relate the effect of non-condensable gases being present in refrigeration systems, but few have looked at domestic appliances, such as household refrigerators.

Cecchinato et al. [36] studied the effect of the presence of air in the refrigerant circuit of a single door refrigerator and an upright freezer. These authors explained that as the condensation process runs, vapour quality decreases and the flow pattern from annular flow tends to bubble flow, which cannot collapse due to the air vapour mixture. Condensation stops when the partial pressure of the refrigerant vapour inside the bubbles becomes equal to the saturation pressure of the surrounding liquid. Thus, bubbles are carried inside the capillary tube and clog the flow. Consequently, the liquid flooding in the condenser increases while air molar fraction increases and the mass flow rate in the capillary tube reduces.

These authors also observed that for a low air quantity, the effect on the performance system is actually positive, and noted an improvement of 3.1% in energy consumption with respect to the no air case. It can be justified by the fact that the capillary tube was oversized, and the presence of air increases capillary tube restriction and system performances.

The same effects were observed by Espindola et al. [37], who set an accelerometer to monitor vibration from refrigerant expansion at the capillary tube outlet. These authors tested different quantities of nitrogen with different compressor speeds (2500, 3000, 4000 rpm).This study revealed:

- An increase in discharge pressure when the quantity of nitrogen was increased (the nitrogen can clog the capillary tube and the condenser is thus flooded and condensation pressure increases, the evaporator is consequently starved of refrigerant and suction pressure is decreases, which causes a mass flow rate reduction.

- An increase in the subcooling, especially in the final part of the condenser. A rapid decrease of the condenser temperature outlet was observed. Figure 43 presents the temperature evolution along the condenser for all refrigerant charge tested. The temperature dropped when a 10.5 m length in the condenser was reached, which may have resulted from the presence of air.

- For the case with lowest nitrogen mass fraction (0.07 and 0.14), they observed a diminution of the compressor consumption as observed by Cecchinato et al. [36].

- At high level of nitrogen (0.53 % of nitrogen), an intermittent acceleration pattern was observed. When the liquid level is very low, there is mostly gas at the inlet of the capillary tube, which partially clogs the capillary tube and reduces the mass flow rate and expansion noise. There is an imbalance between the mass flow displaced by the compressor and mass flow entering the capillary tube when the quantity of air is important.

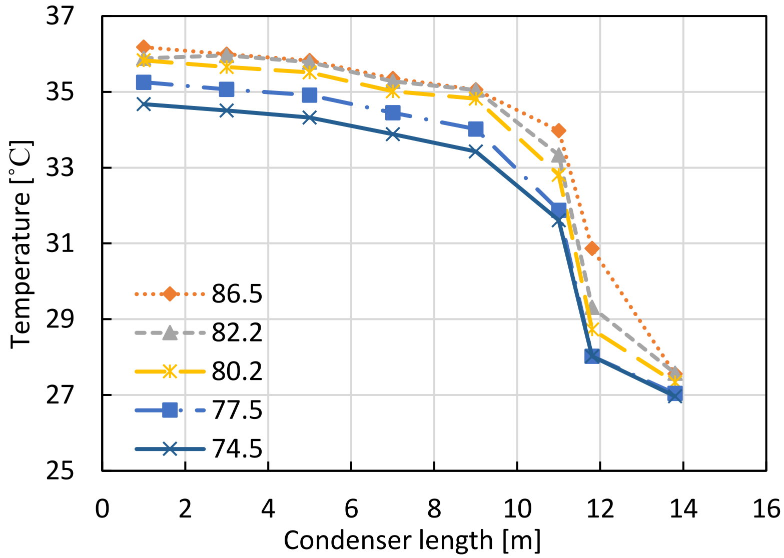

Figure 43: Temperature along condenser for different charges tested

i. Experimental set up

To determine if the refrigerant circuit contained air, a gas chromatography was performed on a refrigerant sample.

A valve was strategically added at the condenser outlet to extract a refrigerant sample. The bottle and its connection, once connected to the refrigerant circuit, were vacuumed using a set of valves, ensuring no contamination of the samples.

The tests were carried out with a CP-4900 Varian microgas chromatograph. Figure 44 presents the experimental set up.

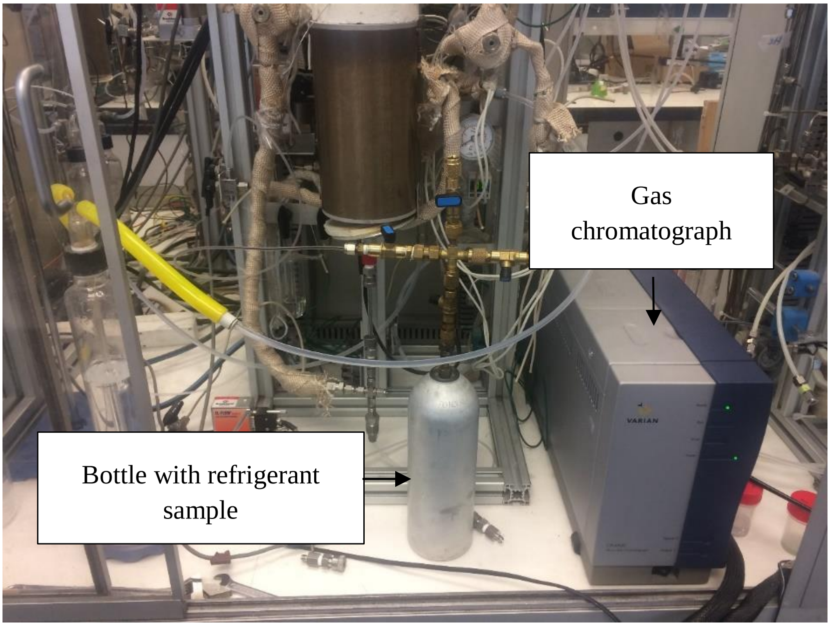

Figure 44: Gas chromatograph experimental set up

ii. Results

The sample contained 15 g of refrigerant. The valve at the bottle outlet was opened and eight measurements were calculated while the refrigerant bottle was emptying. Table 40 presents the percentage of nitrogen and oxygen detected for the different measurements.

It was noted that the oxygen and nitrogen percentage decreased while the bottle was emptying, likely because the first measurement was mostly vapour; afterwards, the liquid present in the bottle was evaporating and thus, the quantity of nitrogen and oxygen was decreasing.

From measurement nº7, the sample bottle was agitated to evaluate if the nitrogen and oxygen quantities would vary, which explains the sudden decrease observed between measurements nº6 and nº7.

Table 40 : Gas chromatography of refrigerant sample

Measurement nº	O_2 (%)*	N_2 (%)*
1	0.162	0.439
2	0.198	0.535
3	0.197	0.54
4	0.193	0.529
5	0.185	0.515
6	0.164	0.458
7	0.104	0.286
8	0.090	0.249
9	0.088	0.247
10	0.085	0.234

*molar percentage

iii. Conclusions and measures taken for the next tests

For the nitrogen and oxygen molar fractions found in the sample, an evaluation of the effect on the condensation temperature was performed using Refprop by defining a mixture of refrigerant, nitrogen and oxygen, with the composition of the first measurement. At equilibrium, and for a given pressure, the effect on the condensation temperature was around 0.3°C (Table 41), which is considered negligible. Furthermore, the quantity of oxygen and nitrogen found in the refrigerant sample is not representative of the actual amount present in the entire refrigerant circuit. Since both liquid and vapour refrigerant states cohabit in the system, and air is contained only in a vapour phase, the actual quantity contained in the complete system is likely to be much lower than the amount found in the sample.

Table 41: Effect of nitrogen and oxygen on condensation temperature

Mole fraction (nitrogen)	Mole fraction (oxygen)	Mole fraction (isobutane)	Pressure (bar)	Temperature (°C)
0.00162	0.00439	0.99399	5	37.45
0	0	1	5	37.71

Nevertheless, to minimize the air contamination during experimental tests, the installation was vacuumed and charged after each experimental campaign or/and every week.

3.3.5 Reproduction of optimal charge air condenser test without heater in the FZ

To more easily and accurately reproduce with the refrigerant-to-water HX the operating conditions determined during experimental campaign 3.1, a test was also run with the optimal charge (80.9 g) maintaining the air condenser and original capillary tube which only regulated the FF temperature, i.e., without the heater in the FZ because the heater value required to reach the target conditions is approximately 0 W. Table 42 presents the test conditions of experimental campaign 3.3. The results of this test are presented in Table 43. The different values obtained were those that had to be reproduced with the refrigerant-to-water heat exchanger.

Table 42: Test conditions for experimental campaign 3.3

Parameter	Configuration
T_{FF_PID} (°C)	8
Climate chamber temperature (°C)	25
Temperature regulation	PID+heater in FF
Compressor speed (rpm)	1600
Refrigerant charge (g)	80.9
Condenser	Air
Control type	Labview
Test type	Steady
Capillary tube diameter (mm)	0.6
Filter position	Horizontal
Test aim	Reproduction of air condenser test conditions without heater in FZ

Table 43: Air condenser conditions to be reproduced

Parameter	Value
SC_{pT} (°C)	9.0
P_{evap} (bar)	0.69
P_{cond} (bar)	4.88
T_{suct} (°C)	12.5
$\dot{m}_{ref}$ ($g.s^{-1}$)	0.238
Compressor power (W)	31.6
T_{FZ} (°C)	-19.3

3.3.6 Reproduce test conditions with refrigerant-to-water HX

The system was first charged with a low refrigerant charge (55 g), which was slowly increased until almost reaching the target values (Table 43), namely, condensation and evaporation pressure, refrigerant mass flow rate, subcooling and compressor power. Then, it was checked whether the suction temperature and temperature reached in the FZ were close to the values obtained in experimental campaign 3.3. Finally, a fine tuning was conducted, varying the water mass flow rate to almost exactly match the target values. Table 44 presents the test conditions of this fine tuning.

Table 44: Test conditions of experimental campaign 3.4

Parameter	Configuration
T_{FF_PID}(°C)	8
Climate chamber temperature (°C)	25
Temperature regulation	PID+heater in FF
Compressor speed (rpm)	1600
Condenser	Water
Water mass flow rate ($kg.min^{-1}$)	from 0.066 to 0.447

Refrigerant charge (g)	64
Control type	Labview
Test type	Steady
Capillary tube diameter (mm)	0.6
Filter position	Horizontal
Test aim	Reproduction of optimal charge air condenser test conditions

3.4 Analysis of the results and discussion

3.4.1 Visualisations

Visualisations of the capillary tube inlet were similar to those found in experimental campaign 2.1. Figure 45 depicts the capillary tube inlet during the entire experimental campaign 3.4. Despite the water mass flow rate variation and thus, condensing conditions differences, it was not possible to fill the inlet of the capillary tube with liquid. Nevertheless, variations in condensing temperature were visible at the condenser outlet, and which strongly modified the flow pattern as the water mass flow rate changed, resulting in a higher presence of vapour phase for lower water mass flow rate, and thus, higher condensation pressure, as visible in Figure 46.

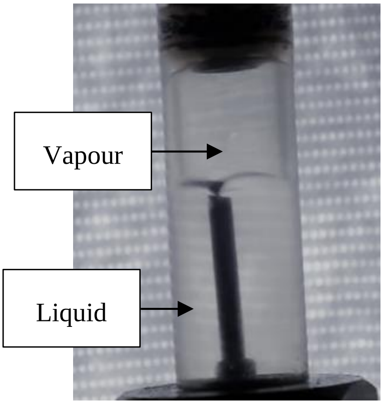

Figure 45: Two-phase flow capillary tube inlet

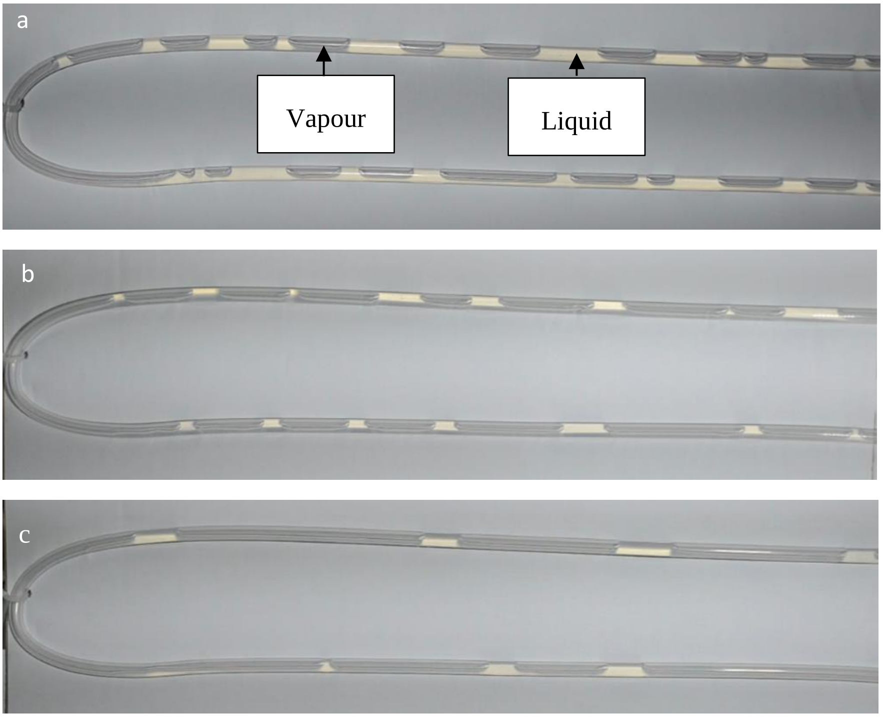

Figure 46: Visualisation of the condenser outlet with a)$\dot{m}_w$*=0.447 kg.min*$^{-1}$
b) $\dot{m}_w$*=0.190 kg.min*$^{-1}$ *c)* $\dot{m}_w$ *=0.066 kg.min*$^{-1}$

3.4.2 Determination of capillary tube inlet conditions

The refrigerant conditions at the condenser outlet has been calculated using the heat balance between water heat capacity (Eq. 3.3) and refrigerant condensing capacity (Eq. 3.4).

$$\dot{Q}_w = \dot{m}_w c_{p_w} (T_{wOUT} - T_{wIN}) \tag{3.3}$$

$$\dot{Q}_w = \dot{Q}_{cond} = \dot{m}_{ref} \left(h_{condIN} - h_{condOUT\_HX} \right) \tag{3.4}$$

From Eqs 3.3 and 3.4, it is possible to calculate the enthalpy at the condenser outlet (Eq. 3.5):

$$h_{condOUT\_HX} = h_{condIN} - \frac{\dot{m}_w}{\dot{m}_{ref}} cp_w (T_{wOUT} - T_{wIN}) \tag{3.5}$$

Calculations of the different parameter uncertainties were carried out using the software EES.

Figure 47 compares the water heat capacity evaluated from the waterside measurements ($\dot{Q}_w$) and condensing capacity calculated from the refrigerant side using the enthalpy calculated with pressure and temperature ($\dot{Q}_{cond}$) with their associated uncertainties (hardly visible because of their low values). Both capacities are represented regarding water mass flow rate. There are two possible reasons for the differences between $\dot{Q}_{cond}$ and $\dot{Q}_w$. First, the refrigerant mass flow rate measurement could be less accurate than expected because of variations in oil concentration or influence of the oil on the measurement, which is unknown. Second, an assumption of thermodynamic equilibrium at the refrigerant outlet for the evaluation of the condensing capacity ($\dot{Q}_{cond}$). In general, it was observed that the water heat capacity was always lower than the refrigerant capacity and that the uncertainty of the measurements could not explain this difference. Both capacities remained constant for water mass flow rates from 0.447 kg.min^{-1} to 0.252 kg.min^{-1}, then continually decreased if the water flow rate decreased. When the water mass flow rate decreased, the capacity of the condenser to reject the heat to the water also decreased, and therefore, the condensation temperature had then to increase, also increasing condensation pressure, as illustrated in Figure 48. At some point, the rise in pressure ratio lead to a decline in the refrigerant mass flow rate (Figure 49). This resulted in the observed decrease of both capacities.

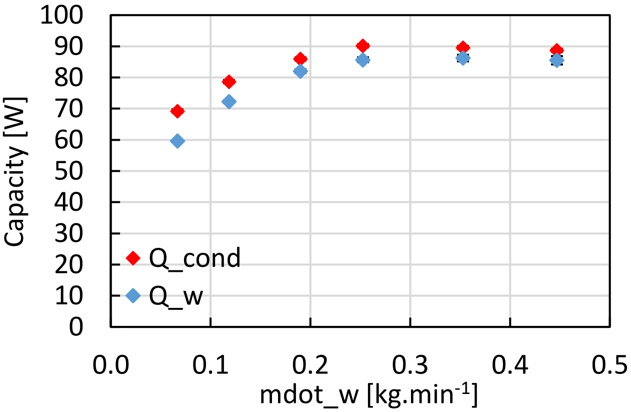

Figure 47: Water and condensing capacities varying water mass flow rate

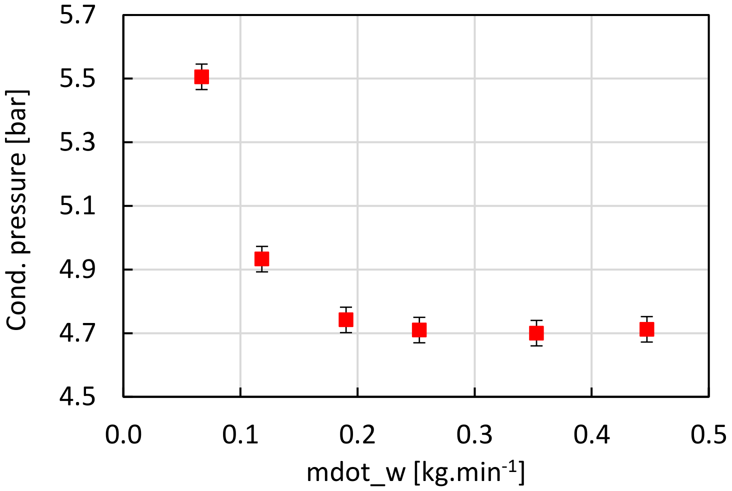

Figure 48: Condensation pressure vs. water mass flow rate

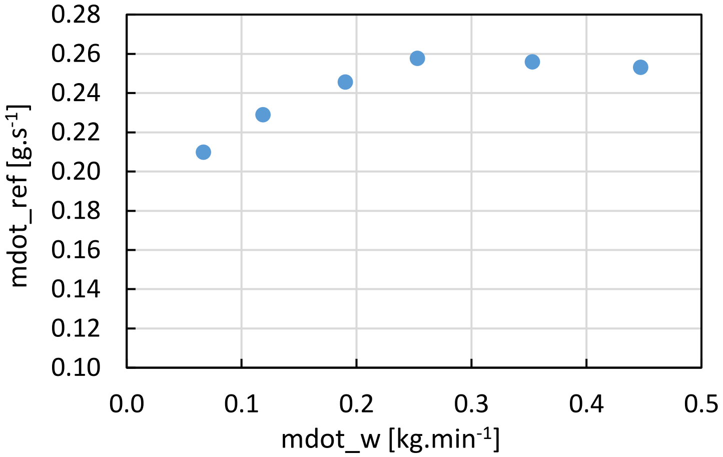

Figure 49: Refrigerant mass flow rate vs. water mass flow rate

Figure 50 depicts the corresponding subcooling, evaluated first from the pressure and temperature measurements and assuming thermodynamic equilibrium for the refrigerant, namely SC_{pT}, and second, subcooling evaluated from the condenser inlet conditions and waterside measured heat, namely SC_{HX}.

SC_{pT} was almost constant around 9 K, except for the lowest tested water flow rate, where it decreased to 7 K. These subcooling values contradicted the visualisation of flow at the capillary tube inlet, which clearly exhibited two-phase flow conditions, or at least, alternating liquid/vapour inlet conditions during the entire campaign (Figure 45). In chapter 2, we already noted this contradiction between the apparent subcooled state, which can be assessed from the pressure and temperature measurements and actual visible conditions of the refrigerant at the capillary tube inlet, with the liquid level always appearing at the capillary inlet mouth. We have revealed that, despite a measured subcooling of 14 K, vapour bubbles were present at the condenser outlet and the capillary tube inlet displayed the two-phase flow pattern.

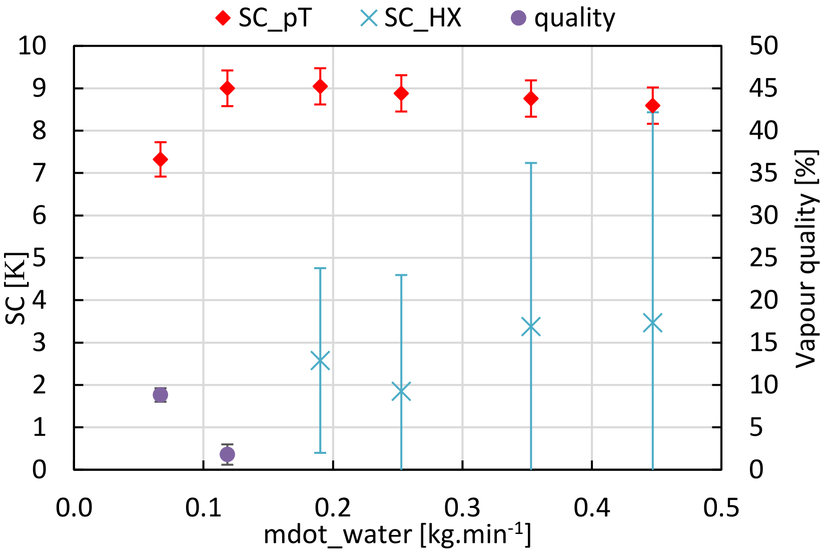

Figure 50: Subcooling evaluated from the pressure and temperature measurements and the assumption of thermodynamic equilibrium, and subcooling evaluated from the inlet refrigerant conditions and the heat measured on the water side.

In contrast with the almost constant value of the SC_{pT} subcooling, SC_{HX} subcooling was much lower and decreased with the decrease of water flow rate, until reaching a point where subcooling ceased. For a water mass flow rate of 0.066 kg.min^{-1} and 0.118 kg.min^{-1}, the calculation of the vapour quality returned 8.8% and 1.7%, respectively. The target values determined in experimental campaign 3.3 were located between two working points corresponding to water mass flow rates between 0.118 kg.min^{-1} and 0.190 kg.min^{-1}, where a transition in refrigerant conditions was observed.

Indeed, a subcooling of 2.5 K was evaluated with a water mass flow rate of 0.190 kg.min^{-1}, while 1.7% vapour quality was found with 0.118 kg.min^{-1}.

Note that despite the attention paid to instrumentation selection, analysis of the propagation error reveals it was challenging to have low uncertainty for SC_{HX} subcooling evaluation. Therefore, it is difficult to conclude the actual state of the refrigerant at the capillary tube inlet. Visual observation confirmed the reported alternating vapour-liquid entrance for all performed tests.

Figure 45 provides an example of the swirl formed at the entrance of the capillary. The heat balance methodology indicated that, except for the two lowest flow rates, all others indicated a certain low subcooling (around 3 K). Pressure and temperature measurements indicated a much higher subcooling. Furthermore, the vapour temperature measured above the filter dryer was always below the saturation temperature, and practically at the same temperature than the subcooled liquid. Figure 51 provides a comparison of the vapour temperature measured at the capillary tube inlet $T_{filterIN}$ and the refrigerant temperature measured at the condenser outlet $T_{condOUT}$.

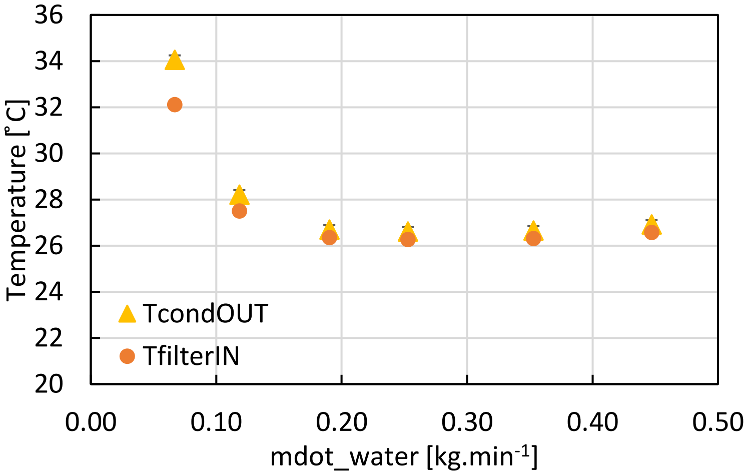

Figure 51: Comparison between condenser outlet temperature and capillary tube inlet temperature

The authors did not find an explanation for the measured refrigerant state since the condensation process happened quite slowly and the vapour bubbles had enough time to condensate along the tube or inside the filter dryer small volume. However, all measurements clearly indicated subcooled conditions for both liquid and vapour, and visualisation of the inlet of the capillary tube revealed the entrance of vapour and liquid. Lee et al. [16] and Ko and Jeong [17] have observed this paradoxical state and attributed it to non-equilibrium conditions. Their results have demonstrated that a two-phase refrigerant flow exists in the subcooled region in both commercial refrigerator-freezers and domestic refrigeration systems. The measured temperatures of the gas phase and liquid phase in the subcooled region were 11.8 °C and 11.5 °C, respectively, but the saturation temperature was 29.6 °C. Thus, these authors concluded that it indicated a thermodynamic non-equilibrium flow coexisted with the subcooled gas and the subcooled liquid was present in the subcooled region, despite the subcooled condition.

They developed an enthalpy calculation method that considered the mixture of subcooled vapour and subcooled liquid. The void fraction calculation method using a video image was proposed to calculate quality. Compared with the provided void fraction value, the calculated void fraction predicted the void fraction well with an error of 2.1%. Compared with the heat balance method, the calculated enthalpy also predicted the specific enthalpy value well with an error of 0.7%. However, the thermodynamic properties table can not be used for non-equilibrium conditions.

Regarding the possible effect of oil in the reported phenomena, a reasonable oil ratio in the circulating fluid would have a small impact on condensation temperature. Figure 52 depicts the refrigerant temperature with respect to the vapour pressure and oil concentration. A vapour pressure of 4 bar and an oil concentration percentage of 70% is assumed. If a higher oil concentration (75%) is reached, the temperature increases by around 5 ºC. Assuming a more reasonable oil concentration percentage than the one depicted in Figure 52, the red curve would be much more horizontal and then the effect on temperature would be much lower. It would have a small effect on the subcooling calculation; oil presence could be part of the explanation for the differences observed between SC_{HX} and SC_{pT} but is not the only reason. Indeed, Lee et al. [16] and Ko and Jeong [17] have performed experiments with an oil separator at the compressor outlet but the difference between $h_{condOUT-pT}$ and $h_{condOUT-HX}$ remained high, as depicted in Figure 53.

From these considerations, it can be concluded that refrigerant conditions at the capillary tube inlet may have been in a non-equilibrium two-phase flow composed of subcooled liquid and subcooled vapour. In addition, the enthalpy at the condenser outlet can thus not be determined using the thermodynamic properties table, which is only valid for an equilibrium condition of the refrigerant.

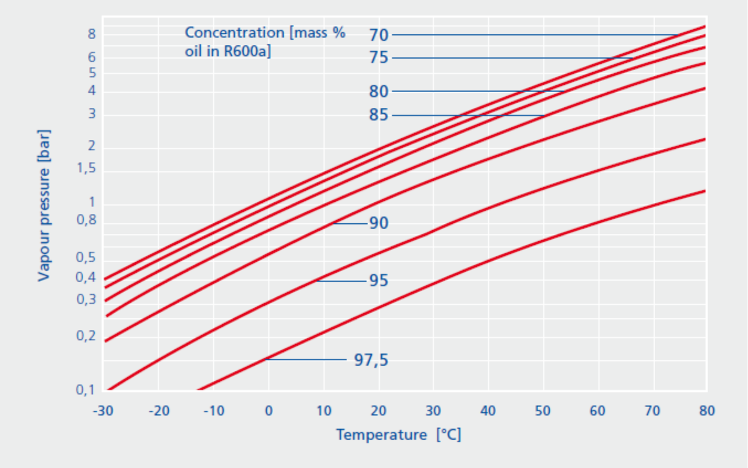

Figure 52: Approximate diagram for R600a/oil

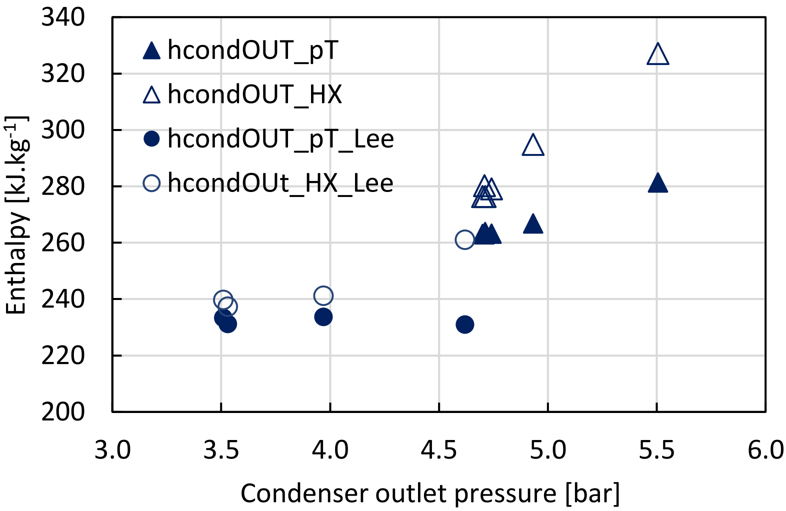

Figure 53: Enthalpies evaluated from the pressure and temperature measurements and the assumption of thermodynamic equilibrium, and enthalpy evaluated from the inlet refrigerant conditions and the heat measured on the water side compared with data obtained by Lee et al. [16].

3.4.3 Possible explanation of vapour at the capillary tube inlet

A possible explanation for this permanent existence of vapour at the capillary tube entrance is that the capillary tube was oversized and therefore, the inlet should be necessary under two-phase flow conditions to match the compressor flow rate with the flow rate through the capillary tube, in a way that flow rate is sufficiently low to match the compressor flow rate.

This potential situation is depicted in Figure 54 where the compressor flow rate is characterised by a line with a negative slope, since it decreases with the pressure ratio increase. A line with positive slope represents the flow rate through the capillary tube, which increases with the pressure ratio. The curves present a qualitative and orientative situation and are not quantitatively representative of an actual working.

The balance point, the intersection of these two lines, represents the stable operation point in which the refrigerant flow rate through the compressor and capillary tube is balanced. The flow rate through the capillary tube with two-phase flow inlet is marked with a dashed line, whereas the zone inlet with liquid refrigerant is indicated by a solid line. That the balance point requires the flow through the capillary tube to be two-phase explains why it is not possible to obtain saturated or subcooled liquid conditions at the tube entrance, and why an alternating liquid-vapour inlet is visualised in a way that the average mass flow rate matches the compressor mass flow rate.

This argument accounts for the presence of vapour at the capillary tube inlet. However, the subcooled state of this vapour is not explained. The balance of mass flow rates would justify that the inlet is two-phase flow. The liquid could certainly be subcooled since the liquid has good contact with the wall, which is at a lower temperature than the condensation.

However, the vapour should keep saturation conditions at the liquid-vapour interface. A combination of subcooled liquid and saturated vapour should be found since the transparent tube set up at the condenser outlet could be defined as adiabatic compared with a normal tube. In this case, refrigerant could have sufficient length to achieve equilibrium state or, at least, reveal some evolution towards the equilibrium. However, this is not what it is measured; vapour seems to be in subcooled conditions, as reported in the present study and by other authors.

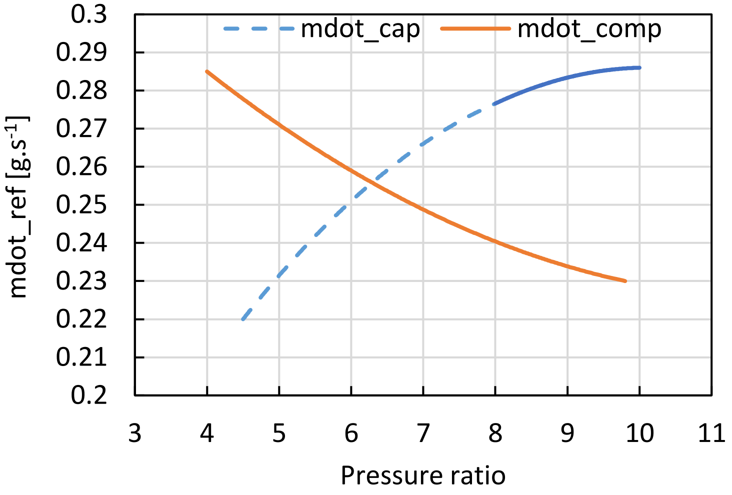

Figure 54: Refrigerant mass flow rates matching

3.5 Conclusions

Conditions at the capillary tube inlet in a commercial household refrigerator were assessed; a refrigerant-to-water heat exchanger was used in place of the original refrigerant-to-air condenser and from the heat balance at the water condenser, refrigerant conditions at the capillary tube inlet were measured.

By varying the water mass flow rate circulating in the water condenser, the condensing conditions on the refrigerant side were modified. Visualisations of the condenser outlet revealed that the presence of vapour in the flow pattern significantly decreased when the refrigerant condensation temperature decreased. Nevertheless, two-phase conditions remained at the capillary tube inlet for each water mass flow rate tested. The heat balance methodology indicated that, except for the two lowest water mass flow rates tested, all others revealed a certain low subcooling (around 3 K). Pressure and temperature measurements indicated a much higher subcooling, which contradicted the visualisation at the capillary tube inlet. Furthermore, the vapour temperature measured above the filter dryer was always below saturation temperature, which was essentially the same as the subcooled liquid.

This paradoxical phenomenon was attributed to the presence of non-equilibrium two-phase flow composed of subcooled liquid and subcooled vapour at the capillary tube inlet. Some authors have observed the same paradoxical phenomenon [16], [17]. The enthalpy at the condenser outlet can thus not be determined using the thermodynamic properties table, which is valid only for an equilibrium condition of the refrigerant. The presence of air and oil in the circuit was ruled out as a possible explanation for the exposed phenomenon. Rather, the presence of vapour at the capillary tube inlet could also be explained by the capillary tube being oversized. Therefore, to match the compressor flow rate with the flow rate through the capillary tube, the capillary inlet should be necessary under two-phase flow conditions, in a way that the flow rate is sufficiently low to match the compressor flow rate. The next chapter proposes a new configuration design to fill the capillary tube inlet with liquid. However, an explanation for why this vapour is found in a subcooled state is not provided.

Chapter 4

How to get full liquid conditions at the capillary tube inlet?

4.1 Objectives

To investigate whether the cause of the two-phase flow inlet, as argued in chapter 3, was the capillary tube being too large for the compressor flow rate, another experimental campaign was performed. The capillary tube was changed to a smaller size, i.e., 0.55 mm nominal diameter (the original was 0.6 mm), and the compressor speed was increased to determine the balance point at which the inlet of the capillary tube could be full of liquid.

The purpose here was not to analyse a commercial refrigerator, but to focus on the possibility of filling the capillary tube only with liquid. Two slight modifications were implemented in the test bench for this experimental campaign, which are described in the following sections.

4.2 Modification of the test bench

For a complete test bench description, see chapter 3, section 3.2. A smaller capillary tube of 0.55 mm was set up in parallel to the original and with the same configuration (Figure 55). The length of the capillary tube was kept identical to the original.

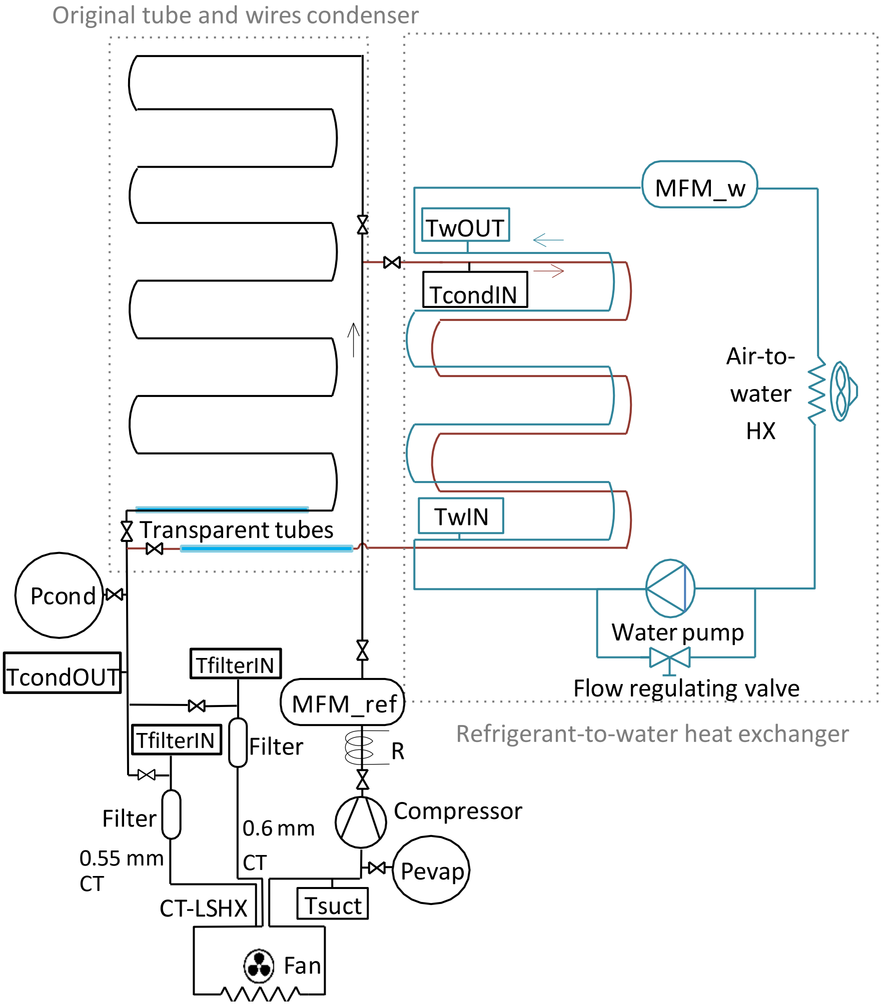
Original tube and wires condenser
MFM_w
TwOUT
TcondIN
Air-to-
water
HX
TwIN
Transparent tubes
Pcond
TcondOUT
TfilterIN
TfilterIN
MFM_ref
Filter
R
Water pump
Flow regulating valve
Refrigerant-to-water heat exchanger
Filter
0.55 mm
CT
0.6 mm
CT
Compressor
Pevap
CT-LSHX
Tsuct
Fan

Figure 55 : Test bench

4.2.1 Temperature regulation

During this experimental campaign, the damper was kept closed, and the tests were run only with the freezer, because, as commented on in the previous section, the purpose was not to analyse a commercial refrigerator, but to focus on the possibility of filling the capillary tube only with liquid. To regulate the temperature in the freezer and ensure the same temperature conditions for the entire test campaign, the previous PID and heater set up was modified. Instead of being placed close to the freezer temperature measurement, the thermocouple used by the PID was placed at the evaporator air inlet (Figure 56).

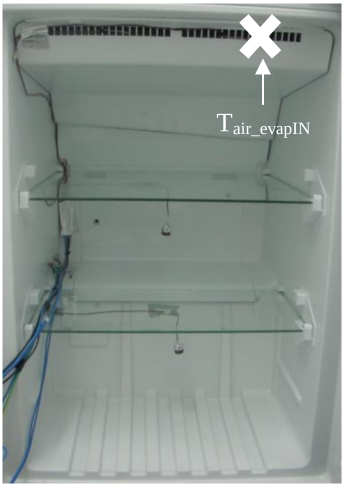

Figure 56: Air evaporator inlet thermocouple location

This type of control insured that the conditions of the secondary fluid at the evaporator inlet were always the same for each operating parameter to be tested, despite the variation of cooling capacity produced by the variation of the compressor speed. The air temperature at the evaporator inlet T_{air_EvapIN} of a household refrigerator is composed of a mix of air coming from the FF compartment (T_{FF}) and air coming from the FZ compartment (T_{FZ}). Eq. 4.1. allows the evaluation of the corresponding mixing temperature:

$$T_{air\_EvapIN} = \alpha T_{FF} + (1-\alpha) T_{FZ} \qquad 4.1$$

Where α represents the air flow ratio supplied to the FF cabinet. This air flow ratio is usually between 0 and 30 %. In the following experimental campaign, T_{air_EvapIN} has been fixed to -13.5 ºC, which corresponds to a air flow ratio of 20 %.

4.2.2 Temperature at the filter inlet

As discussed in chapter 3, the vapour at the capillary tube inlet appeared to be subcooled. This conclusion was based on the temperature reading at the top of the vapour separation device (installed above the filter), which provided a value below saturation. Given that the RTD was placed vertically in the middle of the tube, it is possible the sensor reading was affected by the heat exchanged by radiation between the sensor tip and the surrounding walls. The device outer wall temperature being quite close to the ambient temperature could justify that a vapour temperature value below saturation was measured. Therefore, an analysis of this possible effect was conducted before initiating the tests.

This situation is presented in Figure 57. Inside the copper tube, the external surface of the RTD transfers heat by radiation towards the copper tube wall, whereas the vapour transfers heat by convection to the RTD rod. The reading of the RTD corresponds to the balance temperature, which is intermediate between the vapour and inner wall temperature.

Eq. 4.2 describes the convection heat calculation and eq. 4.3 the equation for the radiation heat. The geometric and temperature parameters explanations for both equations is presented in Figure 57. Table 45 presents the different parameters and their values.

$$\dot{Q}_{conv} = \pi dint_{RTD} L h (T_{vap} - T_{filterIN}) \tag{4.2}$$

$$\dot{Q}_{rad} = \sigma \frac{T_{filterIN} - T_{wall}}{\frac{1-\varepsilon_{RTD}}{\pi dint_{RTD} L \varepsilon_{RTD}} + \frac{1}{\pi dint_{RTD} L} + \frac{1-\varepsilon_{tube}}{\pi Dint_{tube} L \varepsilon_{tube}}} \tag{4.3}$$

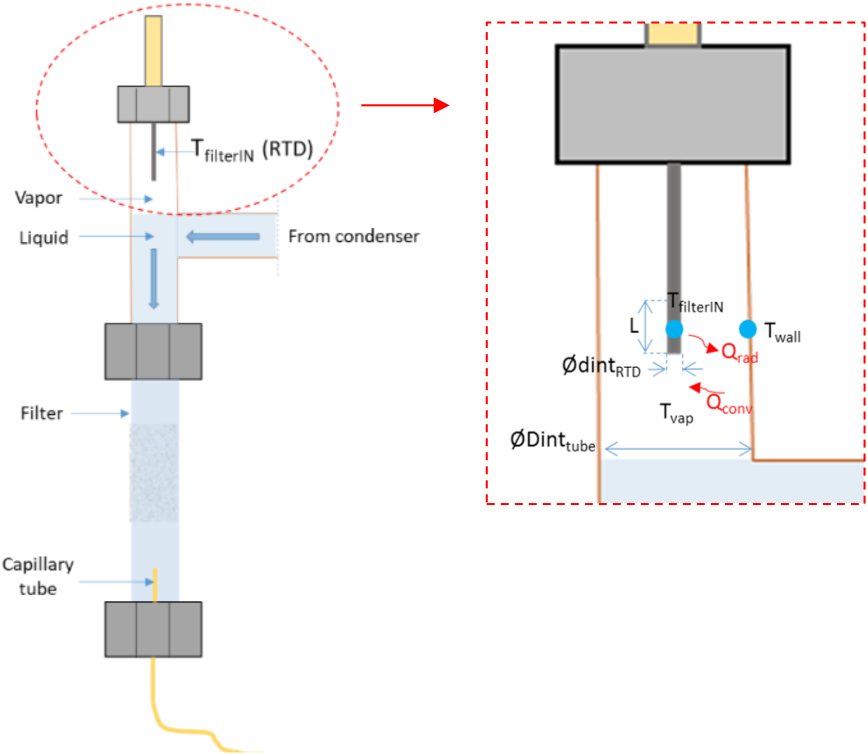
$T_{filterIN}$ (RTD)
Vapor
Liquid
From condenser
Filter
Capillary tube
$T_{filterIN}$
L
T_{wall}
Q_{rad}
$Ødint_{RTD}$
Q_{conv}
T_{vap}
$ØDint_{tube}$

Figure 57: Heat exchange inside refrigerant circuit

If the inner surface of the copper tube is at ambient temperature, the maximum error in the evaluation of the vapour temperature would be 3.3°C. In the case of a vapour temperature of 35℃, then 31.7°C would be the actual vapour temperature. Result sensitivity of the considered emissivities is low. Considering that the recorded values of vapour subcooling are much larger, e.g., 10 K, the effect of the error due to potential radiation would only explain a fraction of the measured subcooling.

That said, to limit the radiation effect on the sensor, a radiation shield manufactured with aluminium foil was installed around the sensor tip, as illustrated in Figure 58. The original copper tube was substituted with a piece of transparent PFA tube to better isolate the vapour and, at the same, allow inspection to ensure the aluminium shield did not touch the RTD surface.

Table 45: Estimation of the radiation effect on the measurement of the vapour temperature at the capillary tube inlet

Parameters	Value
$\varnothing dint_{RTD}$ (mm)	1.5
$\varnothing Dint_{tube}$ (mm)	10
L (mm)	0.28
T_{wall} (°C)	25
T_{vap}(°C)	35
ε_1, RTD surface emissivity	0.5
ε_2, tube surface emissivity	0.7
h, heat transfer coefficient ($W.m^{-2}.K^{-1}$)	6
σ, Stefan-Boltzmann constant ($W.m^{-2}.K^{-4}$)	$5.67.10^{-8}$
Result	
$T_{filterIN}$ (°C)	31.7

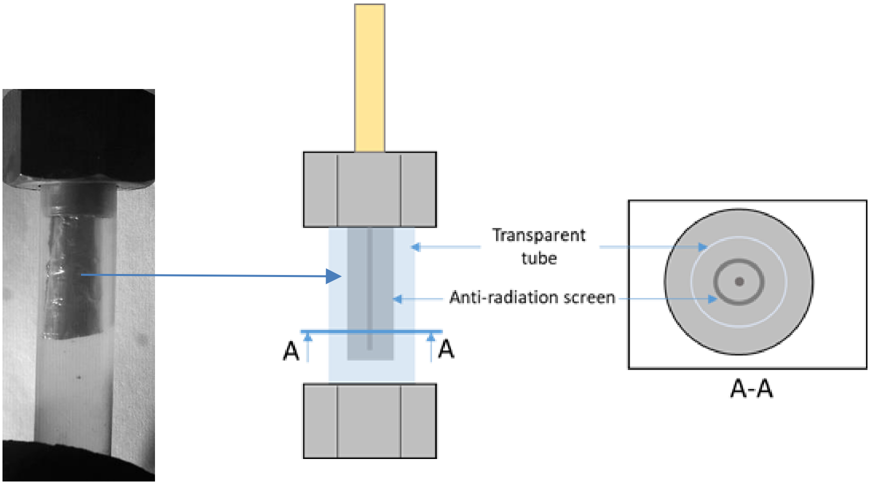

Figure 58: Set up of the anti-radiation shield around the RTD

As shown in Figure 58, some droplets were visible at the radiation shield during the experiments. Therefore, there was slight condensation around the shield, and as such, the shield should have been close to saturation temperature. However, the RTD readings were below saturation and thus confirming the existence of subcooled vapour. New measured subcooling values with the anti-radiation shield proved to be similar to the previous ones.

4.3 Experimental campaign

4.3.1 Tests conditions

Different velocities were tested, namely 1800 rpm, 2500 rpm and 3500 rpm. Each compressor speed tested was maintained during at least six-hour tests. The compressor speed was returned to 1800 rpm between each point tested. The sequence of tests was performed with a unique refrigerant charge and a fixed water mass flow rate at the condenser side. The air temperature at the inlet of the evaporator was kept constant for each compressor speed tested by manually regulating the power of the heater inside the FZ. Table 46 describes the test conditions for experimental campaign 4.1.

Table 46: Test conditions for experimental campaign 4.1

Parameter	Configuration
T_{air_EvapIN} (°C)	-13.5
Water mass flow rate (kg.min^{-1})	0.28
Climate chamber temperature (°C)	25
Compressor speed (rpm)	From 1800 to 3500
Temperature regulation	Heater
Refrigerant charge (g)	64
Control type	Labview
Test type	Steady
Condenser	Refrigerant-to-water

Capillary tube diameter (mm)	0.55
Filter position	Vertical
Test aim	Fill with liquid the capillary inlet

4.3.2 Flow visualisation varying compressor speed

Figure 59 schematically depicts the liquid level observed at the capillary tube inlet for each test and each compressor speed.

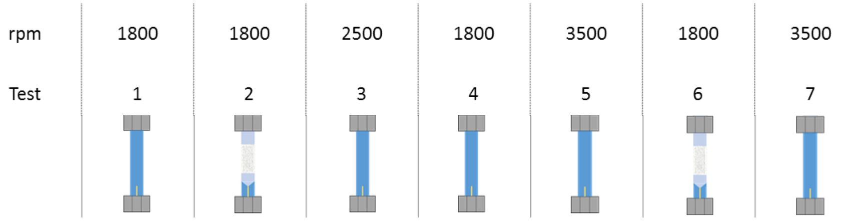

Figure 59: Observed refrigerant liquid level for the different tests

Tests numbered 1, 3, 4, 5 and 7 correspond to a filter full of liquid, as depicted in Figure 60.a. All transparent parts of the filter were full of liquid but the level did not reach the upper transparent section where the RTD with the anti-radiation shield was installed. Liquid conditions at the capillary tube inlet were maintained along these tests. However, tests labelled 2 and 6 were alternated between two different liquid level situations at the capillary tube inlet: apparent liquid level about 5 mm above the capillary tube inlet (Figure 60.c) and a swirl with two-phase inlet (Figure 60.b). Importantly, this only happened at the lowest speed: 1800 rpm. A qualitative analysis of the alternating flow was performed for a five-second test (Figure 61). A high speed PCO camera was used to record the sequence. The blue area represents times when the liquid level was above the capillary tube and the white area, times when the capillary tube inlet was two-phase flow. The alternating flow does not seem to follow a regular pattern. Nevertheless, the capillary tube is mostly sucking only liquid, a proportion of 95%, during the five-second test. Visualisation of the condenser outlet

(Figure 62) allows clear observation of the void fraction evolution, i.e., the highest the compressor speed, the lower the void fraction.

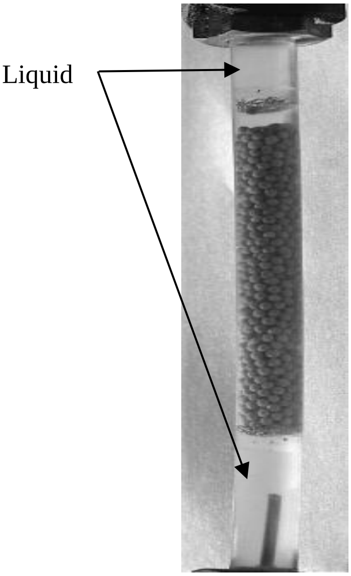

a) Full liquid inlet at 1800 rpm: tests 1 and 4 ; at 2500 rpm: test 3 ; at 3500 rpm: tests 5 and 7

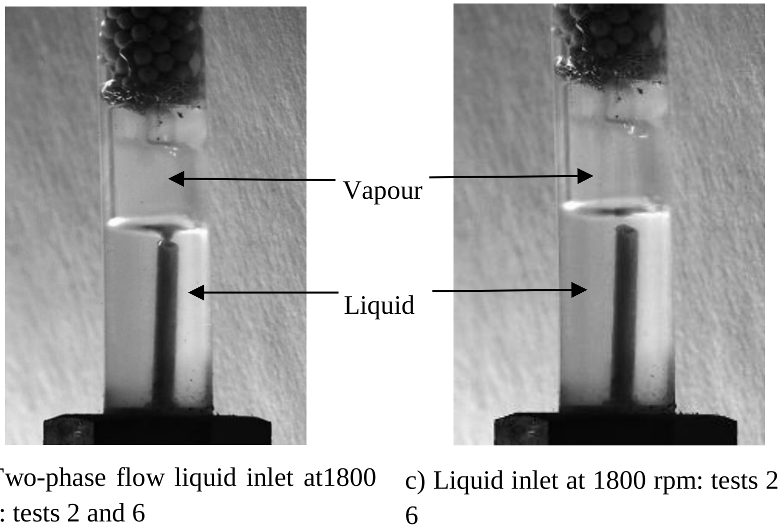

b) Two-phase flow liquid inlet at1800 rpm: tests 2 and 6

c) Liquid inlet at 1800 rpm: tests 2 and 6

Figure 60: Different liquid levels at the capillary tube inlet

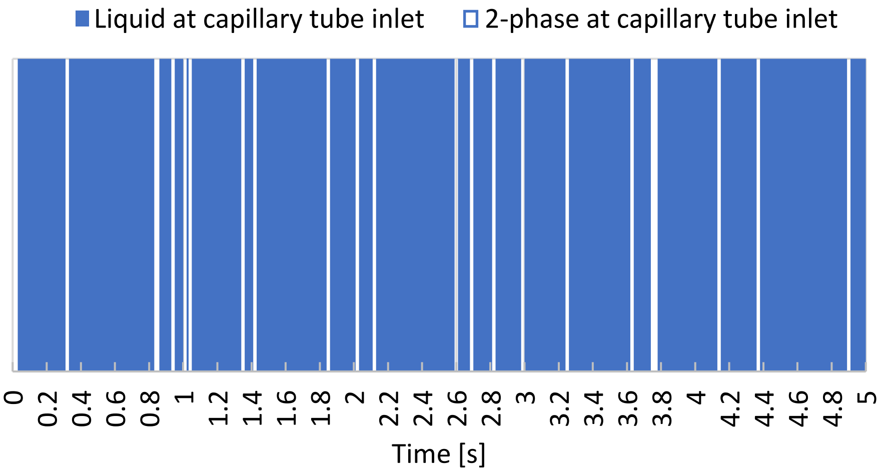

Figure 61: Liquid level evolution at the capillary tube inlet for tests 2 and 6

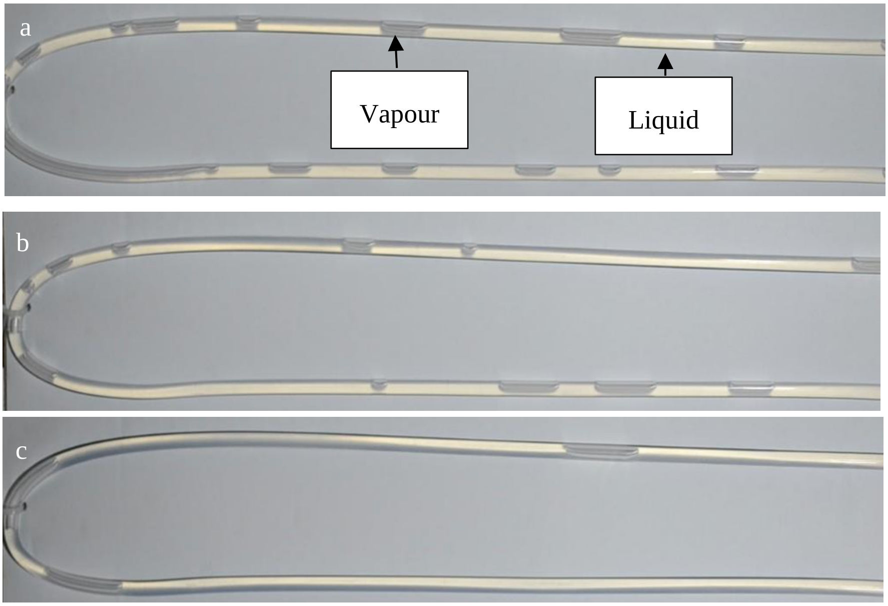

Figure 62: Condenser outlet for different compressor speeds a) 1800 rpm b) 2500 rpm and c) 3500 rpm

4.3.3 Results and discussion

Even though at 3500 rpm, the lower part of the filter was full of liquid and the void fraction upstream was almost negligible, the difference between the two subcooling measurements, e.g. SC_{pT} and SC_{HX}, persisted, as depicted in Figure 63.

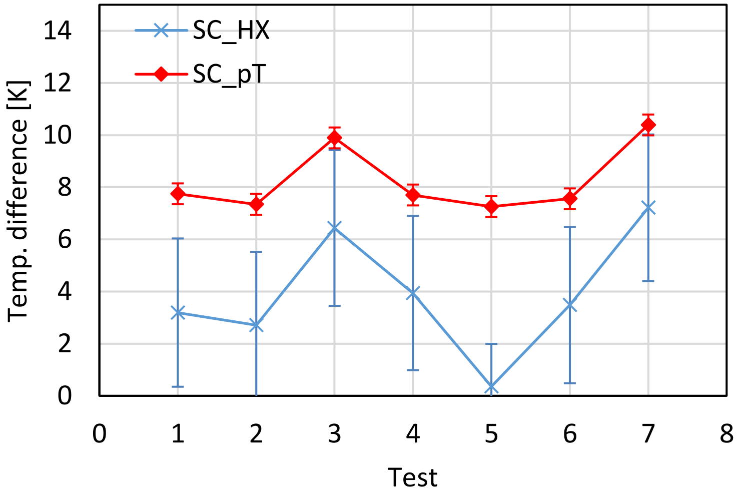

Figure 63: Subcooling evaluated from the pressure and temperature measurements and the assumption of thermodynamic equilibrium (SC_pT), and subcooling evaluated from the inlet refrigerant conditions and the heat measured on the water side (SC_HX)

Although both means of estimating the subcooling led to different values, both indicated a subcooled refrigerant state at the capillary tube inlet, except for test 5.

As explained in the previous chapter, the presence of subcooled vapour did not allow for calculating the actual subcooling from the thermodynamic charts (SC_{pT}) because of the assumption of equilibrium conditions. Interestingly, the difference between both ways to estimate subcooling is highly variable, with the values of SC_{pT} being high and quite constant, as was observed in the previous test campaign (experimental campaign 3.4, chapter 3). For all tests run at 1800 rpm, the difference between SC_{pT} and SC_{HX} remained constant and equal to 4 K. Note that for both points tested at 3500 rpm (points 5 and 7), the difference between the subcoolings was not the same. From point 5 to 7, the SC_{pT} increased from 7.3 K to 10.4 K. From almost no SC_{HX} for point 5, the value increased to 7.2 K for point 7. This large difference can be explained by the refrigerant flow rate value that suddenly “jump” during test 5 and increased by around 45% to reach 0.41 $g.s^{-1}$ (Figure 64).

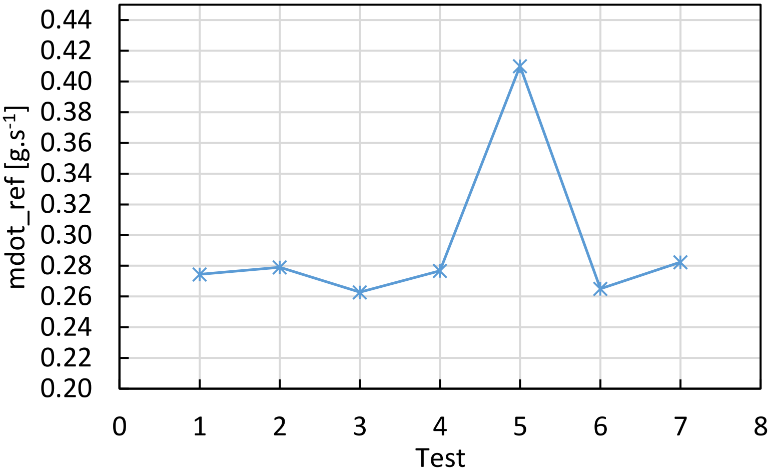

Figure 64: Refrigerant mass flow rate through tests campaign

Could the variation of the controllable parameters (water mass flow rate and air inlet evaporator temperature) be the reason for this difference in operating conditions? Indeed, both points presented a water mass flow rate difference of 1.5% (Figure 65), which might have affected the operating conditions.

A brief analysis of the presented experimental campaign and, more generally, all data collected during various repetition of the tests, demonstrated that this assumption was invalid. For example, points 1 and 4 presented a difference of 5% in water mass flow rate, but the operating conditions did not seem to be affected since both points presented the same refrigerant mass flow rate (Figure 64).

Two different working points were obtained at 3500 rpm due to a sudden “jump” in the mass flow rate, which led the system to a completely different working point. The low variation of the controllable parameters did not seem to be a valid explanation for this change. To reach the same air conditions at the evaporator inlet, the heater power was increased by around 16% from point 5 to point 7 and the compressor power decreased by the same proportion (Figure 66).

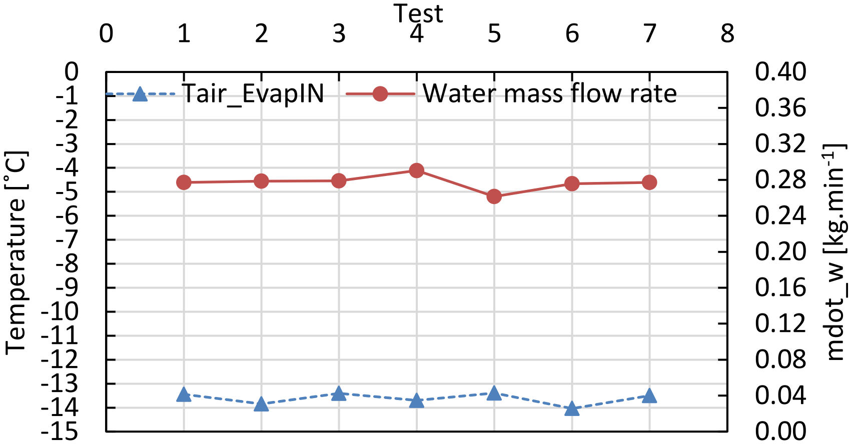

Figure 65: Controlled parameters through tests campaign

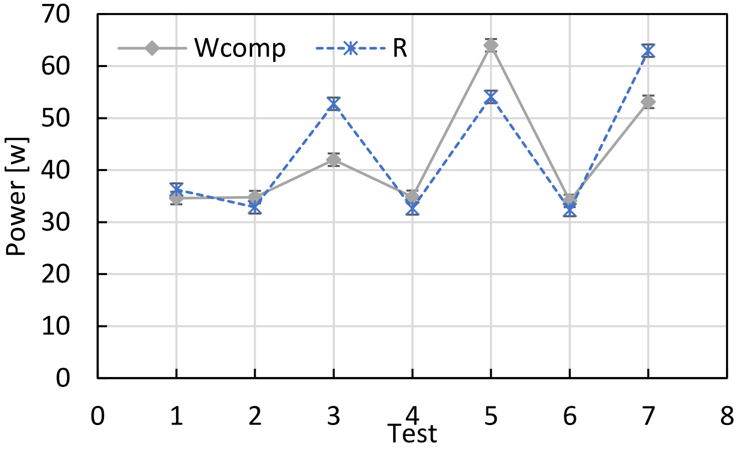

Figure 66: Compressor power and resistance power through tests campaign

This had already been detected on other occasions, indicating that the test results depended somewhat on the history of how the test conditions were obtained, with some random variation not possible to control. As a result, we could obtain stable operation with the same conditions but different performance. An explanation of the difference in refrigerant mass flow was found in the literature.

As demonstrated in chapter 1, a certain hysteresis effect of the refrigerant mass flow rate can occur and a metastable length can be created inside the capillary tube (chapter 1, section 1.3.3). The next section provides more detail to explain the experimental results of the present work.

Meyer and Dunn [26] have found the existence of a hysteresis effect on the mass flow rate with respect to subcooling variation. The authors carried out an experimental test by increasing, then decreasing, the level of subcooling. As depicted in Figure 67, two different levels of refrigerant mass flow rate were found, depending on how the subcooling was obtained. Figure 67 also illustrates the jump in mass flow rate at 9 ºF subcooling, which declined by more than 5% during the decreasing subcooling profile.

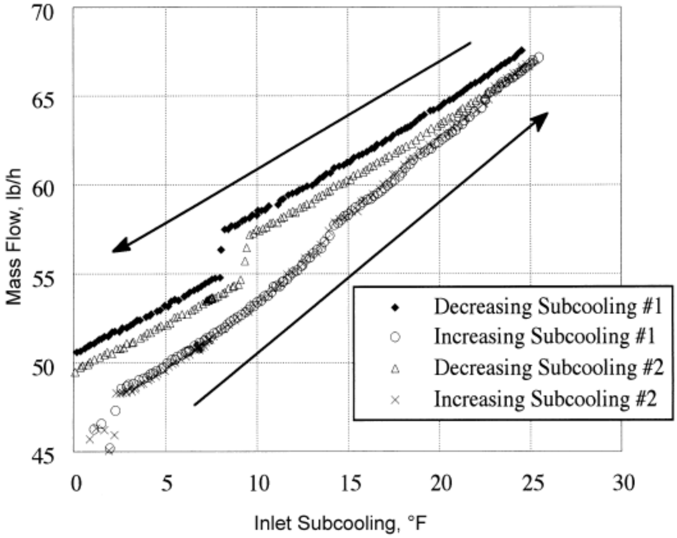

Figure 67: Hysteresis in the capillary tube mass flow rate [26]

The authors explained that when the subcooling is decreasing, a metastable region inside the capillary tube may be created and lengthened, thus resulting in a substantially higher mass flow. Once the underpressure of vaporisation becomes too high, the metastable region collapses to a shorter one. The authors also found that the capillary tube roughness played a dominant role in the length of the metastable region. Meyer and Dunn also highlighted that the lower the capillary tube inlet pressure, the higher the effect of the metastable length and thus, the higher the difference between mass flow rates for the increasing subcooling condition and the decreasing subcooling condition. The importance of the history of how operating conditions have been approached was also emphasised.

Similar results were found by Liu and Bullard [13], who demonstrated that the hysteresis effect on mass flow rate could have an influence of 6% on the COP. However, this hysteresis effect was not repeatable.

Bittle [27] studied the repeatability of the metastable liquid region effect and dependency of the controllable parameters. To this end, he compared two response rates of the capillary tube inlet temperature to reach a given steady state. In the first set of tests, he rapidly increased the temperature rate at the capillary tube inlet (fast response test). In the second set of tests, he gradually increased this temperature. These tests demonstrated some dependence of the refrigerant mass flow rate with respect to the inlet response rate; the mass flow rate was 19% higher for slow response test. Like Liu and Bullard [13] and Meyer and Dunn [26], Bittle demonstrated that the mass flow rate level of variation was much higher for lower subcoolings.

Figure 68 illustrates the variation in the mass flow rate with respect to the SC_{pT} level for various experimental campaigns. For lower SC_{pT}, higher variation in mass flow rate was observed. For each compressor speed, only the point with the same metastable length is represented, so as to be comparable (e.g., the mass flow rate obtained for test 5 is not depicted).

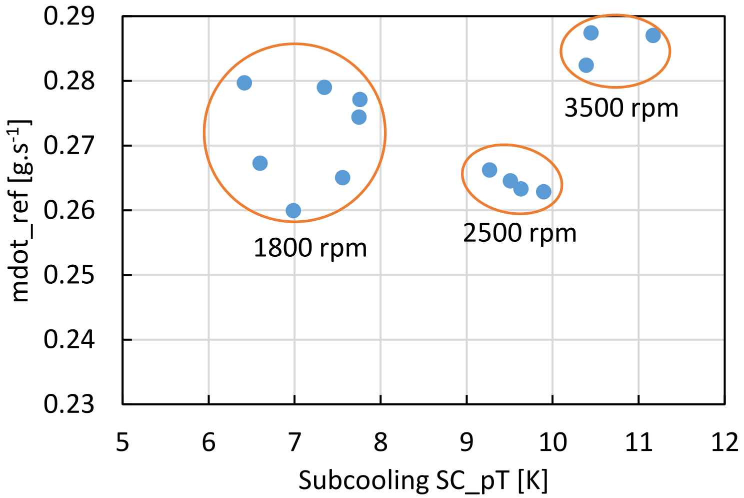

Figure 68: Mass flow rate variation vs. SC_PT measured subcooling for different compressor speeds

Therefore, the explanation for the two working points obtained with the same input parameters (tests 5 and 7) could be that during test 5, a metastable liquid region was present, while, during test 7, the metastable liquid region was non-existent or minimal.

Furthermore, it would explain why refrigerant mass flow rate for test 3 (at 2500 rpm) was lower than for test 1 (at 1800 rpm), as depicted in Figure 69. Indeed, when compressor revolutions were increased, the refrigerant mass flow rate started increasing as expected. Then, the rate decreased and became lower than for 1800 rpm. This would mean that a metastable region was present at 1800 rpm but collapsed when revolutions were increased from 1800 rpm to 2500 rpm.

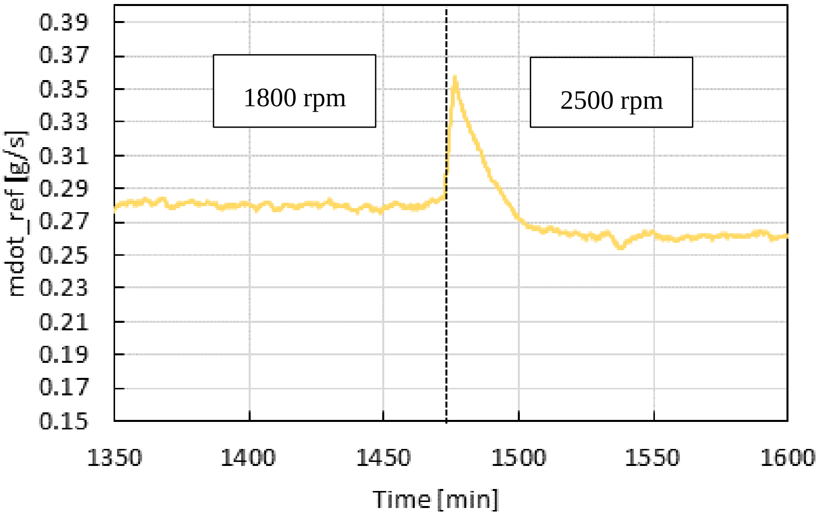

Figure 69: Change in refrigerant mass flow rate from 1800 rpm to 2500 rpm

Even though the purpose of the present work is not to study this effect, it appeared interesting to try to verify this assumption. The test with 1800 rpm was repeated with attempts to collapse the metastable length, actuating on the controllable parameters. Both water mass flow rate and air temperature at the evaporator inlet were modified, as listed in Table 47.

Table 48 lists the results of test one and test two of experimental campaign 4.2. Test 1 (respectively, test 2) corresponds to the values of the operating conditions before (respectively, after) the increase in the observed refrigerant mass flow rate. The cooling capacity was calculated using Eq. 4.4:

$$\dot{Q}_{cool} = \dot{m}_{ref}\left(h_{suct} - h_{condOUT\_\mathrm{HX}}\right) \qquad 4.4$$

The refrigerant mass flow rate dropped by around 15% between the two tests and the condensation temperature remained stable, whereas the evaporation temperature decreased by 10%. The suction temperature increased to around 20 °C. This difference in operating conditions shifted the system to a completely different working point.

Table 47: Test conditions for experimental campaign 4.2

Parameter	Configuration
T_{air_EvapIN} (°C)	-12
Water mass flow rate (kg.min^{-1})	0.46
Climate chamber temperature (°C)	25
Temperature regulation	Heater
Refrigerant charge (g)	64
Control type	Labview
Test type	Steady
Condenser	Air
Capillary tube diameter (mm)	0.55
Filter position	Vertical
Compressor speed (rpm)	1800
Test aim	Metastable length inside capillary tube study

The liquid level in both tests was also different. Before the metastable length in the capillary tube collapsed (test 1), the capillary tube was alternating both liquid and two-phase flow inlet, as seen in experimental campaign 4.1. An initial conclusion could be that when a metastable length is present inside the capillary tube, it is not possible to fill the filter. However, this is not always the case since, as seen in experimental campaign 4.1, full liquid conditions at the capillary tube inlet were obtained at 1800 rpm without change in the refrigerant mass flow rate. Tests 2 and 4 had the same refrigerant mass flow rate, but the liquid level inside the filter was notably different.

Table 48: Comparison of test with (test 1) and without (test 2) metastable length in capillary tube

Parameter	Value for test 1	Value for test 2	Difference
SC_pT (K)	5.9	6.7	+0.8°C
SC_HX (K)	2.2	5.8	+3.6°C
T_{evap} (°C)	-20.6	-22.6	-10.0%
T_{cond} (°C)	33.4	33.7	0.8%
T_{suct} (°C)	0.9	19.7	+18.8°C
$\dot{m}_{ref}$ $(g.s^{-1})$	0.288	0.245	-14.9%
$\dot{m}_{w}$ $(kg.min^{-1})$	0.455	0.468	2.8%
$\dot{Q}_{cool\_ref}$ (W)	82.4	79.7	-3.3%
$\dot{W}_{comp}$ (W)	34.9	33.1	-5.3%
COP	2.36	2.41	+2.1%
R (W)	39.5	46.8	18.5%
T_{air_EvapIN} (°C)	-12.0	-12.3	2.7%
Filter level	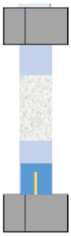	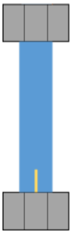	

The same air evaporator inlet temperature as test 1 was obtained for test 2 by increasing the heater power to 7.3 W.

With fan power and temperature parameters (ambient temperature and air evaporator inlet temperature) being constant, an increase of heater power R from test

1 to test 2 should have resulted in an increased refrigerant cooling capacity by the same proportion. However, the opposite occurred; the cooling capacity (calculated at the refrigerant side) in test 2 was 3.3% lower than in test 1.

For some cases, the error on the cooling capacity calculation was higher, as observed in Figure 70, which represents cooling capacity at the refrigerant side, compressor power and heater power for test campaign 4.1. The increase in heater power did not match the increase of cooling capacity for tests 3 and 7—cases where there was no or minimal metastable length. For test 3, from 1800 rpm to 2500 rpm, the heater power was increased to 19.9 W (Figure 70) to maintain air temperature at the evaporator inlet. Thus, it was expected that the cooling capacity would increase by the same proportion. However, the cooling capacity only increased by 6.7 W. Comparing both tests with 3500 rpm (tests 5 and 7), the increase in the heater power of 21.5 W from test 4 to test 5 results in an increase of cooling capacity by 21.1W. These values did not match but the difference was more reasonable than for test 7. In test 7, it is believed that the metastable length inside the capillary tube was minimal, and the increase of 30.7 W in heater power from test 6 to test 7 corresponded to an increase in the cooling capacity by only 15.5 W.

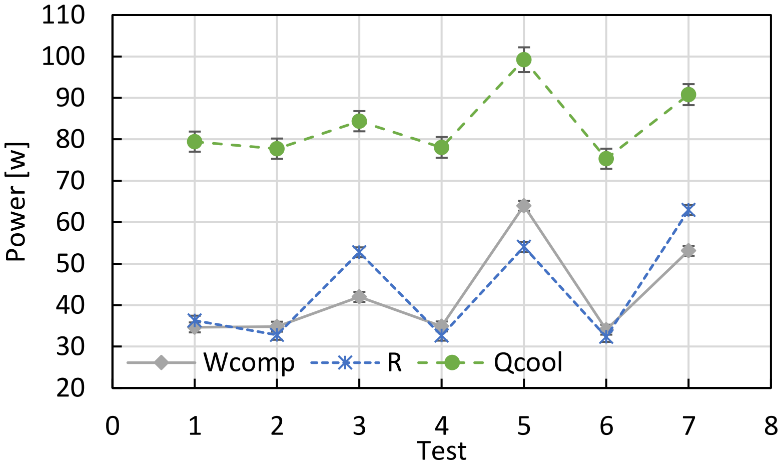

Figure 70: Evolution of cooling capacity, resistance power and compressor power across the tests

Therefore, when a metastable length was present in the capillary tube, it seems that the error in the cooling capacity calculation was lower than for cases with no metastable length. Further tests would be required to find an explanation of this phenomenon.

To estimate the actual cooling capacities, a calculation of the cooling capacities from the air side measurements was conducted. The cooling capacity at air side $\dot{Q}_{cool\_air}$ is a function of fan power W_f, resistance power R and heat gain from ambient, as stated in Eq. 4.5, where UA_{FZ} is the freezer overall thermal conductance, T_{amb} the ambient temperature and T_{air_evapIN} the air temperature at the evaporator inlet.

$$\dot{\mathrm{Q}}_{\mathrm{cool\_air}} = \mathrm{UA}_{\mathrm{FZ}}(\mathrm{T}_{\mathrm{amb}} - \mathrm{T}_{\mathrm{air\_evapIN}}) + \dot{\mathrm{W}}_{\mathrm{f}} + \dot{\mathrm{R}} \qquad 4.5$$

An estimation of the heat gain from ambient can be performed using the cooling capacity calculated at the refrigerant side for cases where a metastable length was present as the calculation matched better for this case (Eq. 4.6).

$$\mathrm{UA}_{\mathrm{FZ}}(\mathrm{T}_{\mathrm{amb}} - \mathrm{T}_{\mathrm{air\_evapIN}}) \approx \dot{\mathrm{Q}}_{\mathrm{cool\_ref}} - \dot{\mathrm{W}}_{\mathrm{f}} - \dot{\mathrm{R}} \qquad 4.6$$

Table 49 compares the cooling capacities of both the refrigerant and air sides for experimental campaign 4.2. Both cooling capacities were equal for test 1 because the heat gain from the ambient was taken as reference for the air cooling capacity calculation. This calculation of cooling capacity at the air side for test 2 output a cooling capacity of 89.7 W instead of the 82.4 W calculated at the refrigerant side. From the same COP value between tests 1 and 2 with $\dot{\mathrm{Q}}_{\mathrm{cool\_ref}}$, an increase of 15% of COP was observed when $\dot{\mathrm{Q}}_{\mathrm{cool\_air}}$ was used for the calculation.The higher COP corresponded to a filter full of liquid.

Although the COP increase is important, it is not possible to conclude that the reason for this increase was the existence of liquid conditions at the capillary tube inlet. Indeed, the large difference in operating conditions of both tests 1 and 2 made the comparison difficult, and that the refrigerant charge remained the same during the entire experimental campaign must also be considered.

An optimisation of the refrigerant charge should be carried out prior to concluding that the existence of full liquid conditions at the capillary tube inlet leads to a better COP. This is the focus of the next chapter.

Table 49: Cooling capacity calculated on the refrigerant side vs cooling capacity calculated on the air side

Parameter	Value for test 1	Value for test 2	Difference
$\dot{Q}_{cool\_ref}$ (W)	82.4	79.7	-3.3%
$\dot{Q}_{cool\_air}$ (W)	82.4	89.7	+8.9%
COP (with $\dot{Q}_{cool\_air}$)	2.36	2.71	+15%

The same exercise was completed with the results from experimental campaign 4.1, taking test 1 as a reference for calculating heat gain from the ambient (different from experimental campaign 4.2 because of the difference in air temperature at the evaporator inlet). The results are presented in Figure 71. The underestimation of the cooling capacity in these tests was visible only when no metastable length was present (tests 3 and 7).

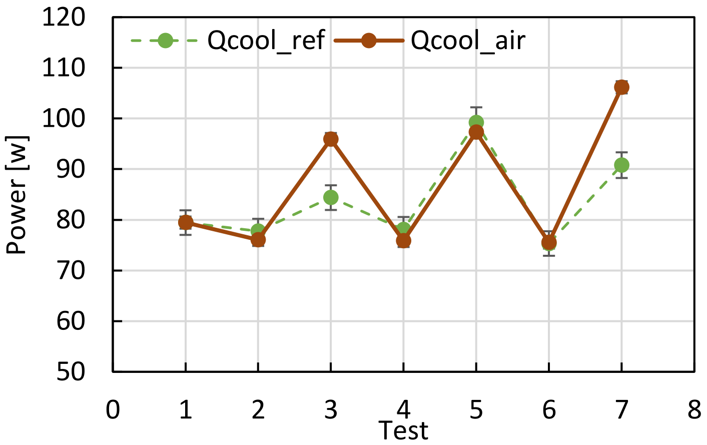

Figure 71: Re-evaluation of cooling capacity of the tests of test campaign 4.1

4.4 Conclusions

These findings demonstrate that a non-matching exists between both the capillary tube and compressor flow rate of a commercial household refrigerator.

Indeed, by increasing the compressor speed from 1600 rpm to 1800 rpm and reducing the capillary tube diameter from 0.6 mm to 0.55 mm, it was possible to fill the filter upstream from the capillary tube inlet with liquid, which resulted impossible with the original capillary tube.

However, at 1800 rpm, during the same experimental campaign and despite identical test conditions, the level of liquid was not repeatable. In this experimental campaign, the filter was always full of liquid at 2500 rpm and upwards. Also, repeatability of the liquid level through all realised tests was not observed.

The transparent tube set up at the condenser outlet revealed that the higher the compressor speed, the lower the void fraction. Nevertheless, although at 3500 rpm, the lower part of the filter was full of liquid and void fraction upstream was almost negligible, the difference between the two subcooling measurements, i.e., SC_{pT} and SC_{HX}, persisted. The subcooling value calculated from the thermodynamic conditions at the condenser outlet, assuming equilibrium, did not provide valid results due to the subcooled state of the vapour, as argued in chapter 3. That said, although the actual subcooling was difficult to assess, the refrigerant state was subcooled, although not in thermodynamic equilibrium. Vapour temperature measurements always resulted in below saturation values.

Additionally, it was found that other phenomena complicated the study of performance in this kind of system. First, by increasing the compressor speed, a sudden change in the operating conditions occurred due to a “jump” in the mass flow rate. The explanation of this phenomenon is attributed to the creation of a metastable region inside the capillary tube, according to the increasing or decreasing profile of the subcooling [13], [26], [27].

Second, the cooling capacity calculation at the refrigerant side did not provide logical results in some cases. Indeed, when changing from a given compressor speed to a higher one, the heater power increase inside the freezer to maintain air temperature at the evaporator inlet should have led to an increase in cooling capacity. However, the reverse occurred. The authors of this work do not have explanations for such a phenomenon.

To assess actual cooling capacity, cooling capacity from the air side was calculated, which confirmed that the cooling capacity calculation at the refrigerant side returned, in some cases, erroneous results.

At 1800 rpm, a higher COP was found when the capillary tube inlet was liquid with respect to a two-phase flow inlet.

Nevertheless, a comparison of both tests was difficult due to the large difference in operating conditions of both tests, which likely have different optimal refrigerant charges. Thus, the purpose of the next chapter is to analyse, through optimisation of the refrigerant charge, whether liquid at the capillary tube inlet results in better performance than two-phase flow inlet.

Chapter 5

Performance comparison between liquid and vapour conditions at the capillary tube inlet

5.1 Objectives

Chapter 4 demonstrated that a non-matching exists between the capillary tube and compressor flow rate of a commercial household refrigerator. Indeed, by increasing the compressor speed from 1600 rpm to 1800 rpm and reducing the capillary tube diameter from 0.6 mm to 0.55 mm, it was possible to fill the filter upstream from the capillary tube inlet with liquid, which would have been impossible with the original capillary tube and compressor speed.

The objective of this chapter is to determine whether there is a performance difference between a liquid and a two-phase flow condition at the capillary tube inlet. To that end, two capillary tubes of different diameters (0.55 mm and 0.6 mm) but same length were used. In the previous chapter, it revealed that it is possible to obtain full liquid conditions with a 0.55 mm diameter capillary tube inlet at higher compressor speeds than the original one. The comparison must be performed at the same compressor speed, i.e., 2900 rpm, which leads to two-phase flow inlet with the 0.6 mm diameter capillary tube and is sufficient to achieve full liquid inlet conditions with the 0.55 mm tube.

5.2 Experimental campaign

5.2.1 Procedure

First, the optimal system charge for each capillary tube must be determined at the established compressor speed to compare performance. The tests were carried out using the original condenser configuration to better assess the difference, if any, in actual refrigerator performance.

5.2.2 Determination of optimal charges with 0.55 and 0.6 mm capillary tubes

5.2.2.1 Test input

Table 50 summarises the test conditions of this experimental campaign.

Table 50: Tests conditions of experimental campaign 5.1

Parameter	Configuration
T_{air_EvapIN} (°C)	-13.4
Climate chamber temperature (°C)	25
Temperature regulation	Heater
Control type	Labview
Test type	Steady
Compressor speed (rpm)	2900
Condenser	Air
Capillary tube diameter (mm)	0.55 / 0.6
Capillary tube length (m)	2.44
Filter position	Vertical
Test aim	Charge study

5.2.2.2 Results

Air temperature at the evaporator inlet was kept constant for each refrigerant charge tested by manually regulating the heater power inside the FZ. Cooling capacity and COP were calculated using Eq. 3.1 and Eq. 3.2 (chapter 3), respectively.

The different COP values obtained during the refrigerant charge study of both capillary tubes are depicted in Figure 72. The different points of the graphs correspond to an average of 50 min of test results once steady conditions were achieved.

The COP values of the 0.6 mm capillary tube were lower than those corresponding to the 0.55 mm tube. However, the difference was small and difficult to quantify. Uncertainty on the COP was equal to ± 0.04 and is not depicted so as to not alter the figure clarity.

For the 0.55 mm tube, the highest COP was 1.97 at 67.5 g, while for the 0.6 mm tube, the highest COP was 1.96 at 65.1 g. As the capillary tube diameter was increased, the optimal refrigerant charge was displaced towards the right of the graphic and therefore, requiring a slightly higher refrigerant charge, which is consistent to findings in the literature [10], [14]. It is interesting to note the drop in COP for both capillary tubes at 62.3 g, however, the authors did not find any physical explanation for this observation since no correlation with observable parameters was found.

Regarding the refrigerant visualisations at the capillary tube inlet, the different liquid levels for the different refrigerant charges tested are depicted in Figure 72. For the 0.6 mm capillary tube, the inlet was always two-phase flow, as represented in the bottom blue frame. For the 0.55 mm capillary tube, different liquid levels were obtained through the refrigerant charge test campaign and are represented in the top red frames. For 67.5g, the filter was full of liquid and the highest COP was found at exactly this refrigerant charge. For the rest of the refrigerant charges tested, the inlet was alternating two-phase flow with mostly liquid inlet similar to that in chapter 4, Figure 61, where the inlet was only liquid 95% of the time.

Figure 73 represents the measured compressor power for both capillary tubes in the refrigerant charge study. At low refrigerant charges, the compressor power was quite similar for both capillary tubes, however, the difference became clear when the refrigerant charge was increased. For the optimal refrigerant charge of each capillary tube, the difference in compressor power was around 3% with the 0.55 mm capillary tube revealing lower consumption.

Figure 74 illustrates the results of the cooling capacity for both capillary tubes evaluated from the enthalpy variation at the evaporator. The cooling capacity was slightly higher for the 0.6 mm capillary tube. However, as argued in chapters 3 and 4, the cooling capacity calculated from the enthalpy variation could be erroneous.

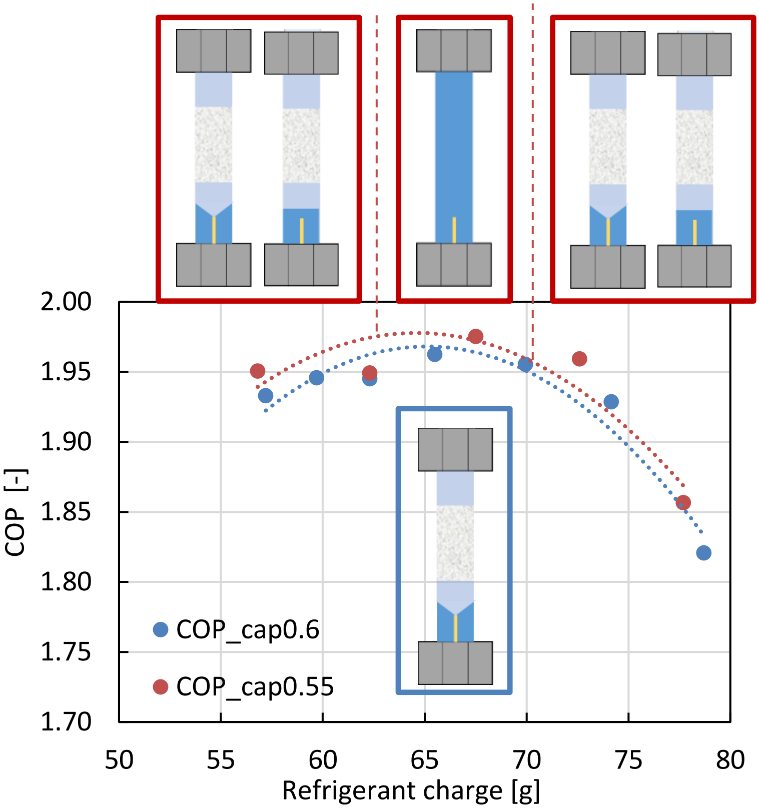

Figure 72: COP and liquid level inside filter for different refrigerant charges for the two tested capillary tubes, of 0.55 mm and 0.6 mm diameter respectively

Figure 75 illustrates the measured input power to the heater used to keep the air temperature constant at the inlet of the evaporator. The power input required was higher for the capillary tube with the smaller diameter, which indicates that cooling capacity with the 0.55 mm tube is slightly higher than the larger capillary tube. This confirms that the use of the refrigerant cooling capacity, evaluated from the estimation of the enthalpy difference at the refrigerant side, did not lead to a logical result. As discussed in chapter 4, section 4.3.3, the cooling capacity variation trend should always be similar to the resistance power trend since the heat gained from the ambient and fan power was identical at each test.

As Figure 73 illustrates, the compressor consumption was lower for the smaller diameter tube, and, as argued, the cooling capacity should thus be higher. This finding leads to the conclusion that the actual COP of the smaller capillary tube diameter was higher than the difference in COP depicted in Figure 72, which was evaluated by the enthalpy variation estimation.

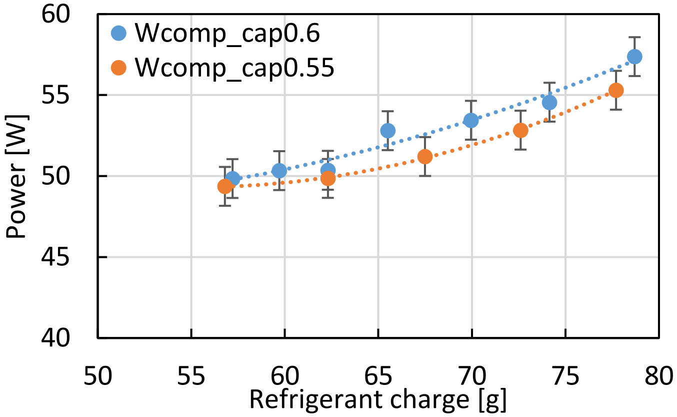

Figure 73: Compressor power for different refrigerant charges for the two tested capillary tubes, of 0.55 mm and 0.6 mm diameter respectively

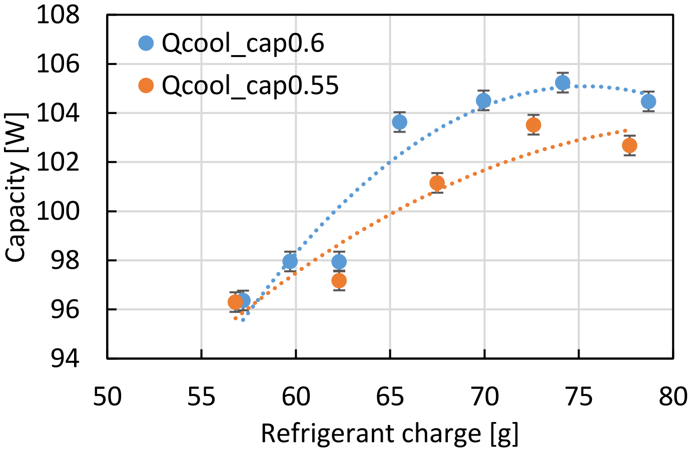

Figure 74: Refrigerant cooling capacity for different refrigerant charges for the two tested capillary tubes, of 0.55 mm and 0.6 mm diameter respectively

Figure 76 depicts the new COP estimation, where the cooling capacity was evaluated at the air side (Eq. 4.5, section 4.3.3) using the input power to the heater and refrigerator heat gain estimation (Eq. 4.6, section 4.3.3), as described in chapter 4. The heat gain estimation was performed for the 0.6 mm capillary tube with the smallest charge of 57.2 g and was considered the same for all the other test points.

All COP values obtained with the 0.55 mm diameter capillary tube were significantly higher than those obtained with the 0.6 mm capillary tube. The average difference of COP between the two capillary tubes was around 4.7%, whereas this difference reached only 0.6% when refrigerant cooling capacity was used to calculate the COP.

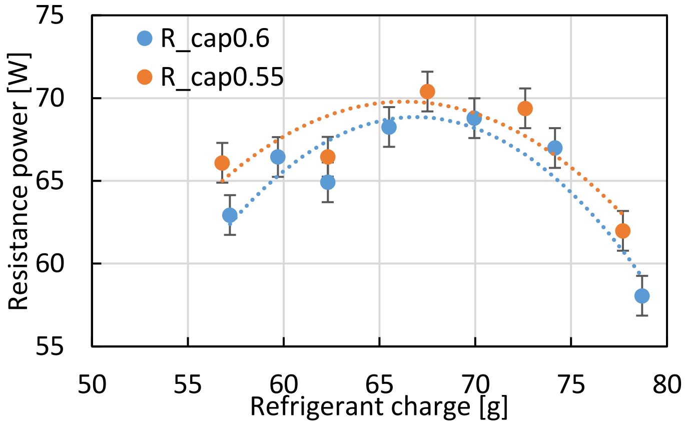

Figure 75: Resistance power of 0.55 mm diameter and 0.6 mm diameter capillary tubes for different refrigerant charges

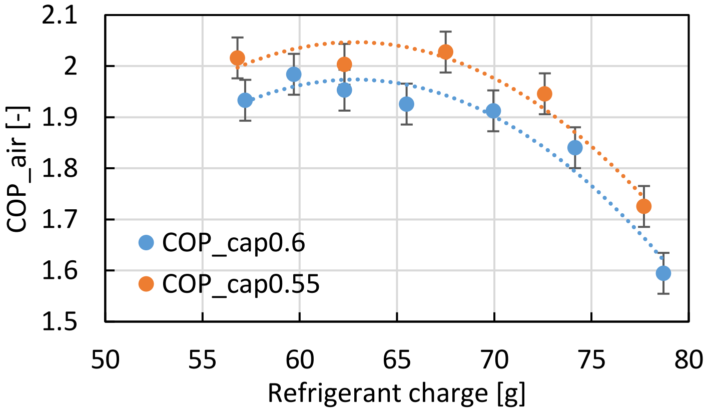

Figure 76: COP using air cooling capacity of 0.55 mm diameter and 0.6 mm diameter capillary tubes for different refrigerant charges

With the COP new estimation, the optimal refrigerant charge for the 0.55 mm tube remained at 67.5 g, whereas, for the 0.6 mm capillary tube, the optimal refrigerant charge was displaced to the left with respect to the previous study. Nevertheless, only the overall trend of both COPs should be analysed instead of focusing on the individual COP values, since the uncertainty was high on this set of results because of the approximation used for the cooling capacity estimation.

5.3 Conclusions

An experimental campaign was carried out using two capillary tubes of different diameters (0.55 mm and 0.6 mm) at the same compressor speed (2900 rpm) to compare performance of a capillary tube with liquid inlet with a capillary tube with two-phase flow inlet.

The COP values were determined by determining the optimal refrigerant charge of each capillary tubes size. In a first analysis, results revealed that the COP was higher for the 0.55 mm capillary tube with liquid inlet than for the 0.6 mm with two-phase inlet. However, the difference is minor and lower than the uncertainty on the COP values.

A second analysis was carried out because some basic observations indicated that the difference between both COP values was underestimated if the refrigerant side cooling capacity was used for the calculation. This second analysis used the estimated air cooling capacity instead of the refrigerant one to estimate the COP. The new COP results revealed a much higher difference between both capillary tubes and seem to confirm that liquid at the capillary tube inlet led to better performance than two-phase flow inlet, with an approximate COP increase of around 4.7%.

Chapter 6

Conclusions and future works

6.1 Conclusions

The main objectives of this thesis (described in chapter 1) are fulfilled:

- A fundamental explanation of the actual conditions at the capillary tube inlet of a household refrigerator is provided (chapters 2 and 3).

- A design improvement of the apparatus was tested to ensure liquid conditions at the capillary tube inlet (chapter 4).

- A performance comparison between the original and new design was performed (chapter 5).

6.1.1 On the actual conditions at the capillary tube inlet

An innovative test bench was designed to enable visualisation of both the condenser outlet and capillary tube inlet of a household refrigerator. The visualisation of the condenser outlet reveals the presence of two-phase flow regardless of filter orientation, capillary tube position and refrigerant charge. In all tested filters, the liquid level followed the capillary entrance, demonstrating that the filter was not operating as a liquid receiver.

A refrigerant-to-water heat exchanger was used instead of the original refrigerant-to-air condenser to assess, from heat balance at the water condenser, refrigerant conditions at the capillary tube inlet. Different water mass flow rates were tested to modify the condensation temperature and study the effect on conditions at the capillary tube inlet. The heat balance methodology indicated that, except for the two lowest water mass flow rates tested, all others revealed a certain low subcooling (around 3 K). Nevertheless, it must be mentioned that despite considerable effort in selecting accurate instrumentation, uncertainty on the measurement was high.

The pressure and temperature measurements revealed a much higher subcooling, which contradicted the visualisation at the capillary tube inlet. Furthermore, the vapour temperature measured above the filter dryer was always below the saturation temperature, that is, practically at the same temperature than the subcooled liquid.

This paradoxical phenomenon was attributed to the presence of non-equilibrium two-phase flow composed of subcooled liquid and subcooled vapour at the capillary tube inlet. The enthalpy at the condenser outlet can thus not be determined using the thermodynamic properties table, which is valid only for an equilibrium condition of the refrigerant. The presence of vapour at the capillary tube inlet can also be explained by the capillary tube being oversized with respect to the compressor. Therefore, the capillary tube inlet should be necessary under two-phase flow conditions in a way that the flow rate is low enough to match the compressor flow rate.

However, a rationale for this vapour being found in subcooled state is not explained here since the condensation process occurred quite slowly and the vapour bubbles had enough time to condensate along the tube or inside the small volume of the filter dryer.

6.1.2 On the design improvement to ensure liquid conditions at the capillary tube inlet

By increasing the compressor speed from 1600 rpm to 1800 rpm and reducing the capillary tube diameter from 0.6 mm to 0.55 mm, it was possible to fill the filter from upstream the capillary tube inlet with liquid, which resulted impossible with the original capillary tube. It has thus been demonstrated that a non-matching existed between the capillary tube and compressor flow rate of this commercial household refrigerator.

Nevertheless, at 1800 rpm, during the same experimental campaign and despite identical test conditions, the level of liquid was not repeatable. From 2500 rpm up, the filter was always full of liquid.

The transparent tube set up at the condenser outlet revealed that the higher the compressor speed, the lower the void fraction. However, at 3500 rpm, the lower part of the filter was full of liquid and the void fraction upstream was almost negligible. That said, the difference between the two subcooling measurements, e.g., SC_{pT} and SC_{HX}, persisted. The subcooling value calculated from the thermodynamic conditions at the condenser outlet, assuming equilibrium, did not provide valid results due to the vapour subcooled state. Although the actual subcooling was difficult to assess, the refrigerant state was subcooled, although not in thermodynamic equilibrium.

Additionally, this study reveals that other phenomena greatly complicate the study of performance in this kind of system. The existence of a hysteresis effect and observation of a “jump” in the mass flow rate was attributed to the creation of a metastable region inside the capillary tube.

Second, the cooling capacity calculation at the refrigerant side did not provide a logical result in some cases. Indeed, when changing from a given compressor speed to a higher speed, the resistance power increase inside the freezer to maintain the air temperature at the evaporator inlet should have led to a cooling capacity increase. However, the reverse occurred. The authors of this work do not have explanations for such a phenomenon.

To assess actual cooling capacity, the cooling capacity from the air side was calculated, which confirmed that the cooling capacity calculation at the refrigerant side returned, in some cases, an erroneous result.

To compare the performance of a capillary tube with liquid inlet to a capillary tube with two-phase flow inlet, an experimental campaign was carried out using two capillary tubes of different diameters (0.55 mm and 0.6 mm) at the same compressor speed (2900 rpm). The COP were determined by determining the optimal refrigerant charge of each capillary tube size. The COP analysis seemed to confirm that liquid at the capillary tube inlet led to better performance than two-phase flow inlet, with an approximate COP increase of around 4.7%.

6.2 Future works

In the present work, it has been a willingness to build a test bench using a domestic refrigerator taking great pains to do not alter the original working by limiting the modification of the piping and components. But the difficulty to reach steady conditions because of the inertia of the system restricted the allowable tests conditions and made very hard to have a wide tests matrix.

It would be interesting to design a test bench with a resistance in the evaporator to simulate the thermal load, instead of using the refrigerator -freezer. The use of a plates condenser could be a way to get a wider range of condensation temperatures in order to study the effect on the void fraction at the condenser outlet. The set up of an oil separator at the compressor outlet would let studying the effect on the oil presence on the condensation pressure and on the mass flow rate measurement.

The reason why the flow is a non-equilibrium mixture composed of subcooled liquid and vapour deserves an explanation.

The metastable effect in the capillary tube certainly worth while a deep study.

References

[1] T. Cleff and K. Rennings, “Are there first mover advantages for producers of energy-efficient appliances? The case of refrigerators,” *Util. Policy*, 2016.

[2] R. Radermacher and K. Kim, “Domestic refrigerators: recent developments,” *Int. J. Refrig.*, vol. 19, no. 1, pp. 61–69, Jan. 1996.

[3] W. J. Yoon, K. Seo, and Y. Kim, “Development of an optimization strategy for insulation thickness of a domestic refrigerator-freezer,” *Int. J. Refrig.*, vol. 36, no. 3, pp. 1162–1172, 2013.

[4] J. Fricke, U. Heinemann, and H. P. Ebert, “Vacuum insulation panels-From research to market,” *Vacuum*, vol. 82, no. 7, pp. 680–690, 2008.

[5] F. Ghadiri and M. Rasti, “The effect of selecting proper refrigeration cycle components on optimizing energy consumption of the household refrigerators,” *Appl. Therm. Eng.*, vol. 67, no. 1–2, pp. 335–340, Jun. 2014.

[6] P. K. Bansal and T. C. Chin, “Modelling and optimisation of wire-and-tube condenser,” vol. 26, pp. 601–613, 2003.

[7] J. R. Barbosa and R. A. Sigwalt, “Air-side heat transfer and pressure drop in spiral wire-on-tube condensers,” *Int. J. Refrig.*, vol. 35, no. 4, pp. 939–951, 2012.

[8] A. Pisano, S. Martínez-Ballester, J. M. Corberán, and A. W. Mauro, “Optimal design of a light commercial freezer through the analysis of the combined effects of capillary tube diameter and refrigerant charge on the performance,” *Int. J. Refrig.*, vol. 52, pp. 1–10, 2015.

[9] J. Boeng and C. Melo, “Mapping the energy consumption of household refrigerators by varying the refrigerant charge and the expansion restriction,” *Int. J. Refrig.*, vol. 41, pp. 37–44, May 2014.

[10] E. Björk and B. Palm, “Performance of a domestic refrigerator under influence of varied expansion device capacity, refrigerant charge and ambient temperature,” *Int. J. Refrig.*, vol. 29, no. 5, pp. 789–798, Aug. 2006.

[11] P. . Bansal and A. . Rupasinghe, “An empirical model for sizing capillary tubes,” *Int. J. Refrig.*, vol. 19, no. 8, pp. 497–505, Nov. 1996.

[12] D. Hartmann and C. Melo, “Popping noise in household refrigerators: Fundamentals and practical solutions,” *Appl. Therm. Eng.*, vol. 51, no. 1, pp. 40–47, 2013.

[13] C. W. Liu, Y., Bullard, “An Experimental and Theoretical Analysis of Capillary Tube-Suction Line Heat Exchangers,” University of Illinois, 1997.

[14] J. Boeng and C. Melo, “A Capillary Tube, Refrigerant Charge Design

Methodology for Household Refrigerators, Part II Equivalent Diameter and Test Procedure," *Int. Refrig. Air Cond. Conf. Purdue*, pp. 1–10, 2012.

[15] C. Inan, T. Gonul, and M. Y. Tanes, "X-ray investigation of a domestic refrigerator. Observations at 25°C ambient temperature," *Int. J. Refrig.*, vol. 26, no. 2, pp. 205–213, 2003.

[16] W.-J. Lee, J.-Y. Seo, J. Ko, and J. H. Jeong, "Non-equilibrium two-phase refrigerant flow at subcooled temperatures in an R600a refrigeration system," *Int. J. Refrig.*, vol. 70, pp. 148–156, 2016.

[17] J. Ko and J. H. Jeong, "Effects of a non-equilibrium two-phase refrigerant flow at subcooled temperatures on the performance of an R-600a refrigeration system," *Int. J. Refrig.*, 2017.

[18] P. K. Bansal and C. Yang, "Reverse heat transfer and re-condensation phenomena in non-adiabatic capillary tubes," *Appl. Therm. Eng.*, vol. 25, no. 17–18, pp. 3187–3202, Dec. 2005.

[19] ASHRAE, "American Society of Heating, Refrigerating, and Air-Conditioning Engineers," in *ASHRAE*, 2010th ed., Georgia: ASHRAE, 2010.

[20] B. Xu and P. . Bansal, "Non-adiabatic capillary tube flow: a homogeneous model and process description," *Appl. Therm. Eng.*, vol. 22, no. 16, pp. 1801–1819, 2002.

[21] C. J. L. Hermes, C. Melo, and J. M. Gonçalves, "Modeling of non-adiabatic capillary tube flows: A simplified approach and comprehensive experimental validation," *Int. J. Refrig.*, vol. 31, no. 8, pp. 1358–1367, Dec. 2008.

[22] N. Ablanque, C. Oliet, J. Rigola, and A. Oliva, "Numerical simulation of non-adiabatic capillary tubes. Special emphasis on the near-saturation zone," *Int. J. Refrig.*, vol. 55, pp. 153–167, Jul. 2015.

[23] M. B. Wolf, D. A., Pate, "Capillary Tube-Suction Line Heat Exchanger Performance with Alternative Refrigerants," *ASHRAE Res. Proj. Rep. 948*, 2002.

[24] A. A. Silva Huerta, F. A. Sanzovo Fiorelli, and O. de Mattos Silvares, "Metastable flow in capillary tubes: An experimental evaluation," *Exp. Therm. Fluid Sci.*, vol. 31, no. 8, pp. 957–966, Aug. 2007.

[25] R. R. Bittle, "An experimental evaluation of capillary tube- suction line heat exchanger performance with alternative refrigerants HFC-134a and HFC-152a," 1994.

[26] J. J. Meyer and W. E. Dunn, "New insights into the behavior of the metastable region of an operating capillary tube," *ASHRAE Trans.*, vol. 104, no. 2, p. 120, 1998.

[27] R. R. Bittle, J. A. Carter, J. V Oliver, R. R. Bittle, and D. Ph, "Extended

Insight into the Metastable Liquid Region Behavior in an Adiabatic Capillary Tube Extended Insight into the Metastable Liquid Region Behavior in an Adiabatic Capillary Tube," vol. 9669, no. August, 2017.

[28] Rui-Yang Li, Sui Lin, Zu-Yao Chen, and Zhi-Hang Chen, "Metastable flow of R12 through capillary tubes," *Int. J. Refrig.*, vol. 13, no. 3, pp. 181–186, 1990.

[29] K. C. Mendoca, C. Melo, R. T. S. Ferreira, and R. H. Pereira, "Experimental Study on Lateral Capillary Tube- Suction Line Heat Exchangers," in *Proceedings of International Refrigeration Conference, Purdue*, 1998, pp. 437–442.

[30] C. Melo, L. A. Torquato Vieira, and R. H. Pereira, "Non-adiabatic capillary tube flow with isobutane," *Appl. Therm. Eng.*, vol. 22, no. 14, pp. 1661–1672, Oct. 2002.

[31] E. Dirik, C. Inan, and M. Y. Tanes, "Numerical and experimental studies on adiabatic and nonadiabatic capillary tubes with HFC-134a," in *Proceedings of the IIR-Purdue Refrigeration Conference, West Lafayette*, 1994, pp. 365–370.

[32] C. J. L. Hermes and C. Melo, "Assessment of the energy performance of household refrigerators via dynamic simulation," *Appl. Therm. Eng.*, vol. 29, no. 5, pp. 1153–1165, 2009.

[33] O. García-Valladeres, "Numerical simulation of non-adiabatic capillary tubes considering metastable region . Part II : Experimental validation," vol. 30, pp. 654–663, 2007.

[34] J. M. Choi and Y. C. Kim, "The effects of improper refrigerant charge on the performance of a heat pump with an electronic expansion valve and capillary tube," *Energy*, vol. 27, no. 4, pp. 391–404, 2002.

[35] J. El Hajal, J. . Thome, and A. Cavallini, "Condensation in horizontal tubes, part 1: two-phase flow pattern map," *Int. J. Heat Mass Transf.*, vol. 46, no. 18, pp. 3349–3363, Aug. 2003.

[36] L. Cecchinato, M. Dell'Eva, E. Fornasieri, M. Marcer, O. Monego, and C. Zilio, "The effects of non-condensable gases in domestic appliances," *Int. J. Refrig.*, vol. 30, no. 1, pp. 19–27, 2007.

[37] C. M. Rodolfo S. ESPÍNDOLA, Fernando T. KNABBEN, "The Influence of Non-condensable Gases on the Thermal-acoustic Behavior of Household Refrigerators," in *International Compressor Engineering, Refrigeration and Air Conditioning, and High Performance Buildings Conferences*, 2016, pp. 1–9.

Publications

Publications in peer-reviewed journals

1. S. Martínez-Ballester, L. Bardoulet, A. Pisano, and J. M. Corberán, "Visualization of refrigerant flow at the capillary tube inlet of a high-efficiency household refrigerator," Int. J. Refrig., vol. 73, pp. 200–208, Jan. 2017.

2. L. Bardoulet, S. Martínez-Ballester, J. M. Corberán, "How to get full liquid conditons at the capillary tube inlet of a household refrigerator," 2018. Manuscript submitted for publication.

Publications in congresses

1. L. Bardoulet, S. Martínez-Ballester, J. M. Corberán, "How to assess subcooling in household refrigerator," in *10th edition of the National Congress of Engineering Thermodynamics, LLeida,* 2017.

2. L. Bardoulet, S. Martínez-Ballester, J. M. Corberán, "Refrigerant conditions at the capillary tube inlet of a household refrigerator," in *13th IIR Gustav Lorentzen Conference, Valencia,* 2018.